

博士論文

Mechanisms of Senescence in Retinal Pigment Epithelial Cells

(網膜色素上皮細胞における加齢のメカニズム)

Murilo Felix Roggia

ムリロ フェリックス ロジャ

Doctoral Dissertation

博士論文

Mechanisms of Senescence in Retinal Pigment Epithelial Cells

(網膜色素上皮細胞における加齢のメカニズム)

The University of Tokyo

東京大学

Murilo Felix Roggia

ロジャ ムリロ フェリックス

2015

To my dear parents

Acknowledgements

It is a pleasure to express my great appreciation to those who supported my journey in Japan. This doctoral dissertation is the result of five years of commitment and hard work.

Firstly, I would like to express my profound gratitude to my adviser and research supervisor, Dr. Takashi Ueta, a great scientist and brilliant ophthalmologist who guided my steps during this doctoral program at the University of Tokyo. It was an honor to join your team and to learn from you. Thank you very much for teaching me and supporting me along the journey.

I am very glad to express my deep appreciation to the Associate Professor Satoshi Kato and to the former professors of the Department of Ophthalmology of the University of Tokyo, Professor Makoto Araie and Professor Shiro Amano, for this great opportunity.

Also, I would like to truly thank the former Associate Professor of the Department of Ophthalmology, Professor Yasuhiro Tamaki, who actively supported my coming to the University of Tokyo.

To my coworkers and collaborators, Dr. Hirotaka Imai, Dr. Yasuo Noda, and Dr. Tomoyasu Shiraya, my sincere gratitude.

To all the members of the Department of Ophthalmology of the University of Tokyo, I sincerely appreciate your kindness and hard work.

I would like to thank the University of Tokyo Center for NanoBio Integration for the confocal microscopy technical support. I also thank Dr. Noboru Mizushima for supporting the evaluation of cathepsin D activity.

I would like to express my deepest gratitude to Dr. Howard Ying, Associate Professor of the Wilmer Eye Institute at the Johns Hopkins Graduate School of Medicine, for his great support, orientation, guidance, and training of my clinical and

surgical skills in ophthalmology, fully supporting my decision to come to Japan to improve my academic studies.

My most sincere gratitude to Dr. Neil Bressler, Professor of Ophthalmology and Chief of the Retina Division of the Wilmer Eye Institute at the Johns Hopkins Graduate School of Medicine.

I would like to thank Professor João Borges Fortes Filho from Brazil for stimulating me to engage in academic research and for supporting my decision to come to Japan to improve my skills. To Dr. Wilson de Oliveira Leite Filho, and Dr. Antônio José Dornelles da Costa Gama, also from Brazil, my gratitude for fully encouraging me to come to Japan.

To my dear parents Valdir Roggia and Vania Maria Felix Roggia, thank you very much for the unconditional love and support always. Your encouragement and example allowed me to achieve my accomplishments. To my dear sisters Mariane Felix Roggia and Cristina Felix Roggia, thank you for always supporting and encouraging me along the journey. Your example inspired me to pursue my objectives. To my dear little Cindy, thank you for always being there for me.

To Dr. Simone Beheregaray, my dear partner and colleague, my very special thanks for always being by my side along the way. Your unconditional support encouraged and inspired me to become a better person. Thank you for your unconditional support always.

To all my friends, thank you for being by my side for all these years. Each one of you contributed to make this real.

I would like to express my deepest gratitude to the Japanese Government and the Japanese Ministry of Education, Culture, Sports, Science and Technology (MEXT) for supporting my doctoral course in Japan.

Murilo Felix Roggia

Contents

Acknowledgements	iii
Contents	v
Abbreviations	viii
Symbols	xi
List of Figures	xii
List of Tables	xix
Abstract	xx
1. Introduction	1
1.1 Retina	1
1.2 Retinal Pigment Epithelium	2
1.3 Age-Related Macular Degeneration	5
1.4 Research Motivation	11
1.5 Pathogenesis of AMD	12
2. Literature Review	15
2.1 Peroxisome Proliferator-Activated Receptor Gamma Coactivator 1-α	15
2.2 Photoreceptor Outer Segments Phagocytosis and the Retinal Pigment Epithelium .	16
2.3 Aging and Metabolism of the RPE Cells	19
2.3.1 Impaired Lysosomal Function in the RPE	20
2.3.2 Oxidative Stress and Mitochondrial Dysfunction in the RPE Cells	21
2.3.3 Impaired Autophagosomal Activity in the RPE Cells and AMD	22
2.4 Choroidal Neovascularization	22
2.4.1 Animal Model of CNV	23
2.4.2 Oxidative Stress and CNV	23

3. Research Purposes	25
4. Senescence and Lysosomal Activity of Retinal Pigment Epithelium Regulated by Binding of Photoreceptor Outer Segments through $\alpha\beta 5$ Integrin/FAK/PGC-1α	26
4.1 Introduction	26
4.2 Methods	28
4.2.1 Animals	28
4.2.2 Experimental protocol	28
4.2.3 POS treatment on ARPE-19 cells	29
4.2.4 Antibodies and reagents	30
4.2.5 Quantification of mRNA and mitochondrial DNA by real-time PCR	31
4.2.6 Western blot analysis	33
4.2.7 Knockdown experiment	33
4.2.8 Intracellular ROS levels	34
4.2.9 Mitochondrial activity assay	34
4.2.10 Cell senescence assay	34
4.2.11 BODIPY C11 assay	35
4.2.12 Transmission electron microscopy (TEM)	35
4.2.13 Statistics	35
4.3 Results	36
4.3.1 Binding of POS upregulates PGC-1 α through $\alpha\beta 5$ integrin and FAK	36
4.3.2 POS exerts antisenescent effects through PGC-1 α in RPE cells	43
4.3.3 PGC-1 α regulates lysosomal activity of POS in RPE cells	47
4.3.4 Senescence-related phenotypes in RPE of PGC-1 α knockout (KO) mice	51
4.4 Discussion	53
5. Protective Role of GPx4 in Laser-Induced Choroidal Neovascularization in Mice	57
5.1 Introduction	57
5.2 Methods	59
5.2.1 Animals	59
5.2.2 Laser-induced CNV model	59
5.2.3 Assessment of RPE/choroid tissue	60
5.2.4 Quantification of mRNA using real-time RT-PCR	61
5.2.5 Protein expression analysis using Western Blot analysis and ELISA	62

5.2.6 Immunohistochemistry using 4-hydroxy-2-nonenal (4-HNE).....	63
5.2.7 Statistical analysis.....	64
5.3 Results	64
5.3.1 Laser-induced CNV and VEGF-A expression in the RPE/choroid tissue in mice	64
5.3.2 Generation of GPx4 ^{+/-} , GPx4 ^{+/+} , and GPx4-overexpressing mice used in the study ..	68
5.3.3 GPx4 and oxidative stress in the mice	71
5.3.4 Animal model of CNV development using laser-induced CNV.....	71
5.4 Discussion.....	75
6. Discussion.....	80
7. Conclusions	87
8. Clinical Viewpoints and Future Perspective.....	88
9. Bibliography	89

Abbreviations

AGE Advanced Glycation End-Product

AICAR AMP-mimetic 5-aminoimidazole-4-carboxamide-1- β -D-ribofuranoside

AMPK AMP-Activated Protein Kinase

AREDS Age-Related Eye Disease Study

AMD Age-Related Macular Degeneration

BCVA Best Corrected Visual Acuity

bFGF Basic Fibroblast Growth Factor

BODIPY Boron Dipyrromethene

CTS Cathepsin

CI Confidence Interval

CNV Choroidal Neovascularization

FAK Focal Adhesion Kinase

FAZ Foveal Avascular Zone

4-HNE 4-Hydroxy 2-Neonenal

GA Geographic Atrophy

GLA Galactosidase α

GPx Glutathione Peroxidase

H₂O₂ Hydrogen Peroxide

H2DCFDA 2',7'-Dichlorodihydrofluorescein Diacetate

HEXA Hexosaminidase A

IGF-1 Insulin Growth Factor 1

KD Knockdown

KO Knockout

MerTK Mer Tyrosine Kinase

mTOR Mechanistic Target of Rapamycin

max Maximum

min Minimum

mm Millimeter

OCT Optical Coherence Tomography

OPL Outer Plexiform Layer

μm Micrometer

nm Nanometer

P Probability

PEDF Pigment Epithelium-Derived Factor

PGC-1α Peroxisome Proliferator Activated Receptor γ Coactivator-1 α

POS Photoreceptor Outer Segments

RPE Retinal Pigment Epithelium

ROS Reactive Oxygen Species

SA- β -gal Senescence-Associated β -galactosidase

SD Standard Deviation

Sirt1 Silence Information Regulator 2-Like 1

SOD Superoxide Dismutase

TFEB Transcription Factor EB

Tg Transgenic

TPPI Tripeptidyl Peptidase I

UCVA Uncorrected Visual Acuity

UEA-I Biotinylated Ulex europaeus agglutinin-I

VEGF Vascular Endothelial Growth Factor

Symbols

$^{\circ}\text{C}$ degrees Celsius

$>$ greater than

$<$ less than

\geq equal or greater than

\leq equal or less than

\sim range of values

List of Figures

Figure 1.1. Histological organization of the retina.

Figure 1.2. Schematic representation of the cellular organization of the retina.

Figure 1.3. Normal fundus.

Figure 1.4. Age-related macular degeneration: early stage.

Figure 1.5. Age-related macular degeneration: late stage (geographic atrophy).

Figure 1.6. Age-related macular degeneration: late stage (neovascular).

Figure 1.7. Progression of AMD: modifications of the retinal structures.

Figure 4.1. POS upregulate PGC-1 α in RPE cells. PGC-1 α mRNA and protein levels were upregulated in: (A) Undifferentiated ARPE-19 cells. (B) Differentiated ARPE-19 cells. (C) *Ex vivo* RPE cells, treated with POS for 3 h for evaluation of mRNA and for 6 h for evaluation of protein level. Morphology of differentiated ARPE-19 cells was confirmed by immunofluorescence for ZO-1 antibody. Mean \pm SEM, n = 6–10 per group for mRNA level, n = 3 per group for protein level, two-tailed Student's *t*-test, **P* < 0.05, ***P* < 0.01, ****P* < 0.001, *****P* < 0.0001. Scale bars in the images of undifferentiated and differentiated ARPE-19 cells represent 100 μ m and 200 μ m, respectively.

Figure 4.2. Upregulation of PGC1- α mRNA was dose-dependent on the number of POS in undifferentiated ARPE-19 cells. Mean \pm SEM, n = 6 per group, *****P* < 0.0001 by ANOVA, followed by a post hoc Tukey's test ***P* < 0.01, ****P* < 0.001, compared with ARPE-19 cells with no treatment.

Figure 4.3. POS binding activates the α v β 5 integrin/FAK/PGC-1 α pathway in undifferentiated ARPE-19 cells. (A) PGC-1 α mRNA levels were not affected in the ARPE-19 cells treated with latex beads (LB) versus the controls. Mean \pm SEM, n = 6

per group; two-tailed Student's *t*-test; ns, not significant. (B) Upregulation of PGC-1 α mRNA in response to POS was significantly suppressed in the ARPE-19 cells pretreated with RGD peptide versus the controls. Mean \pm SEM, n = 6 per group, two-tailed Student's *t*-test, *****P* < 0.0001. (C) Time course of PGC-1 α mRNA levels in the ARPE-19 cells after treatment with POS.

Figure 4.4. Knockdown efficacy of siRNAs for β 5 integrin, CD36, MerTK, and Atg5 knockdown was analyzed in undifferentiated ARPE-19 cells. (A) β 5 integrin mRNA levels measured by RT-PCR. Mean \pm SEM, n = 6 per group, two-tailed Student's *t*-test, *****P* < 0.0001. β 5 integrin protein levels measured by western blot analysis. Mean \pm SEM, n = 3 per group, two-tailed Student's *t*-test, ****P* < 0.001. (B) CD36 mRNA levels measured by RT-PCR. Mean \pm SEM, n = 6 per group, two-tailed Student's *t*-test, ****P* < 0.001. CD36 protein levels measured by western blot analysis. Mean \pm SEM, n = 3 per group, two-tailed Student's *t*-test, ****P* < 0.001. (C) MerTK mRNA levels measured by RT-PCR. Mean \pm SEM, n = 6 per group, two-tailed Student's *t*-test, *****P* < 0.0001. MerTK protein levels measured by western blot analysis. Mean \pm SEM, n = 3 per group, two-tailed Student's *t*-test, ****P* < 0.001. (D) Atg5 mRNA levels measured by RT-PCR. Mean \pm SEM, n = 6 per group, two-tailed Student's *t*-test, ****P* < 0.001. Atg5 protein levels measured by western blot analysis. Mean \pm SEM, n = 3 per group, two-tailed Student's *t*-test, ****P* < 0.001.

Figure 4.5. POS binding activates the α β 5 integrin/FAK/PGC-1 α pathway in undifferentiated ARPE-19 cells. (A) Upregulation of PGC-1 α mRNA levels in response to POS was significantly suppressed in the ARPE-19 cells pretreated with siRNA against β 5 integrin, enhanced in those pretreated with siRNA against CD36 or MerTK, and not influenced in those pretreated with siRNA against Atg5. Mean \pm SEM, n = 6 per group, *****P* < 0.0001 by ANOVA, followed by a post hoc Tukey's test **P* < 0.05, ***P* < 0.01, ****P* < 0.001, ns [not significant], compared with the control group. (B) Upregulation of PGC-1 α mRNA levels in response to POS was enhanced in the ARPE-19 cells pretreated with CD36 antibody (2 μ g/mL) versus control. Mean \pm SEM, n = 6 per group, two-tailed Student's *t*-test, ***P* < 0.01. (C) Upregulation in PGC-1 α mRNA in response to POS was enhanced in the ARPE-19 cells pretreated with MerTK antibody (3.44 μ g/mL) versus control. Mean \pm SEM, n = 6 per group, two-tailed

Student's *t*-test, **** $P < 0.0001$. (D) Upregulation in PGC-1 α mRNA in response to POS was suppressed in the ARPE-19 cells pretreated with FAK inhibitor 14 (500 μ M) versus control. Mean \pm SEM, $n = 6$ per group, two-tailed Student's *t*-test, **** $P < 0.0001$.

Figure 4.6. The upregulation of PGC1- α was independent of AMPK activity. (A) Pretreatment of undifferentiated ARPE-19 cells with STO-609 (10 μ g/ml) for 10 min enhanced the upregulation of PGC1- α mRNA level by POS. Mean \pm SEM, $n = 6$ per group, two-tailed Student's *t*-test, ** $P < 0.01$. (B) Pretreatment with AICAR for 12 h decreased the PGC1- α mRNA level in the ARPE-19 cells. Mean \pm SEM, $n = 6$ per group, * $P < 0.05$ by ANOVA, followed by a post hoc Tukey's test * $P < 0.05$, compared with control.

Figure 4.7. POS increased antioxidant enzymes and decreased ROS level in undifferentiated ARPE-19 cells through PGC-1 α . (A) mRNA levels of anti-oxidant enzymes including GPx1, GPx4, SOD1 and catalase, but not of SOD2, were upregulated in the ARPE-19 cells treated with POS. Mean \pm SEM, $n = 6$ per group, two-tailed Student's *t*-test, ** $P < 0.01$, *** $P < 0.001$; ns, not significant. (B) ROS levels in the ARPE-19 cells evaluated by H₂DCFDA were downregulated in the ARPE19 cells treated with POS. Mean \pm SEM, $n = 16$ per group, two-tailed Student's *t*-test, **** $P < 0.0001$. (C) ROS levels were downregulated in response to POS in the ARPE-19 cells transfected with control siRNA, but upregulated in cells transfected with PGC-1 α siRNA. Mean \pm SEM, $n = 9$ –12 per group, two-tailed Student's *t*-test, **** $P < 0.0001$.

Figure 4.8. Efficacy of PGC-1 α knockdown was analyzed in undifferentiated ARPE-19 cells. (A) PGC-1 α mRNA levels measured by RT-PCR. Mean \pm SEM, $n = 8$ per group, two-tailed Student's *t*-test, **** $P < 0.0001$. (B) PGC-1 α protein levels measured by western blot analysis. Mean \pm SEM, $n = 3$ per group, two-tailed Student's *t*-test, ** $P < 0.01$.

Figure 4.9. POS treatment upregulated mitochondrial biogenesis in undifferentiated ARPE-19 cells through PGC-1 α . (A) Relative mitochondrial DNA level, as determined by cytochrome b/GAPDH, were upregulated in the ARPE-19 cells treated with POS.

Mean \pm SEM, $n = 6$ per group, two-tailed Student's t -test, **** $P < 0.0001$. (B) Western blot analysis showed increased protein level of the mitochondrial marker prohibitin in the ARPE-19 cells treated with POS. Mean \pm SEM, $n = 6$ per group, two-tailed Student's t -test, * $P < 0.05$. (C) In the ARPE-19 cells transfected with control siRNA, mitochondrial complex I activity was significantly upregulated in response to the POS treatment ($n = 8$ per group, **** $P = 0.0001$ by ANOVA, followed by a post hoc Tukey's test *** $P < 0.001$). However, in the ARPE-19 cells transfected with PGC-1 α siRNA, the change in mitochondrial complex I activity with POS treatment was not statistically significant.

Figure 4.10. POS treatment rescues H₂O₂-induced senescence through PGC-1 α . (A) Undifferentiated ARPE-19 cells were incubated with or without POS for 3 h and then treated with 100 μ M H₂O₂ for 2 h to induce senescence. In the RPE cells pretreated with control siRNA, POS treatment almost completely suppressed SA- β -gal staining by H₂O₂-induced senescence. In contrast, in the RPE cells transfected with PGC-1 α siRNA, H₂O₂ induced significantly stronger and more frequent SA- β -gal staining in the RPE cells, and the rescue effect by POS treatment was significantly smaller compared with the RPE cells pretreated with control siRNA. (B) Quantification of SA- β -gal staining in the ARPE-19 cells. Mean \pm SEM, $n = 3$ per group, **** $P < 0.0001$ by ANOVA, followed by a post hoc Tukey's test * $P < 0.05$, ** $P < 0.01$. The scale bars in large pictures and in insets are 100 μ m and 500 μ m, respectively.

Figure 4.11. PGC-1 α regulates lysosomal activity in undifferentiated ARPE-19 cells. (A) Nuclear immunofluorescence with TFEB antibody was weaker in the ARPE-19 cells transfected with PGC-1 α siRNA compared with those with control siRNA. (B) Quantification of nuclear immunofluorescence with TFEB antibody. Mean \pm SEM, $n = 6$ per group, two-tailed Student's t -test, **** $P < 0.0001$; scale bar, 50 μ m. (C) In the ARPE-19 cells transfected with PGC-1 α siRNA, mRNA levels of TFEB target genes including GLA, HEXA, TPPI, and CTSF were downregulated when compared with those with control siRNA. Mean \pm SEM, $n = 6$ per group, two-tailed Student's t -test, ** $P < 0.01$, *** $P < 0.001$, **** $P < 0.0001$. (D) In the ARPE-19 cells pretreated with FAK inhibitor 14, mRNA levels of TFEB target genes including GLA, HEXA, TPPI, and CTSF were downregulated when compared with those with control

pretreatment. Mean \pm SEM, n = 6 per group, two-tailed Student's *t*-test, $**P < 0.01$, $****P < 0.0001$. (E) In the ARPE-19 cells transfected with PGC-1 α siRNA, cathepsin D activity was significantly downregulated compared with those with control siRNA. Mean \pm SEM, n = 11–12 per group, two-tailed Student's *t*-test, $***P < 0.001$.

Figure 4.12. PGC-1 α facilitates lysosomal degradation of POS in undifferentiated ARPE-19 cells. (A) In the ARPE-19 cells transfected with PGC-1 α siRNA, oil red O staining was more intense after POS treatment than in those with control siRNA. Scale bar, 200 μ m. (B) In the ARPE-19 cells transfected with PGC-1 α siRNA, the accumulation of peroxidized lipid evaluated by BODIPY C11 fluorescence increased after POS treatment when compared with those with control siRNA. Mean \pm SEM, n = 6–10 per group, $***P < 0.001$ by ANOVA, followed by a post hoc Tukey's test $*P < 0.05$, ns [not significant].

Figure 4.13. Accelerated senescence is observed in the RPE of PGC-1 α KO mice. The phenotypes of the RPE, Bruch's membrane, and choriocapillaris of 6-month-old PGC-1 α KO mice were compared with those of age-matched control littermates. (A and B) Accumulation of melanolipofuscin on TEM was observed in the PGC-1 α KO mice when compared with the control mice. Note that many melanin granules in the KO mice are more whitish, which indicates lipofuscin accumulation in the melanin granules. CC; choriocapillaris; scale bar, 5 μ m. (C and D) Bruch's membrane (BM) and choriocapillaris (CC) on TEM. Note that BM of the KO mice is thicker and has greater electron density than that of the control mice. CC beneath the BM was not often observed in KO mice, while it was abundant in the control mice. Scale bar, 1 μ m. (E and F) Magnified view of BM and CC. Scale bar, 500 nm. (G and H) CC evaluated by UEA-I staining was poor in the KO mice when compared with the control mice. Scale bar, 5 μ m. (I and J) Autofluorescence reflecting lipofuscin accumulation in the RPE was more intense in the KO mice than in the control mice. (K) Magnified views of melanolipofuscin in the RPE cells of the KO mice. Scale bar 1, μ m.

Figure 4.14. Schematic drawing of the signaling pathway revealed in the present study. In the RPE cells, POS binding activates the α v β 5 integrin/FAK/PGC-1 α pathway, which facilitates lysosomal activity and prevents senescence to counteract POS-induced metabolic stress.

Figure 5.1. VEGF-A expression in the RPE/choroid with laser-induced CNV. (A) Relative VEGF-A mRNA levels in the RPE/choroid of wild-type mice before and after induction of the CNV model at 6, 12, 24, 48 and 72 h. Mean \pm SEM, n = 10–21, *** P < 0.0001 by ANOVA, followed by a post hoc Tukey's test *** P < 0.001 compared with the no laser group. (B) VEGF-A protein expression in the RPE/choroid of wild-type mice before and after 72 h of CNV induction by laser, measured by ELISA. Mean \pm SEM, n = 4, *** P < 0.001, Student's t -test.

Figure 5.2. Change in VEGF-A mRNA levels in the RPE/choroid after CNV induction in wild-type mice. For the same samples shown in Figure 1, different primer pairs for VEGF-A were used for RT-PCR. The primers sequences are shown in Table 1. (A) A primer pair 2 (Hu et al., 2009) was used. (B) A primer pair for VEGF 164 (Mizutani et al., 2009) was used. (C) A primer pair 3 (Xie et al., 2011) was used. Mean \pm SEM, n = 10–21 per group, **** P < 0.0001, ns [not significant] by ANOVA, followed by a post hoc Tukey's test * P < 0.05, *** P < 0.001, ns [not significant], compared with the no laser group.

Figure 5.3. GPx4 expression in the RPE/choroid. (A) Similar appearance of GPx4^{+/-}, GPx4^{+/+} and GPx4^{+/+}:Tg (GPx4) mice at 3 months of age expressing different levels of GPx4. (B) Hematoxylin-eosin staining of the retina and RPE/choroid of the mice expressing different levels of GPx4. (ONL, outer nuclear layer; INL, inner nuclear layer; GCL, ganglion cells layer; Scale bar, 30 μ m).

Figure 5.4. GPx4 expression in the mice. (A) Western blot analysis of β -actin and GPx4 protein expression in the RPE/choroid. (B) Statistical evaluation for the comparative differences in GPx4 protein in the RPE/choroid. Mean \pm SEM, n = 8, ** P < 0.01 by ANOVA, followed by a post hoc Tukey's test * P < 0.05, ** P < 0.01, compared with GPx4^{+/-} mice.

Figure 5.5. Protein expression of GPx1 and GPx2 in the RPE/choroid. (A) Western blot analysis of β -actin and GPx1/2 protein expression in the RPE/choroid. (B) Statistical evaluation for the comparative differences in GPx1/2 protein in the RPE/choroid. Mean \pm SEM, n = 5; ns, not significant by ANOVA.

Figure 5.6. Accumulation of peroxidized lipids. (A) Immunoreactivity to 4-hydroxi-2-neonenal (4-HNE, red) in the retina and RPE/choroid of mice expressing different levels of GPx4. Nuclei was counterstained with 4,6-diamidino-2-phenylindole (DAPI, blue). Scale bar, 30 μm . (B) Statistical evaluation of the immunofluorescence for 4-HNE in the RPE/choroid. Mean \pm SEM, $n = 4$, $***P < 0.001$ by ANOVA, followed by a post hoc Tukey's test $*P < 0.05$, $***P < 0.001$, compared with GPx4^{+/-} mice.

Figure 5.7. Laser-induced CNV model. The CNV area size was evaluated on flatmount culture on day 7. (A) CNV induced by laser exposure in the mice expressing different levels of GPx4. Scale bar, 500 μm . (B) The area size of the CNV in these 3 types of mice (μm^2). Mean \pm SEM, $n = 4-5$, $****P < 0.0001$ by ANOVA, followed by a post hoc Tukey's test $**P < 0.01$, $****P < 0.0001$ compared with GPx4^{+/-} mice.

Figure 5.8. VEGF-A expression in the RPE/choroid before and after CNV induction. (A) Relative VEGF-A mRNA levels were measured by RT-PCR before and 3 days after the CNV induction by laser exposure. Mean \pm SEM, $n = 4-6$. P values for ANOVA are described inside the figure. A post hoc Tukey's test $*P < 0.05$, ns [not significant], compared with GPx4^{+/-} mice that underwent the same treatment. (B) VEGF-A protein expression in the RPE/choroid was measured by ELISA before and 3 days after the CNV induction. Mean \pm SEM, $n = 4-6$. P values for ANOVA are described inside the figure. A post hoc Tukey's test $*P < 0.05$, $**P < 0.01$, ns [not significant], compared with GPx4^{+/-} mice that underwent the same treatment.

List of Tables

Table 4.1. Primers sequences used for real time RT-PCR in the study.

Table 5.1. Primers sequences used for real time RT-PCR in the study.

Abstract

Age-related accumulation of lipids in the retinal pigment epithelium (RPE) is important for the development of age-related macular degeneration (AMD), a major cause of legal blindness worldwide. Photoreceptor outer segments (POS) are constantly shed to RPE cells, and if not efficiently metabolized, can result in accumulation of hazardous lipid byproducts. Previous studies reported that the inhibition of POS phagocytosis is associated with oxidative stress and aging of RPE cells. In late stage neovascular AMD, vascular endothelial growth factor (VEGF) plays a central role in the establishment of choroidal neovascularization (CNV). The importance of VEGF in the pathogenesis of the disease has also been determined in animal model of laser-induced CNV. Oxidative stress has not only been associated with the development of AMD, but also participates in the progression from early stage to late stage neovascular AMD. The current study identified a regulatory role of POS binding in senescence and lysosomal activity in the RPE cells through $\alpha\text{v}\beta\text{5}$ integrin/focal adhesion kinase (FAK)/peroxisome proliferator activated receptor γ coactivator-1 α (PGC-1 α) pathway. POS-induced PGC-1 α decreased reactive oxygen species (ROS), increased mitochondrial biogenesis, and prevented senescence. Furthermore, FAK and PGC-1 α were involved in the activation of transcription factor EB (TFEB), a master regulator of autophagy/lysosomal pathway, and the silencing of PGC-1 α led to decreased cathepsin D activity and accumulation of peroxidized lipids after POS treatment. PGC-1 α knockout (KO) mice exhibited phenotypes of aged RPE, including lipofuscin accumulation, thickening of Bruch's membrane, and atrophic choriocapillaris. Overall,

these results suggest the regulatory role of POS binding in senescence and metabolism in the RPE cells to counteract the potential metabolic stress of POS phagocytosis. With regards to neovascular AMD, this study demonstrated that GPx4 influences VEGF-A expression in the RPE/choroid, suppressing the increase in VEGF-A protein levels after laser-induced CNV. Furthermore, GPx4 demonstrated a protective effect against CNV development *in vivo*.

Keywords: Age-related macular degeneration, retinal pigment epithelium, photoreceptor outer segments, peroxisome proliferator activated receptor γ coactivator-1 α , α v β 5 integrin, focal adhesion kinase, senescence, lysosomal degradation, oxidative stress, antioxidant enzymes, vascular-endothelial growth factor, glutathione peroxidase 4, choroidal neovascularization.

1. Introduction

1.1 Retina

The retina is known as the sensorineural part of the eye. Anatomically it can be divided into the central and peripheral retina. The posterior pole, also known as the anatomic macula, is the central area of the retina located between the superior and inferior temporal arcades. Characteristically it is the area surrounding the fovea, measuring approximately 6 mm in diameter (Hildebrand and Fielder, 2011).

The macula, also known as the anatomic fovea centralis, is the area located approximately 3 mm temporal to the optic disc, measuring about 1.5 mm in diameter. This region was named the macula because of the presence of xanthophyll, a yellow carotenoid pigment (Hildebrand and Fielder, 2011). The most central part of the macula is called the fovea. The fovea is formed by a central depression measuring around 0.35 mm in diameter. This is the region of the greatest visual acuity of the retina (Oyster, 1999). The foveola presents the highest population of cone photoreceptors, approximately 200,000/mm², characteristically narrowed and elongated (Curcio et al., 1990). Rod photoreceptors are usually absent in this very central area, but dense elsewhere. The central 500 μm of the fovea contains no retinal capillaries and is called the foveal avascular zone (FAZ) (Hildebrand and Fielder, 2011).

The peripheral retina is the remaining area of the retina located outside the temporal retinal arcades. This region presents a dense population of rod photoreceptors.

The retina extends anteriorly towards the ora serrata, which delineates the termination of the sensory retina (Hildebrand and Fielder, 2011).

Retinal cells and their processes are organized in layers that can be identified histologically (Figures 1.1 and 1.2).

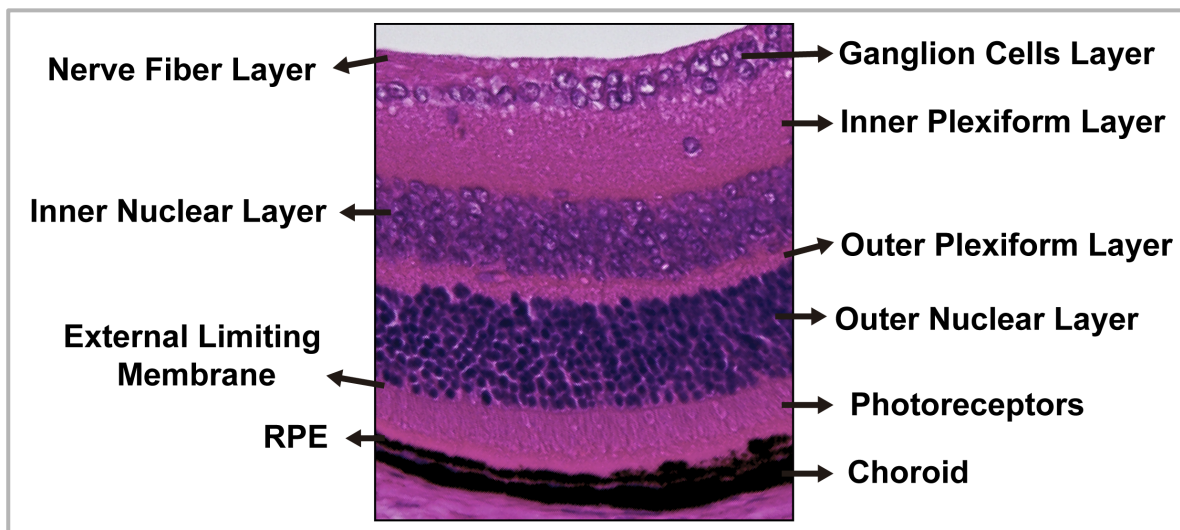


Figure 1.1. Histological organization of the retina.

1.2 Retinal Pigment Epithelium

The RPE consists of a monolayer of specialized pigmented epithelial cells responsible for the transportation of nutrients and metabolic end products between the subretinal space and the choriocapillaris (Steinberg, 1985). A healthy adult individual has approximately 3.5 million RPE cells (Panda-Jonas et al., 1996). Characteristically, the RPE cells are symmetrically arranged as hexagonal tiles with tight-junction between adjacent cells (Strauss, 2005).

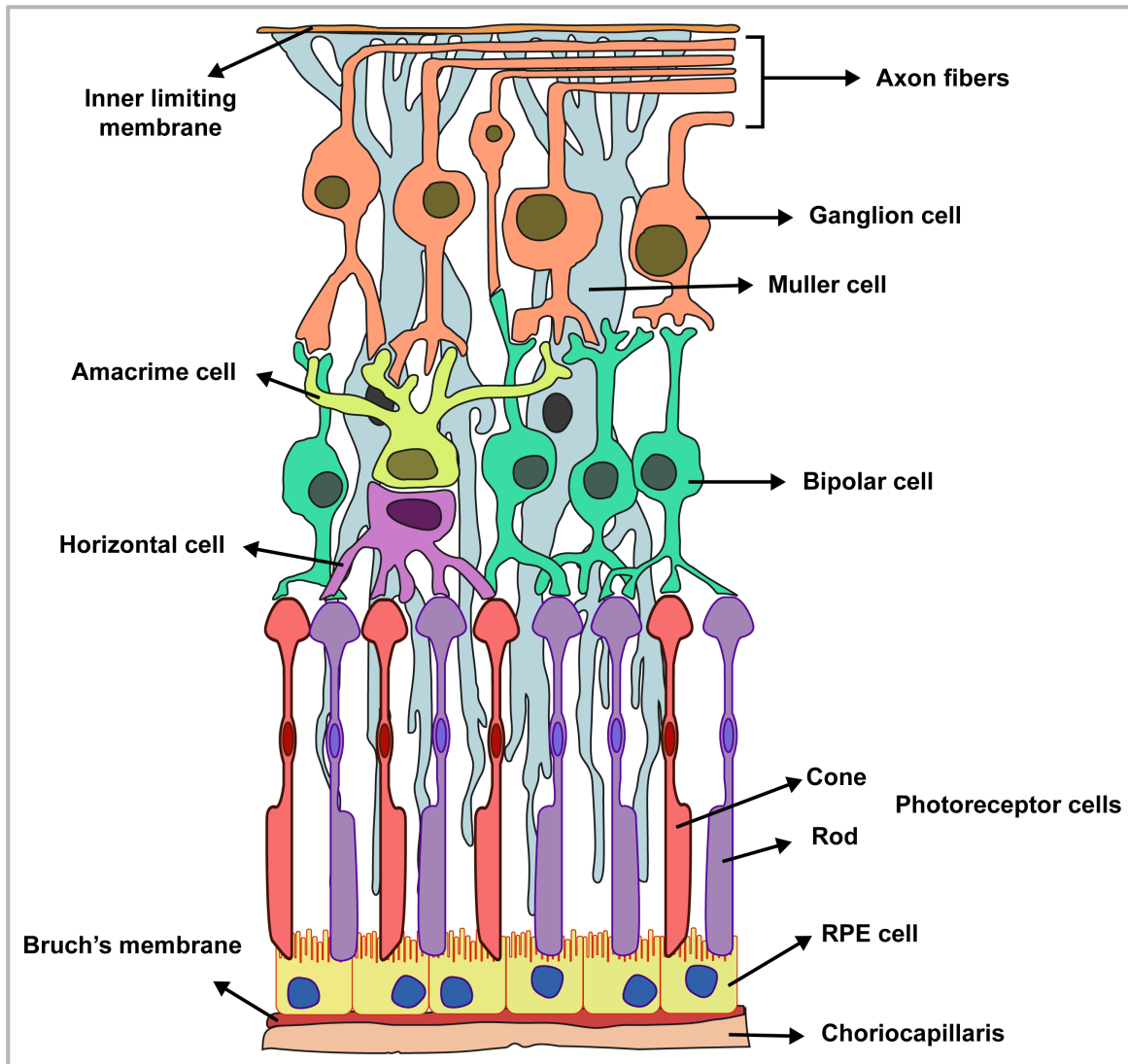


Figure 1.2. Schematic representation of the cellular organization of the retina.

Considered one of the most metabolically active tissues of the human body, the RPE is essential for photoreceptor survival and differentiation (King and Suzuma, 2000; Strauss, 2005). For this reason, RPE viability is crucial for the function of both photoreceptors and choriocapillaris, and essential for visual maintenance (Strauss, 2005).

Owing to intense absorption of light that enters the eye, high oxygen concentration from the choriocapillaris, and intense metabolic reactions, RPE cells are constantly exposed to oxidative damage (Strauss, 2005). A healthy RPE cell is capable of defending

itself against these toxins by the filtering and absorbing of light by the melanosomes (Boulton, 1998) and lipofuscin (Delori et al., 2001; Weiter et al., 1986). Additional light absorption by the photoreceptor-containing pigments, such as lutein and zeaxanthin (Strauss, 2005) promotes further protection against photooxidation (Beatty et al., 1999; Beatty et al., 2001). The existence of antioxidant activity in RPE cells, as well as the ability to repair damaged proteins and DNA are also associated with protection (Strauss, 2005).

Photoreceptor outer segments phagocytosis is one of the most important functions of the RPE. In humans, each RPE cell faces an average of 23 photoreceptors (Gao and Hollyfield, 1992), and the turnover rate is approximately 10 days for an entire photoreceptor outer segment (Young, 1971). Each photoreceptor consists of an outer segment, an inner segment, a nucleus, an inner fiber, and the synaptic terminal (Roof and Makino, 2000). In the outer segment, the retinal photopigment is stacked inside flat discs. The inner segment contains the metabolic-related structures responsible for the survival and function of the photoreceptor cells (Strauss, 2005).

RPE cells are also responsible for secreting a wide range of different growth factors as well as other substances, which are important for the maintenance of the structural integrity of the retina and choriocapillaris, contributing to the survival of photoreceptors (Strauss, 2005). VEGF is produced and secreted in low concentrations by the RPE in physiologic conditions (Adamis et al., 1993; Lopez et al., 1996; Witmer et al., 2003). This vascular factor secretion occurs at the basal side of the RPE cell acting on the choroidal endothelium (Blaauwgeers et al., 1993). It is associated with endothelial cell protection against apoptosis, and is essential for maintaining the integrity of the choriocapillaris endothelial cells (Burns and Hartz, 1992).

Interestingly, secretion of growth factors by the RPE can change in accordance with damage or injury. This mechanism protects both RPE cells and photoreceptors against light-induced damage (Cao et al., 2001; Walsh et al., 2001). Upregulation of VEGF by RPE cells under intensive light of physiologic range has also been described (Ueta et al., 2012b).

1.3 Age-Related Macular Degeneration

Age-related macular degeneration (AMD) is the leading cause of irreversible visual loss in people aged older than 65 years around the world (Kawasaki et al., 2010; Smith et al., 2001). Commonly afflicting the elderly population, the disease is also present in younger individuals. Approximately 2% of the population at 40 years of age is diagnosed with AMD, while one in every four people at the age of 80 has the disease (Friedman et al., 2004). Longer life expectancy, increasing prevalence of chronic systemic diseases, and exposure to environmental risk factors are some of the reasons why the incidence of AMD has climbed over the last few years. The estimated prevalence of the disease is expected to increase over 50% by the year 2020 (Friedman et al., 2004).

Several risk factors for the development and progression of AMD have already been strongly established. Advancing age is clearly one of the main factors associated with the incidence and progression of the disease. The prevalence of early stage AMD has been reported to increase from 8% among those aged between 43 and 54 years, to 30% among those individuals aged older than 75 years. With regards to the late stage AMD, the

prevalence increased from 0.1% among people aged between 43 to 54 years to 7.1% in the population aged over 75 years (Klein et al., 1992).

Genetic related factors are also associated with the establishment of the disease. Family inheritance has been proved to play an important role as a risk factor for the development of AMD (Jager et al., 2008). The complement system has a clear role in the development of the disease. Polymorphisms of the complement factors H, B, and C2 genes have been reported to be associated with the increased risk for development of AMD (Jager et al., 2008).

According to de Jong (2006), smoking shows a consistent association with AMD. The author described greater risk for developing late stage AMD among currently active smokers in contrast with an insignificant risk among former smokers. Moreover, a history of smoking more than 10 packs/year was associated with the development of neovascular AMD as an independent factor.

Jager et al. (2008) have found that systemic diseases such as high blood pressure, obesity, high intake of vegetal fat, and low dietary intake of antioxidants and zinc are also associated with the development of advanced stage AMD. The authors showed that high dietary intake of β -carotene, vitamins C and E, zinc, as well as polyunsaturated fatty acids and fish independently decreased the risk of developing neovascular AMD.

Degeneration of the RPE cells is widely considered the initial step in AMD development. Oxidative damaged molecules gradually accumulate in the macular area serving as a source of chronic oxidative stress (Handa, 2012). Age-related increase in oxidative stress reactions along with accumulation of lipofuscin in the lysosomes of the RPE cells contributes for drusen formation in the extracellular space underneath the RPE

(Kaarniranta et al., 2013). Additionally, immunological events are also associated with the pathogenesis of the disease. Production of inflammation-related mediators, macrophages recruitment, and activation of complement system are present in the development of AMD (Kaarniranta et al., 2013).

Avascular AMD is characterized by the absence of the neovascular component (Bressler and Bressler, 2013b). The first clinical finding in the early stage of dry AMD is the presence of drusen. Drusen are extracellular deposits of lipids and protein debris that accumulate beneath the RPE cells (Hageman et al., 2001). Geographic atrophy (GA) is the late stage of avascular AMD, which is characterized by large and confluent areas of RPE atrophy in the macular area (Bressler and Bressler, 2013b).

Neovascular AMD is characterized by the invasion of abnormal blood vessels from the choroid towards the retina (Bressler and Bressler, 2013a). As a consequence, leakage of fluid and hemorrhage characteristically occur with the progression of the disease (Ambati et al., 2003). Typically, the first symptoms of exudative AMD are central visual blurring and distortion. Examination of the macula usually reveals an exudative macular lesion along with other features of early AMD such as drusen and pigmentary irregularities. Subretinal or sub-RPE neovascularization, serous detachment of the neurosensory retina, RPE detachment, hemorrhages (subretinal, intraretinal or preretinal) and hard exudates (lipids) are commonly observed in the progression of the disease (Bressler and Bressler, 2013a).

AMD can be classified according to the severity of the macular alterations associated with the disease. Although more than one classification system exists, the grading system proposed by the Age-Related Eye Disease Study (AREDS) has been

increasingly used (Age-Related Eye Disease Study Research Group, 2000). Therefore, the disease may be classified according to four stages:

- **No AMD (AREDS category 1):** any of the following:
 - no alterations
 - few small drusen (< 63 μm in diameter);
- **Early AMD (AREDS category 2):** any or all of the following:
 - multiple small drusen
 - few (less than 20) intermediate drusen (63 - 124 μm in diameter)
 - RPE abnormalities
- **Intermediate AMD (AREDS category 3):** any or all of the following:
 - extensive intermediate drusen (63 - 124 μm in diameter)
 - at least one large druse (≥ 125 μm in diameter)
 - geographic atrophy not involving the center of the fovea
- **Advanced AMD (AREDS category 4);**
 - geographic atrophy involving the fovea
 - any of the features of neovascular AMD



Figure 1.3. Normal fundus

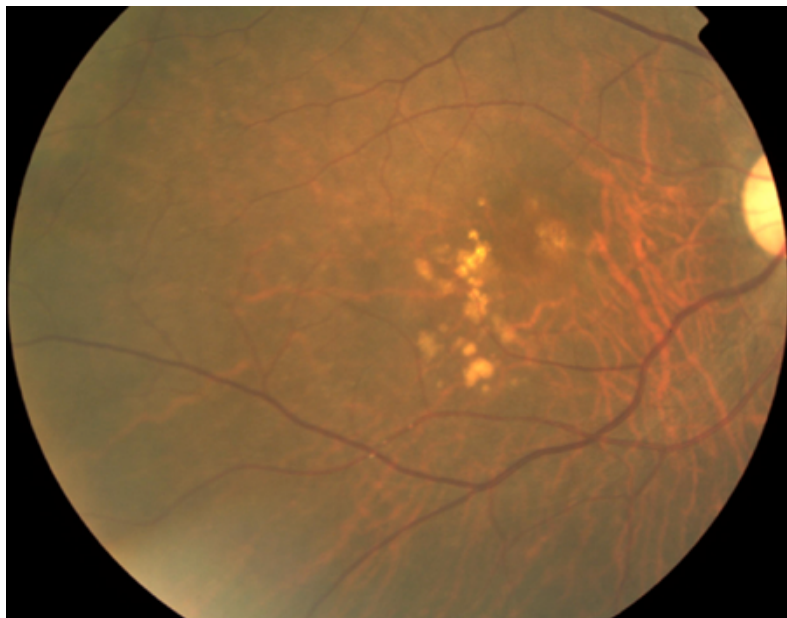


Figure 1.4. Age-related macular degeneration: early stage

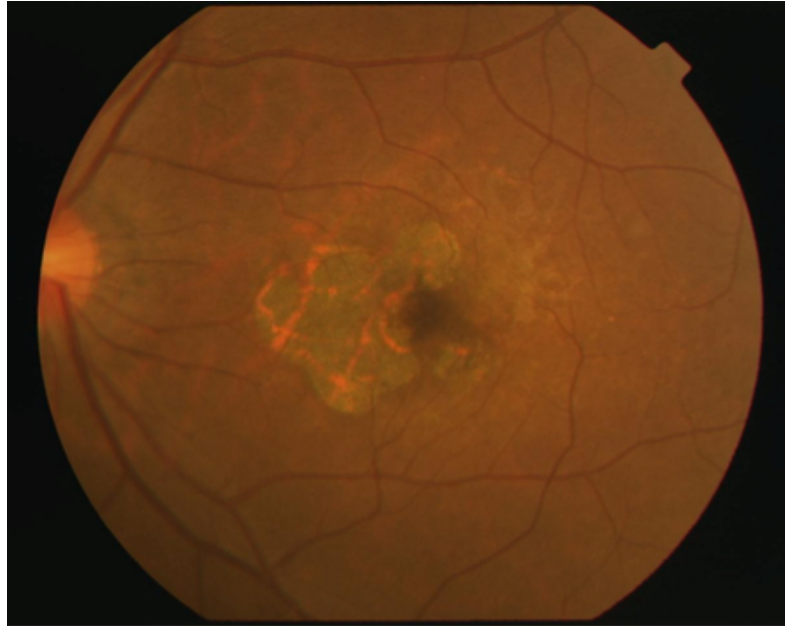


Figure 1.5. Age-related macular degeneration: late stage (geographic atrophy)

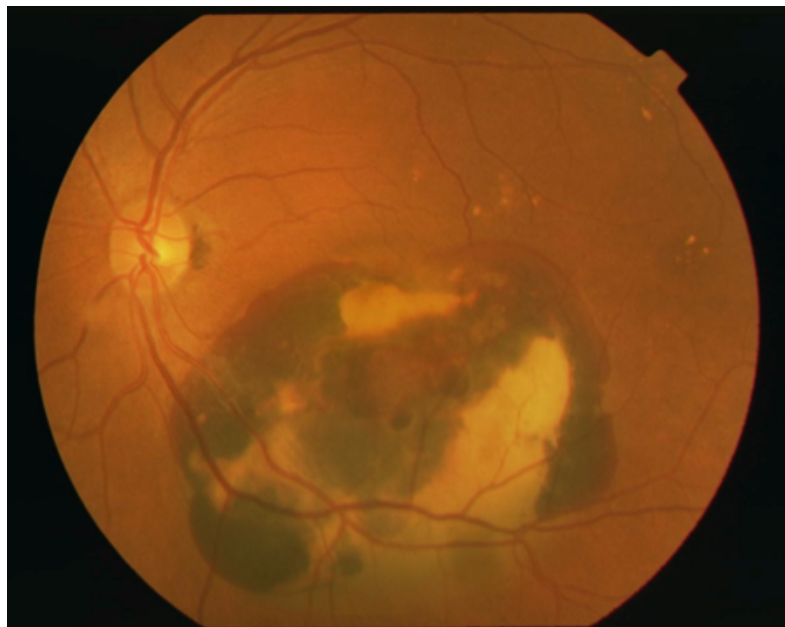


Figure 1.6. Age-related macular degeneration: late stage (neovascular)

Treatment of avascular AMD is limited and consists mainly of counseling, smoking cessation, visual rehabilitation, and prescription of vitamins to reduce the risk of progression. The AREDS demonstrated that daily oral supplementation with antioxidant vitamins C, E, β -carotene and zinc reduced the risk of developing advanced AMD by 25% at five years (Age-Related Eye Disease Study Research Group, 2001). The AREDS 2 trial investigated whether the addition of daily oral supplementation with omega-3 long-chain polyunsaturated fatty acids (DHA and EPA) to the AREDS formulation might be associated with a reduction in the progression of the disease (Age-Related Eye Disease Study 2 Research Group, 2013). However, the findings showed that no extra reduction in risk of progression to advanced AMD was evident in AREDS 2 by the addition of lutein and zeaxanthin, or of DHA and EPA, or all of these to the AREDS formulation.

Treatment of neovascular AMD is based on the inhibition of the development of abnormal new blood vessels localized in the choroidal and retinal tissues. Currently, the primary therapy for the management of exudative AMD consists of intravitreal administration of antiangiogenic drugs. Intravitreal injections with VEGF blockers are then delivered directly into the vitreous.

1.4 Pathogenesis of AMD

The pathogenesis of early AMD is characterized by thickening of the Bruch's membrane due to lipid and protein accumulation that leads to formation of sub-RPE deposits, called drusen.

Lipid accumulation is believed to be a consequence of a dysfunction of the RPE. Consequently, increased accumulation of lipofuscin in the RPE cells inflicts further damage on RPE function, affecting lysosomal activity and aggravating cellular distress. As a consequence of decreased flow of nutrients across the Bruch's membrane, physical displacement caused by drusen accumulation, and loss of RPE cells, areas of hypopigmentation surrounded by focal hyperpigmentation become visible at the RPE. Late stage AMD is characterized by confluent loss of RPE cells, originating as GA in non-exudative AMD (Bowes Rickman et al., 2013). In exudative AMD, the late stage of the disease is characterized by abnormal angiogenesis of the choroidal vessels that grow into the retina (Ambati et al., 2003) (Figure 1.7).

1.5 Research Motivation

Given that AMD is the leading cause of visual loss worldwide and that its development is associated with aging-related processes, many factors are relevant for the progression of the disease. The pathogenesis of AMD is directly dependent on abnormalities of the RPE cells, Bruch's membrane, and choriocapillaris. In the natural course of AMD, different molecular alterations act synergistically to determine the progression of the disease. Impaired degradation of POS by the RPE cells is responsible for damaging the RPE, initiating modifications that will contribute to the deterioration of cellular function, leading to aging-associated disorders. Although the beneficial effects of POS phagocytosis and digestion for RPE cells have been recognized, the mechanisms regulating RPE metabolism and senescence have not been fully elucidated. Thus, a study

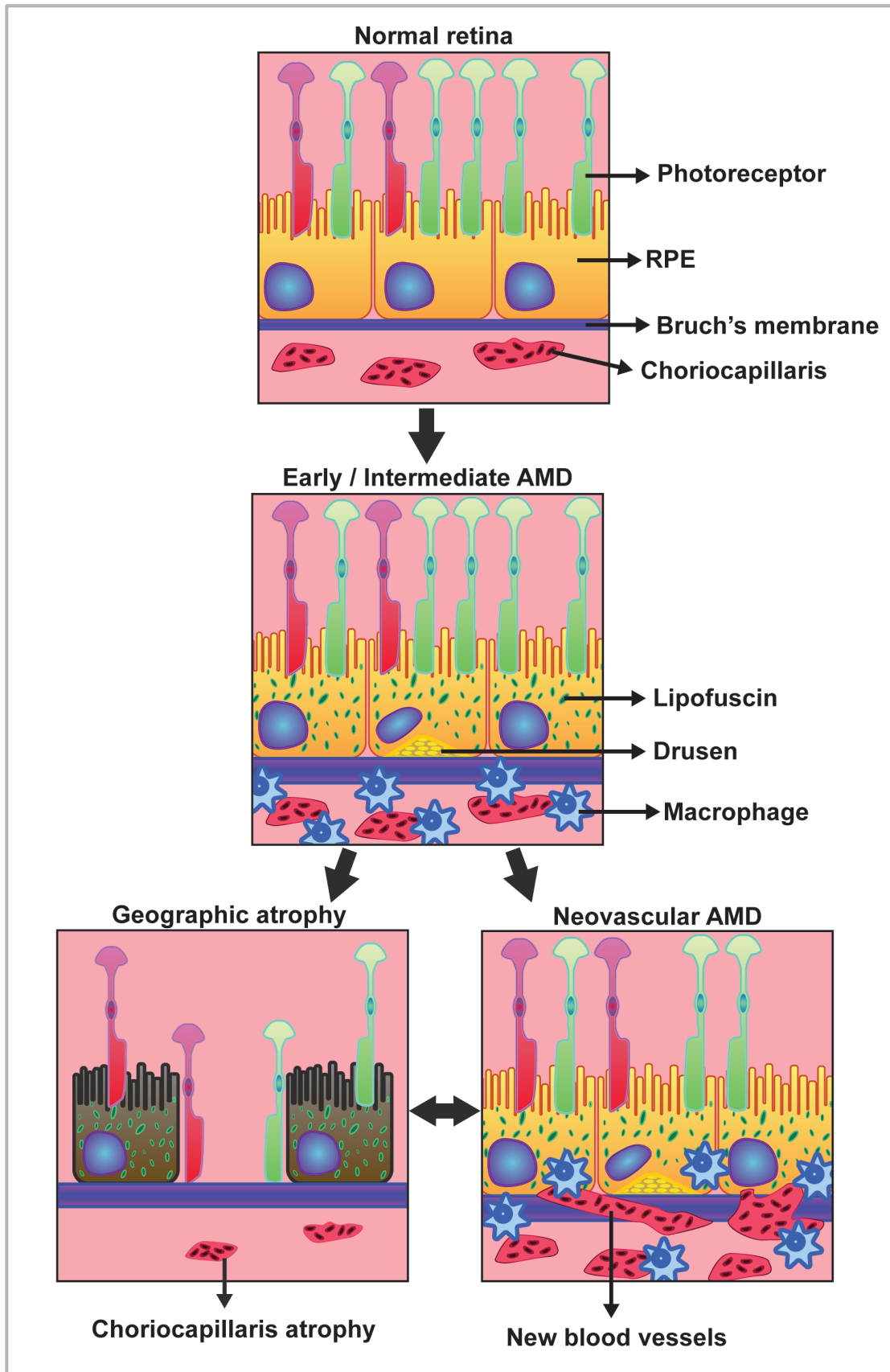


Figure 1.7. Progression of AMD: modifications of the retinal structures.

aiming to further explore the aging-related mechanisms of RPE cells remains vital for better comprehension of the pathogenesis of AMD.

The choroidal neovascularization present in the late stages of AMD is strongly associated with VEGF. Oxidative stress has been demonstrated to influence the development of neovascular AMD, although the role of endogenous antioxidant enzymes remains incompletely understood. Additionally, few reports suggest the implication of superoxide-dismutase 1 in the establishment of CNV in animal models, although its implication in the regulation of VEGF remains unclear. Thus, a study investigating the role of the antioxidant enzyme GPx4 in the establishment of CNV would be important for better understanding the influence of the antioxidant system in the pathogenesis of neovascular AMD.

Therefore, I decided to conduct this research to further explore the mechanisms underlying the metabolism and senescence modifications of RPE cells and to investigate the influence of GPx4 in the development of CNV and in the regulation of VEGF in the RPE/choroid tissue. I believe that the results of the current study will strongly contribute to better understanding of the development and progression of AMD, as well as revealing possible new targets for the management of AMD.

2. Literature Review

2.1 Peroxisome Proliferator-Activated Receptor Gamma Coactivator 1- α

Peroxisome proliferator-activated receptor gamma coactivator 1- α (PGC-1 α) is a transcriptional coactivator that plays an important role in the regulation of adaptive energy metabolism in multiple tissues and has been enrolled in the control of the normal circadian rhythm (Liu et al., 2007). PGC-1 α is a master regulator of mitochondrial biogenesis, and physiologically activated by increased energy demand, temperature oscillations, physical activity, and fasting (Handschin and Spiegelman, 2006). The generation of PGC-1 α null mice further demonstrated its importance in different metabolic reactions. Reduced expression of mitochondrial genes in the liver, brain, skeletal muscle, and heart was observed in mice lacking the expression of PGC-1 α (Arany et al., 2005; Leone et al., 2005; Lin et al., 2004). Mutant mice were extremely cold-sensitive, suggesting a strong requirement of PGC-1 α in adaptive thermogenesis. Additionally, PGC-1 α KO mice displayed multiple neurodegenerative lesions in the brain as well as behavioral abnormalities (Leone et al., 2005; Lin et al., 2004). PGC-1 α also has an important role as a regulator of reactive oxygen species (ROS) metabolism, because it is required for the induction of different antioxidant enzymes responsible for detoxifying ROS, such as the superoxide-dismutase (SOD) and the glutathione peroxidase (GPx) enzymes (St-Pierre et al., 2006).

Wenz et al. (2009) demonstrated that elevated expression of muscular PGC-1 α strongly increases mitochondrial mass and preserves mitochondrial oxidative phosphorylation capacity in aging mice. Elevation of PGC-1 α expression buffered against decline in OXPHOS function during aging, maintaining the metabolic fitness and exercise capacity. The antioxidant capacity was also increased, and the levels of superoxide dismutase 2 (SOD2) and catalase were overexpressed in mutant mice overexpressing PGC-1 α . Additionally, Koltai et al. (2012) reported that regular exercise training stimulates mitochondrial biogenesis through PGC-1 α .

2.2 Photoreceptor Outer Segments Phagocytosis and the Retinal Pigment Epithelium

Despite working as an outer blood-retinal barrier wherein exchange of nutrients and waste products between the choroidal blood vessels and the overlying photoreceptors is constantly controlled (McBee et al., 2001), the RPE is responsible for phagocytizing the shed POS membrane discs maintaining the physiologic renewal of the photoreceptors (Nguyen-Legros and Hicks, 2000). This is an important process by which the RPE cells efficiently dispose of shed POS and return important molecules back to the photoreceptors. Any inefficiency in POS clearance will result in a gradual accumulation of undigested photoreceptor components in the neural retina.

Photooxidative stress causes accumulation of greater amounts of oxidized proteins, radicals and lipids at the tips of the POS. Those structures are shed from the photoreceptors, and new POS are then generated, maintaining a constant POS length.

After been phagocytized by the RPE, shed POS undergo intracellular digestion and important molecules are redelivered to photoreceptors (Bibb and Young, 1974; Bok, 1993).

Shedding of the distal tips of POS takes place every morning, and this process is synchronized by light and circadian rhythm. Thenceforth, the RPE cells initiate its phagocytic activity by efficiently removing shed POS from the retina (La Vail, 1976).

The basis of the coordination between POS shedding and phagocytosis is the presence of POS on the apical surface of the RPE cells (Strauss, 2005). The initial step of the phagocytosis is the specific binding of POS at the apical membrane of the RPE (Strauss, 2005). Next, the recognition of the POS binding is transferred to the intracellular space by activation of a second messenger pathway, consequently activating the internalization of the bound POS (Hall and Abrams, 1987). Finally, the already internalized POS are digested through the activation of the autophagy/lysosomal pathway.

Particle binding occurs during the first 2 h from the start of POS challenging, proceeding a phase of internalization of bound particles, occurring between 2 h and 6 h following POS challenge (Finnemann et al., 1997; Finnemann and Rodriguez-Boulan, 1999). Recently, Westenskow et al. (2012) reported that binding of POS reaches its maximum rates at 2 h, and internalization started within 30 minutes of challenging the cells, showing its maximum rates at 3 h after initiated challenging with POS.

Binding of shed POS to RPE cells is mediated by the integrin adhesion $\alpha\beta5$ receptor. Finnemann et al. (1997) demonstrated that blocking the $\alpha\beta5$ receptor using a neutralizing antibody efficiently decreased binding of POS, although no effect was observed on the POS already bound to the RPE. Thus, $\alpha\beta5$ integrin receptor has a

primary role in initiating and controlling the rhythm of POS phagocytosis *in vivo* (Nandrot et al., 2004).

Internalization of shed POS is the next step of the phagocytic process by the RPE cells. The scavenger receptor CD36 and the Mer tyrosine kinase (MerTK) are the main mediators of the POS engulfment by the RPE (Finnemann and Silverstein, 2001). Finnemann and Silverstein (2001) demonstrated that CD36 ligation is necessary for activating POS internalization. Blocking CD36 ligation using specific antibodies had no effect on POS binding, but affected the internalization rate, for both POS binding to the $\alpha\beta5$ integrin receptor and for POS already bound to the RPE. They demonstrated that CD36 works as a signaling molecule in the postbinding steps of RPE phagocytosis.

MerTK also has an important role in the process of POS engulfment. Redistribution of MerTK to the sites of internalized POS, and increased tyrosine phosphorylation of MerTK were demonstrated by challenging the RPE cells with POS (Feng et al., 2002; Finnemann, 2003). After binding to the $\alpha\beta5$ integrin receptor, focal adhesion kinase (FAK) is activated through Tyr861 phosphorylation. Activated FAK then migrates and binds to the cytoplasmic face of $\alpha\beta5$ integrin receptor, forming the complex FAK- $\alpha\beta5$ integrin, which stimulates the phosphorylation of FAK Tyr397 and Tyr576. The simultaneous formation of FAK- $\alpha\beta5$ integrin complex and the increase in FAK activity during POS binding strongly suggests that FAK activation in RPE phagocytosis requires its association with $\alpha\beta5$ integrin (Finnemann and Silverstein, 2001). Furthermore, Finnemann (2003) described increased levels of FAK in $\alpha\beta5$ integrin protein complexes during the early POS binding phase, but loss of FAK from the integrin complex during the later POS internalization phase. These results suggest that RPE cells activate FAK recruited to its apical $\alpha\beta5$ integrin receptors in response to POS phagocytic

challenge (Finnemann and Nandrot, 2006). Analysis of RPE defective in either FAK or MerTK function demonstrates that FAK signaling upon POS binding is independent of and required for MerTK tyrosine phosphorylation. FAK provides a critical molecular link between particle binding and particle engulfment via MerTK in phagocytosis by RPE cells. Thus, FAK acts upstream of MerTK to stimulate the internalization machinery of the RPE (Finnemann and Nandrot, 2006).

2.3 Aging and Metabolism of the RPE Cells

ROS generation is strongly associated with increased oxidative stress and cell death. Irreversible damage decreases cellular degradation systems, especially lysosomes (Kurz et al., 2008).

Lipofuscin accumulation compromises the autophagic degradative capacity, impairing the turnover of damaged organelles and waste material digestion. Delayed degradation of mitochondrial material results in increased damage by self-produced ROS, additionally contributing to further lipofuscinogenesis. At the same time, accumulation of extralysosomal material originates as indigestible protein aggregates (Kurz et al., 2008). Progressive accumulation of nondegraded waste material underlies the development of age-related diseases. Lipofuscin accumulation in the RPE cells is associated with the pathogenesis of AMD, preventing the phagocytosis of POS and leading to loss of RPE cells and photoreceptors death.

2.3.1 Impaired Lysosomal Function in the RPE

Lysosomal clearance can be disturbed by assorted mechanisms during RPE cell degeneration and development of AMD (Kaarniranta et al., 2013). Lysosomes have the ability to interact with different cleaning processes to proceed to protein degradation. The cathepsins are proteases with the biological task of protein digestion. More specifically, the main responsibility of cathepsins in RPE cells is the degradation of POS and rhodopsin into glycopeptides within the lysosomes. Cathepsin-deficient mice have been shown to develop retinal degeneration (Koike et al., 2003).

Oxidized low-density lipoproteins and lipid peroxidation end products reduce the degradation of phagocytized POS, contributing to greater cellular stress in the RPE cells (Kaarniranta et al., 2013). Intracellular storage of these metabolites represents the initial stage of lipofuscinogenesis. Lipofuscin toxic components have both photosensitizer and autooxidant properties, increasing mitochondrial stress and irreversibly inhibiting lysosomal cathepsin activity, which leads to further RPE damage (Kaarniranta et al., 2013). Once lipofuscin is formed and accumulated in the lysosomes it cannot be degraded by the proteasomal or lysosome enzymes, nor transported to the extracellular space via exocytosis (Kaarniranta et al., 2013). Both POS clearance and lysosome enzyme activity seem to be related to lysosomal pH. It is a fact that lysosomal activity depends on acidic pH. Elevated lysosomal pH was observed both in the RPE cells of a mouse model of retinal degeneration and in cultured human RPE cells exposed to lipofuscin components (Kaarniranta et al., 2013).

2.3.2 Oxidative Stress and Mitochondrial Dysfunction in the RPE Cells

The central retina is constantly exposed to a high load of oxidative stress, which increases during the aging process (Winkler et al., 1999). Different studies have already demonstrated the role of oxidative stress in the pathogenesis of AMD, since the retina and the RPE cells provide an ideal environment for the generation of ROS (Kaarniranta et al., 2013). Oxidative stress originates mainly from retinal irradiation, lipid peroxidation, photochemical damage of the chromophores, and the respiratory burst. As a consequence, these oxidative processes contribute to the clinical manifestations of pigment dispersion, accumulation of intracellular lysosomal lipofuscin, and extracellular drusen deposits. Thus, nondegradable lipofuscin is formed by the polymerization of oxidative products and accumulates inside the lysosomes. Lipofuscin itself can be cytotoxic because of its ability to provide a redox-free surface by the incorporation of oxidative labile iron. Therefore, formation of oxygen radicals causes oxidative modification of proteins, lipids, and nucleic acids. In addition to increased storage of lipofuscin, impaired lysosomal function, continuous light exposure, and increased oxidation, defects in mitochondrial function exacerbate the stimulation of further increase in oxidative stress (Kaarniranta et al., 2013). Finally, due to the high metabolic activity, impaired mitochondrial function leads to accelerated degeneration of RPE cells and photoreceptor death (Kaarniranta et al., 2013). Since mitochondrial DNA has greater susceptibility to oxidative damage and light exposure than nuclear DNA (Kaarniranta et al., 2013), oxidative stress easily mutates mitochondrial DNA, increasing ROS generation and reducing the metabolic capacity. AMD patients present enhanced mitochondrial stress and dysfunction of RPE cells

(Kaarniranta et al., 2013). Thus, removal of damaged mitochondria through autophagy is essential for cell survival.

2.3.3 Impaired Autophagosomal Activity in the RPE Cells and AMD

Declining autophagic capacity along with increased accumulation of lipofuscin accelerates ROS production and stimulates the expression of protein aggregation. Consequently, activation of the inflammatory response further provokes long-term, low-grade retinal inflammation, which accelerates the aging process (Salminen et al., 2012).

Lysosomal destabilization, mitochondrial dysfunction and oxidative stress can successfully activate inflammasomes (Salminen et al., 2012). Under normal conditions, the autophagy process is able to control the activation of inflammasomes. However, when autophagy declines, inflammasomes become strongly activated owing to the dysregulation of mitochondrial homeostasis (Nakahira et al., 2011).

2.4 Choroidal Neovascularization

Choroidal neovascularization is the hallmark of wet AMD. Angiogenesis of abnormally formed new vessels predisposes to leaking and hemorrhage (Bora et al., 2014).

Physiologic proliferation of choroidal and retinal blood vessels respects a fine balance between antiangiogenic and proangiogenic factors. However, when this balance is disrupted, levels of proangiogenic molecules increase, while expression of antiangiogenic

factors decreases. Consequently, choroidal and retinal endothelial cells become activated and start to proliferate, originating new blood vessels (Bora et al., 2014).

Blockade of VEGF-A, the most important proangiogenic messenger, is the basis of the therapy for neovascular AMD (Schmidt-Erfurth et al., 2014).

2.4.1 Animal Model of CNV

The importance of VEGF in the pathogenesis of human AMD has been widely established. Furthermore, VEGF is also involved in the pathogenesis of an animal model of laser-induced CNV (Lambert et al., 2013; Rosenfeld et al., 2006).

Laser-induced CNV is widely accepted and considered the most frequently used experimental model of CNV in mice. It is characterized by the rupture of the Bruch membrane by laser photocoagulation, which leads to growth of new blood vessels from the choroid into the subretinal space, successfully mimicking the main features of the neovascular form of AMD (Lambert et al., 2013). The use of laser-induced CNV has consolidated angiogenesis as an important target for AMD treatment. The animal model of CNV along with transgenic mouse technologies have allowed the exploration of key regulators of pathologic angiogenesis, leading to the identification of different molecules as mediators of CNV development (Lambert et al., 2013).

2.4.2 Oxidative Stress and CNV

Oxidative stress has been implicated in the development of AMD. According to the AREDS study, supplementation with antioxidant vitamins was demonstrated to

suppress the development of neovascular AMD (Chew et al., 2013). Moreover, studies using animal models of CNV have also implicated oxidative stress in the pathogenesis of the disease (Dong et al., 2009; Ebrahim et al., 2006; Hara et al., 2010; Imamura et al., 2006). Antioxidant enzymes represent the key endogenous defense system against oxidative stress, and its implication in neovascular AMD has been demonstrated in studies on superoxide dismutase 1 deficient mice (Dong et al., 2009; Imamura et al., 2006).

Imamura et al. (2006) investigated the age-related changes of the choroid and retina of mice lacking SOD1. They showed that the lack of SOD1 leads to the development of age-related changes in many of the features of human AMD. Drusen, thickened Bruch membrane, CNV, and dysfunction of the RPE were identified, suggesting a major role for the antioxidant molecules as a defense system against AMD. Dong et al. (2009) reported that oxidative stress enhances several types of ocular neovascularization. They showed that mice lacking SOD1 present a proangiogenic environment in the choroid and retina and that treatment with antioxidants was associated with decreased ischemia-induced retinal neovascularization, reduced VEGF-induced subretinal neovascularization, and decreased choroidal neovascularization. Thus, while oxidative stress may directly create a proangiogenic environment for the development of retinal and subretinal neovascularization, generation of ROS may stimulate CNV by fostering a proangiogenic environment in the RPE-choroid and at the same time contribute to a progressive compromise of the Bruch's membrane (Dong et al., 2009). N-acetyl-cysteine (NAC), an antioxidant known as a precursor of glutathione, inhibited the expression of both VEGF and VEGF receptor-1 and suppressed the CNV formation in animal mouse model of CNV (Hara et al., 2010).

3. Research Purposes

The purposes of this study were as follows:

1. To explore the mechanism responsible for the induction of PGC-1 α by POS phagocytosis in the RPE cells;
2. To evaluate the involvement of PGC-1 α and POS phagocytosis in the regulation of senescence and POS metabolism by the RPE cells;
3. To evaluate the role of the antioxidant enzyme GPx4 in the development of laser-induced CNV;
4. To analyze the effect of the antioxidant enzyme GPx4 in the expression of VEGF in laser-induced CNV.

4. Senescence and Lysosomal Activity of Retinal Pigment Epithelium Regulated by Binding of Photoreceptor Outer Segments through $\alpha\beta 5$ Integrin/FAK/PGC-1 α

4.1 Introduction

AMD is a leading cause of legal blindness worldwide, and its pathogenesis lies in age-related abnormalities in the RPE as well as in its closely related tissues including the Bruch's membrane and the choriocapillaris (de Jong, 2006; Jager et al., 2008). Physiologically, the RPE cells coordinate with photoreceptors for the homeostasis of phototransduction, where absorption of light, nutritional trafficking, and degradation of photoreceptor outer segments (POS) are some of the essential roles of the RPE cells. POS comprise stacks of phospholipid bilayer membranes, and tips of POS are constantly shed by photoreceptors and phagocytosed by the RPE cells to renew POS in photoreceptors. Shed POS need to be efficiently processed in the RPE cells through distinct steps (Finnemann, 2003; Finnemann and Silverstein, 2001; Kaarniranta et al., 2013; Kim et al., 2013). Binding or recognition of POS at the apical surface of the RPE cells is the first step and this step is mediated by $\alpha\beta 5$ integrin. The second step is internalization of POS that is mediated by CD36 and Mer tyrosine kinase (MerTK) receptors. Finally, the internalized POS are digested through the autophagy/lysosomal pathway. Autophagic capacity declines with age (Cuervo et al., 2005), and the disruption of autophagy in the RPE cells leads to the accumulation of improperly degraded lipid byproducts called lipofuscin,

which are phenotypes of senescent RPE cells (Kaarniranta et al., 2013; Valapala et al., 2014).

While the pathogenic effects of impaired POS degradation in the RPE cells have become more recognized, there is a line of evidence suggesting beneficial effects of POS for the RPE cells. For example, in cultured RPE cells, POS treatment confers protection against oxidative stress-induced apoptosis (Mukherjee et al., 2007). In mice lacking $\beta 5$ integrin where physiologic POS phagocytosis was disturbed, lipofuscin accumulated in the RPE (Nandrot et al., 2004). Excessive POS phagocytosis has been described to upregulate the expression of peroxisome proliferator-activated receptor gamma coactivator 1-alpha (PGC-1 α) in undifferentiated ARPE-19 cells, which was responsible for increasing VEGF in the RPE cells under intensive light of physiological range (Ueta et al., 2012b). While PGC-1 α works as an important coactivator of estrogen-related receptor alpha ERR α to induce VEGF transcription (Arany et al., 2008; Ueta et al., 2012b), it is a well-known master regulator of metabolism (Liu et al., 2007) and is associated with senescence (Wenz et al., 2009).

These data from the previous literature look contradictory in terms of the effect of POS for the RPE cells, yet they also imply that an unidentified mechanism activated by POS may exist, preventing senescence and facilitating the autophagy/lysosomal pathway in the RPE cells. To date, the mechanisms regulating senescence and metabolism in the RPE cells have remained largely unclear despite their critical importance. The current study aimed to explore the mechanism underlying the induction of PGC-1 α by POS and its involvement in the regulation of senescence and POS metabolism.

4.2 Methods

4.2.1 Animals

All procedures were performed in accordance with the Association for Research in Vision and Ophthalmology Statement for the Use of Animals in Ophthalmic and Vision Research (Association for Research in Vision and Ophthalmology, 1994) and were approved by the Institutional Animal Research Committee of the University of Tokyo. Mice were housed in a temperature-controlled room with access to fresh water and fed a rodent-specific diet. Mice were kept under a 12-h light/dark cycle. PGC-1 α KO mice were purchased from Jackson Laboratory. For the *ex vivo* culture experiment, RPE/choroid flat-mounts from C57BL/6 mice were used and the RPE cells were isolated after dispase treatment.

4.2.2 Experimental protocol

Firstly, the upregulation of PGC-1 α by POS was confirmed in the RPE cells using different culture conditions. Next, the mechanism of the POS-induced upregulation of PGC-1 α was explored in undifferentiated ARPE-19 cells using siRNAs, blocking antibodies, and specific inhibitors. Then, the protective effect conferred by the activation of α v β 5 integrin/FAK/PGC-1 α pathway by POS binding was investigated from the viewpoints of oxidative stress, mitochondrial biogenesis, senescence-associated β -galactosidase activity, and lysosomal activity. Finally, the phenotype of the RPE in PGC-1 α -deficient mice was evaluated.

4.2.3 POS treatment on ARPE-19 cells

ARPE-19 is a human RPE cell line derived from the RPE cells of a human donor. These cells exhibit characteristic features of the original RPE, such as the expression of RPE-specific markers and functional phagocytosis of POS (Dunn et al., 1996). In addition, ARPE-19 cells can be differentiated to have similar polarity and morphology as the RPE cells present *in vivo* (Dunn et al., 1998). Several studies have demonstrated that ARPE-19 cells in various culture conditions use the $\alpha\beta5$ integrin/FAK mechanism to recognize POS, which is the same mechanism used by the RPE cells *in vivo* (Chowers et al., 2004; Finnemann et al., 1997; Mazzoni et al., 2014; Olchawa et al., 2013; Qin and Rodrigues, 2012). Therefore, ARPE-19 cells are commonly used to investigate the physiologic and pathologic mechanisms of the RPE cells. In this study undifferentiated ARPE-19 cells were used in all the *in vitro* experiments except the initial experiment in which the upregulation of PGC-1 α by POS was confirmed similarly in undifferentiated/differentiated ARPE-19 cells and *ex vivo* RPE cells.

POS were isolated from normal porcine eyes under dim red light, as described previously (Ueta et al., 2012b). Freshly prepared POS were used in every experiment and not preserved for use in further experiments. Differentiated or undifferentiated ARPE-19 cells were treated with POS at a concentration of 10 POS/cell for 3–6 h depending on the type of assay. The cells were incubated in Dulbecco's modified Eagle's Medium (DMEM; Nissui Pharmaceutical) supplemented with 10% fetal bovine serum (FBS) and antibiotics (50 $\mu\text{g}/\text{mL}$ streptomycin and 50 U/mL penicillin) at 37°C in an atmosphere of 5% CO₂. To induce differentiation, the ARPE-19 cells were cultured in laminin-coated transwells

for 3 weeks in a medium supplemented with 1% FBS (Kannan et al., 2006; Sonoda et al., 2009) and antibiotics.

4.2.4 Antibodies and reagents

The following antibodies were used in this study: ZO-1 (1:100) (sc-10804, Santa Cruz), prohibitin (1:100) (sc-28259, Santa Cruz), TFEB (1:100) (sc-11004, Santa Cruz), CD36 (2 µg/ml) (ab23680, Abcam), MerTK (3.44 µg/ml) (ab52968, Abcam), PGC-1 α antibody (1 µg/ml) (ST1202, Calbiochem), β 5 Integrin (1:200) (sc-14010, Santa Cruz), CD36 (1:200) (sc-9154, Santa Cruz), MerTK (1:2000) (ab52968, Abcam), Atg5 (Apg5) (1:200) (sc-8667, Santa Cruz), β -actin (1:2000) (A5316, Sigma-Aldrich). ARPE-19 cells were pretreated with anti-CD36 and anti-MerTK antibodies for 1 h before POS treatment. 0.6 µm Latex beads (10/cell) (LB6) and Arg-Gly-Asp (RGD) peptide (0.5 mM) (A8052) were from Sigma-Aldrich. ARPE-19 cells were pretreated with RGD peptide for 30 min before POS treatment. FAK inhibitor 14 (500 µM) (sc-203950) was from Santa Cruz Biotechnology. STO-609 (10 µg/ml) (S1318) was from Sigma-Aldrich. AICAR (0.1 and 1.0 µM) (2627-69-2) was from Wako. ARPE-19 cells were pretreated with FAK inhibitor 14 for 30 min before POS treatment. Biotinylated Ulex europaeus agglutinin-I (UEA-I, 1:50) and Avidin Texas red (1:100) were from Vector Laboratories. Cathepsin D activity assay kit (ab65302) was from Abcam. Oil red O solution (O1391) was from Sigma-Aldrich.

4.2.5 Quantification of mRNA and mitochondrial DNA by real-time PCR

RNA was extracted from homogenized samples of ARPE-19 cells or isolated mouse RPE cells using Trizol reagent (Invitrogen). cDNA was prepared using Superscript III for RT-PCR (Invitrogen). Real-time PCR was performed using the Thermal Cycler Dice Real Time System (Takara Bio, Inc., Shiga, Japan). Values for each gene were normalized to expression levels of glyceraldehyde 3-phosphate dehydrogenase (GAPDH). The primer sequences used in this study were confirmed using Primer-BLAST (<http://www.ncbi.nlm.nih.gov/tools/primer-blast/>) (Table 1).

Relative amounts of nuclear and mitochondrial DNA were determined by comparisons with GAPDH and cytochrome b, respectively, and the ratio of mitochondrial DNA to nuclear DNA was used to reflect mitochondrial DNA replication. DNA was isolated from the ARPE-19 cells using the Wizard® SV Genomic DNA Purification System (Promega). The following primer sequences were used for real-time PCR of DNA samples: cytochrome b (Fwd: 5'-TATTCCTTCATGTCGGACGA-3' and Rev: 5'-AAATGCTGTGGCTATGACTG-3') and GAPDH (Fwd: 5'-CAAGGTCATCCATGACA ACTTTG-3' and Rev: 5'-ACCACAGTCCATGCCATCACTGCCA-3').

Table 4.1. Primer sequences used for real time RT-PCR in the study

Genes	Sequences
Mouse GAPDH	Forward: CACATTGGGGTAGGAACAC Reverse: AACTTTGGCATTGTGGAAGG
Mouse PGC-1α	Forward: AATGCAGCGGTCTTAGCACT Reverse: GTGTGAGGAGGGTCATCGTT
Human GAPDH	Forward: TTGATTTTGGAGGGATCTCG Reverse: GAGTCAACGGATTTGGTCGT
Human PGC-1α	Forward: GTGAAGACCAGCCTCTTTGC Reverse: TCACTGCACCACTTGAGTCC
Human GPx1	Forward: CTCTTCGAGAAGTGCGAGGT Reverse: TCGATGTCAATGGTCTGGAA
Human GPx4	Forward: GCACATGGTTAACCTGGACA Reverse: CTGCTTCCCGAACTGGTTAC
Human SOD1	Forward: TGGCCGATGTGTCTATTGAA Reverse: GGGCCTCAGACTACATCCAA
Human SOD2	Forward: TCCACTGCAAGGAACAACAG Reverse: TCTTGCTGGGATCATTAGGG
Human catalase	Forward: GCCTGGGACCCAATTATCTT Reverse: GAATCTCCGCACTTCTCCAG
Human HEXA	Forward: GTCATTGAATACGCACGGCT Reverse: GACTGGGATTCACCTGGTCCA
Human TPPI	Forward: GATGTGGCTGCACTTTCTGA Reverse: AGCCACGGGTACATCAAAG
Human GLA	Forward: CATCAGCCCTCAAGCCAAAG Reverse: ACCAATCTCCTGCCGGTTTA
Human CTSF	Forward: GCCTGTCCGTCTTTGTCAAT Reverse: TTGTTGCCAGGCTCTTTCTT
Human β5 Integrin	Forward: CTGGAACAACGGTGGAGATT Reverse: TACCCCATCTTGGCAGGTAG
Human CD36	Forward: AGATGCAGCCTCATTCCAC Reverse: GCCTTGGATGGAAGAACAAA
Human MerTK	Forward: ACTTCAGCCACCCAAATGTC Reverse: GGGCAATATCCACCATGAAC
Human Atg5	Forward: TGGGATTGCAAAATGACAGA Reverse: TTCCCATCTTCAGGATCAA

4.2.6 Western blot analysis

Total protein extracts from the ARPE-19 samples were separated by sodium dodecyl sulfate polyacrylamide gel electrophoresis and transferred to nitrocellulose membranes, which were then blocked with 5% nonfat dry milk in phosphate-buffered saline plus 0.1% Tween-20 (PBS-T buffer). Samples were incubated with primary antibodies overnight at 4°C in PBS-T buffer. After washing, the membranes were incubated with horseradish peroxidase-labeled anti-mouse/rabbit/goat secondary antibody (Amersham Biosciences, Chalfont St. Giles, UK) for 1 h. After washing, the membranes were developed with ECL Plus Western Blotting Detection Reagents (GE Healthcare). The levels of proteins of interest were calculated by normalization to the level of β -actin.

4.2.7 Knockdown experiment

siRNAs designed to specifically knockdown PGC-1 α (sc-38884), β 5 integrin (sc-35680), CD36 (sc-29995), MerTK (sc-37127), or Atg5 (sc-41445) (Santa Cruz) were transfected to the ARPE-19 cells using Lipofectamine® RNAiMAX Reagent (Life Technologies) according to the manufacturer's instructions. These siRNAs consisted of three or more different sequences to minimize off-target effects. The following experiments were conducted after 48 h of siRNA transfection. Transfection of negative control scramble siRNA (sc-37007, Santa Cruz) was used for comparison.

4.2.8 Intracellular ROS levels

ROS levels in the ARPE-19 cells were determined after 3 h of POS treatment using the fluorescent dye 2,7-dichlorodihydrofluorescein diacetate (H2DCFDA) (C6827, Molecular Probes) according to the manufacturer's instructions. Wells without dye were measured and subtracted from all readings.

4.2.9 Mitochondrial activity assay

Mitochondrial complex I is the first enzyme in the mitochondrial respiratory chain. It creates a potential difference across the inner membrane, which is used for the ATP synthesis. NADH oxidation to NAD⁺ by the mitochondrial complex I in the ARPE-19 cells was analyzed after 3 h of POS treatment using the Mitochondrial Complex I Activity Assay Kit (AAMT001, EMD Millipore).

4.2.10 Cell senescence assay

ARPE-19 cells were incubated with or without POS for 3 h and then treated with 100 μ M H₂O₂ for 2 h to induce senescence (Yu et al., 2009). After 24 h, the cells were fixed and stained with β -galactosidase using the SA- β -Gal Kit (K320-250, BioVision) according to the manufacturer's instructions. The proportions of stained cells from three microscopic views for each well were averaged, and three wells were used for each treatment group.

4.2.11 BODIPY C11 assay

ARPE-19 cells were treated with or without POS for 6 h and then incubated in the medium alone for 22 hours. After washing, the cells were incubated with 10 μ M BODIPY C11 fluorescence dye (D3861, Molecular Probes) for 30 min at 37°C and then rinsed. The plate was read at an excitation wavelength of 485 nm and an emission wavelength of 535 nm. Bodipy C11 is a fluorescent fatty acid analog that resides in the organelle membranes, changing its fluorescence when oxidized. It is considered a reliable reporter of lipid oxidation.

4.2.12 Transmission electron microscopy (TEM)

Mouse eyes were processed for histology, and 70-nm-thick transverse sections were cut through the central retina and mounted onto grids. The sections were stained with lead citrate and uranyl acetate. Images were obtained by TEM (80 kV, model JEM-1200EX; JEOL Ltd., Tokyo, Japan) using a charge-coupled device digital camera (model VELETA; JEOL Ltd.).

4.2.13 Statistics

All statistical analyses were performed using JMP11 software (SAS Institute). Two-tailed student's t-test was used for comparisons between unpaired groups. One-way analysis of variance (ANOVA) followed by the post hoc Tukey's test was used for

comparisons among three or more groups. Probability (*P*) value < 0.05 was regarded as statistically significant.

4.3 Results

4.3.1 Binding of POS upregulates PGC-1 α through α v β 5 integrin and FAK

First the effect of POS treatment on PGC-1 α expression by cultured RPE cells under several conditions was evaluated. In the present study, undifferentiated ARPE-19 cells were used to evaluate PGC-1 α -related signaling in RPE cells. POS treatment increased PGC-1 α mRNA and protein levels in undifferentiated ARPE-19 cells (Figure 4.1A). The same effect of POS was confirmed in differentiated ARPE-19 cells (Figure 4.1B) and in *ex vivo* RPE cells in flat-mount culture (Figure 4.1C).

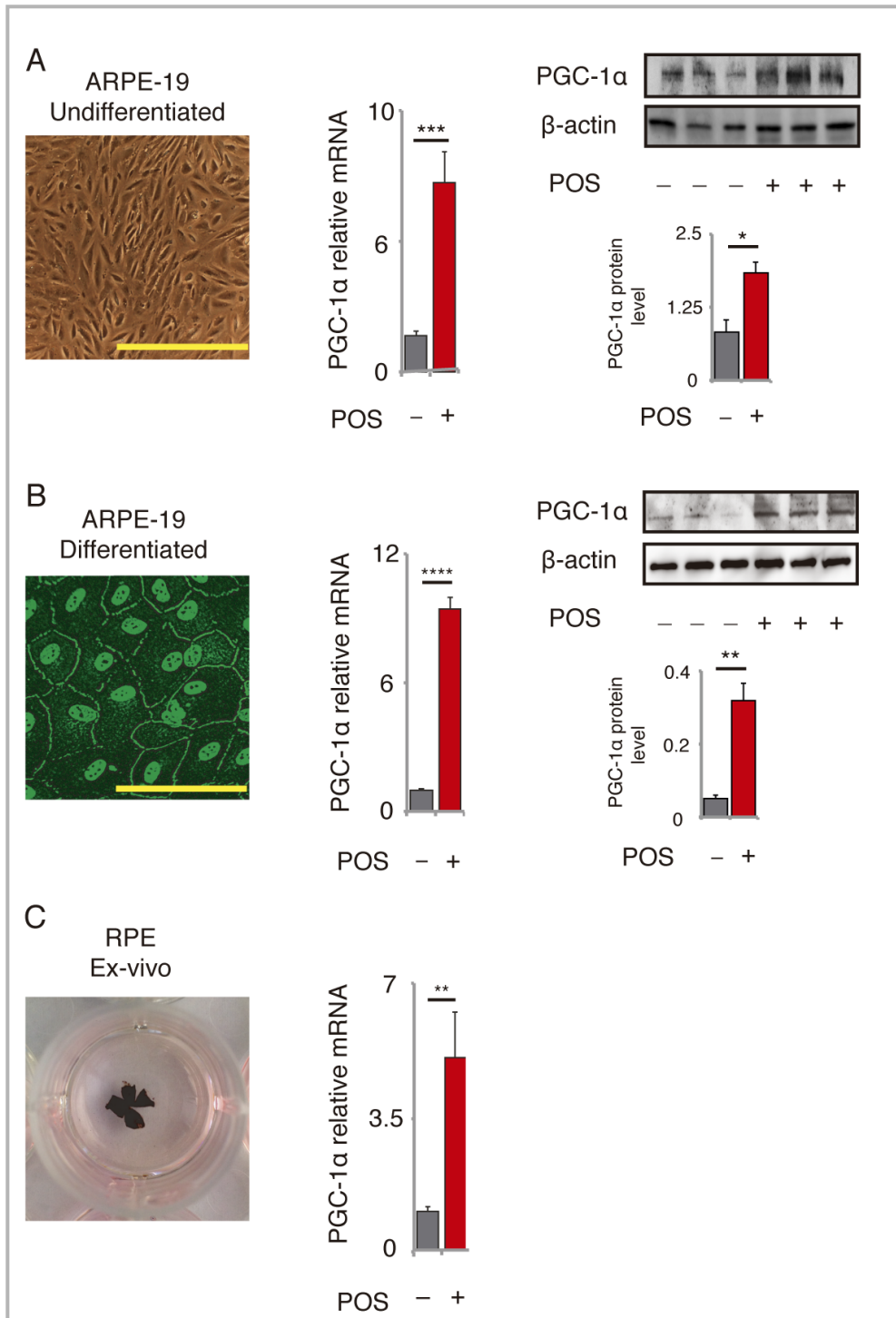


Figure 4.1. POS upregulate PGC-1 α in RPE cells. PGC-1 α mRNA and protein levels were upregulated in: (A) Undifferentiated ARPE-19 cells. (B) Differentiated ARPE-19 cells. (C) *Ex vivo* RPE cells, treated with POS for 3 h for evaluation of mRNA and for 6 h for evaluation of protein level. Morphology of differentiated ARPE-19 cells was confirmed by immunofluorescence for ZO-1 antibody. Mean \pm SEM, $n = 6-10$ per group for mRNA level, $n = 3$ per group for protein level, two-tailed Student's t -test, * $P < 0.05$, ** $P < 0.01$, *** $P < 0.001$, **** $P < 0.0001$. Scale bars in the images of undifferentiated and differentiated ARPE-19 cells represent 100 μm and 200 μm , respectively.

The upregulation of PGC-1 α was dose-dependent of the number of POS (Figure 4.2).

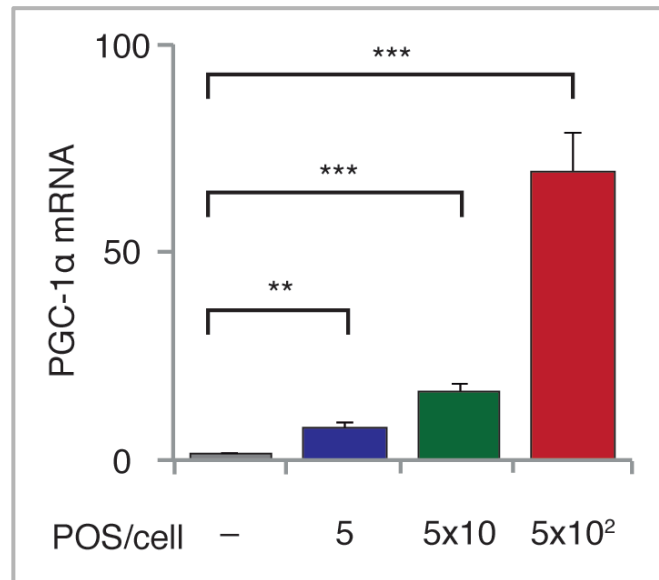


Figure 4.2. Upregulation of PGC1- α mRNA was dose-dependent on the number of POS in undifferentiated ARPE-19 cells. Mean \pm SEM, n = 6 per group, **** P < 0.0001 by ANOVA, followed by a post hoc Tukey's test ** P < 0.01, *** P < 0.001, compared with ARPE-19 cells with no treatment.

To test if the effect was specifically due to the phagocytosis of POS, treatment with latex beads, which have been used for the assessment of phagocytic activity of RPE cells, was done (Burke and Zareba, 2009; Higgins et al., 2003). In contrast to POS treatment, treatment with latex beads did not increase PGC-1 α mRNA levels (Figure 4.3A), suggesting a specific role of POS phagocytosis in the upregulation of PGC-1 α . In addition, to rule out the possibility that other impurities in the isolated POS might influence the results, the ARPE-19 cells were pretreated for 30 minutes with Arg-Gly-Asp (RGD) peptides (0.5 mM) that inhibit POS binding (Finnemann et al., 1997). This pretreatment significantly suppressed the upregulation of PGC-1 α mRNA induced by POS supplementation (Figure 4.3B). Evaluation of the time course of PGC-1 α mRNA

upregulation after POS treatment revealed that the increase began as early as 30 minutes after POS treatment (Figure 4.3C).

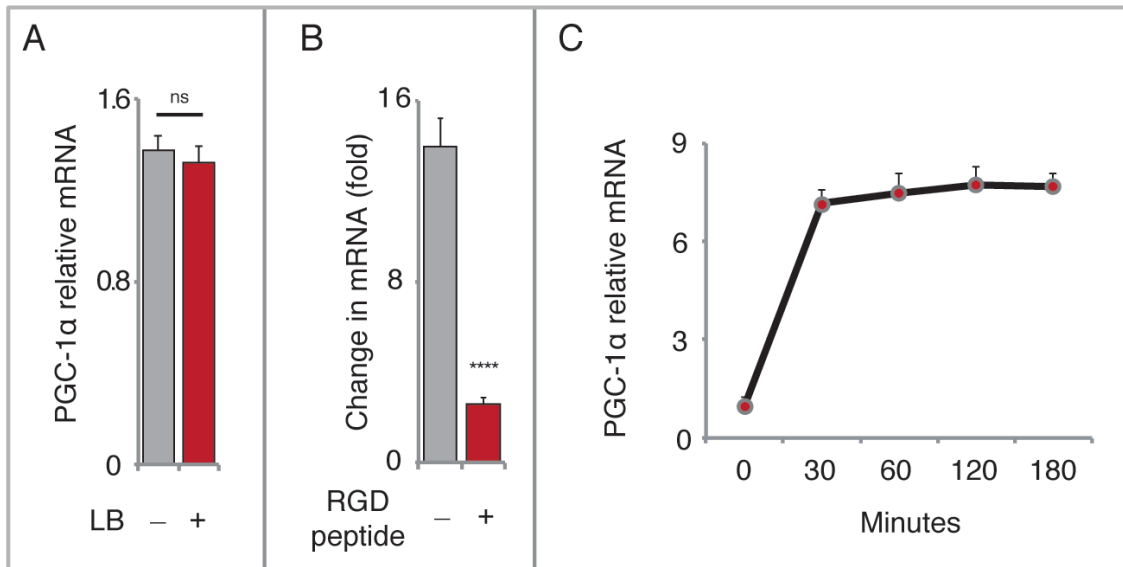


Figure 4.3. POS binding activates the $\alpha v\beta 5$ integrin/FAK/PGC-1 α pathway in undifferentiated ARPE-19 cells. (A) PGC-1 α mRNA levels were not affected in the ARPE-19 cells treated with latex beads (LB) versus the controls. Mean \pm SEM, $n = 6$ per group; two-tailed Student's t -test; ns, not significant. (B) Upregulation of PGC-1 α mRNA in response to POS was significantly suppressed in the ARPE-19 cells pretreated with RGD peptide versus the controls. Mean \pm SEM, $n = 6$ per group, two-tailed Student's t -test, **** $P < 0.0001$. (C) Time course of PGC-1 α mRNA levels in the ARPE-19 cells after treatment with POS.

A previous study reported that POS internalization by RPE-J cells occurred after 90 minutes of POS treatment (Finnemann and Silverstein, 2001), while another recent study reported that POS internalization by ARPE-19 and human fetal RPE cells occurred within 30 minutes of POS treatment (Westenskow et al., 2012). Therefore, the present study explored which stage of POS phagocytosis (i.e., binding, internalization, or digestion) was specifically related to PGC-1 α upregulation by POS treatment. After the efficacy of siRNAs for $\beta 5$ integrin, CD36, MerTK, and Atg5 was confirmed in the ARPE-

19 cells (Figure 4.4), the influence of silencing of these genes on the upregulation of PGC-1 α mRNA by POS was tested (Figure 4.5A).

In the RPE cells in which β 5 integrin expression was silenced (i.e. binding was

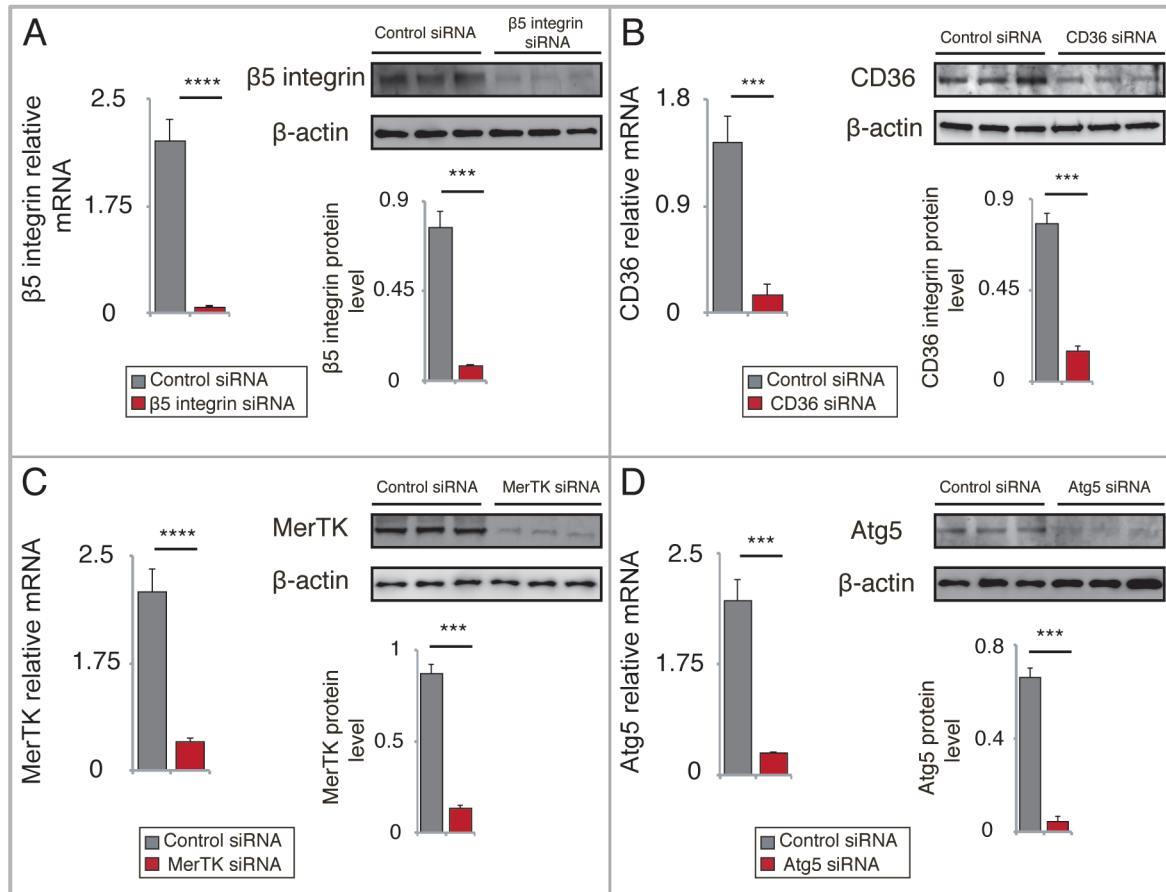


Figure 4.4. Knockdown efficacy of siRNAs for β 5 integrin, CD36, MerTK, and Atg5 was analyzed in undifferentiated ARPE-19 cells. (A) β 5 integrin mRNA levels measured by RT-PCR. Mean \pm SEM, n = 6 per group, two-tailed Student's *t*-test, **** P < 0.0001. β 5 integrin protein levels measured by western blot analysis. Mean \pm SEM, n = 3 per group, two-tailed Student's *t*-test, *** P < 0.001. (B) CD36 mRNA levels measured by RT-PCR. Mean \pm SEM, n = 6 per group, two-tailed Student's *t*-test, *** P < 0.001. CD36 protein levels measured by western blot analysis. Mean \pm SEM, n = 3 per group, two-tailed Student's *t*-test, *** P < 0.001. (C) MerTK mRNA levels measured by RT-PCR. Mean \pm SEM, n = 6 per group, two-tailed Student's *t*-test, **** P < 0.0001. MerTK protein levels measured by western blot analysis. Mean \pm SEM, n = 3 per group, two-tailed Student's *t*-test, *** P < 0.001. (D) Atg5 mRNA levels measured by RT-PCR. Mean \pm SEM, n = 6 per group, two-tailed Student's *t*-test, *** P < 0.001. Atg5 protein levels measured by western blot analysis. Mean \pm SEM, n = 3 per group, two-tailed Student's *t*-test, *** P < 0.001.

discouraged), PGC-1 α upregulation by POS was markedly suppressed. However, when CD36 or MerTK was silenced (i.e. internalization was discouraged), PGC-1 α upregulation was significantly enhanced rather than suppressed. In addition, PGC-1 α upregulation by POS was not affected by Atg5 silencing (i.e. digestion was discouraged). The effect of antibodies against CD36 and MerTK receptors at the concentrations that inhibit POS internalization was also tested. Similarly, PGC-1 α upregulation was not suppressed but was rather enhanced in the RPE cells pretreated with antibodies against CD36 (2 μ g/mL) (Figure 4.5B) or MerTK (3.44 μ g/mL) (Figure 4.5C) for 1 hour. These results are in line with those of a previous report showing that MerTK negatively controlled POS binding by limiting β 5 integrin activity (Nandrot et al., 2012). The results of the current study also suggest that CD36 has similar effects on β 5 integrin. Supposedly the POS recognition by RPE cells (i.e. POS binding) was associated with upregulated PGC-1 α expression. Thus it was hypothesized that focal adhesion kinase (FAK), a major intracellular mediator of β 5 integrin activation in RPE cells (Finnemann, 2003; Nandrot et al., 2004), was involved in this signaling. Consequently, the RPE cells were pretreated with FAK inhibitor 14 (500 μ M) for 30 minutes, followed by treatment with or without POS. The increase in PGC-1 α mRNA levels by POS treatment was significantly reduced when the RPE cells were pretreated with FAK inhibitor versus control (Figure 4.5D), suggesting that FAK is at least partly responsible for the upregulation of PGC-1 α by POS binding.

Recent studies have revealed the importance of the AMP-activated protein kinase (AMPK)-PGC-1 α pathway in the regulation of autophagy (Viscomi et al., 2011; Yang et al., 2014). The present study tested whether AMPK played a role in the upregulation of PGC-1 α by POS binding. However, pretreatment with AMPK inhibitor STO-609 (10 μ g/ml) for 10 minutes enhanced, but did not suppress, the upregulation of PGC-1 α by

POS (Figure 4.6A). Furthermore, pretreatment with AMPK-specific activator AMP-mimetic 5-aminoimidazole-4-carboxamide-1- β -D-ribofuranoside (AICAR) for 12 hours decreased, but did not increase, mRNA levels of PGC-1 α (Figure 4.6B), indicating an AMPK-independent mechanism of PGC-1 α upregulation by POS binding.

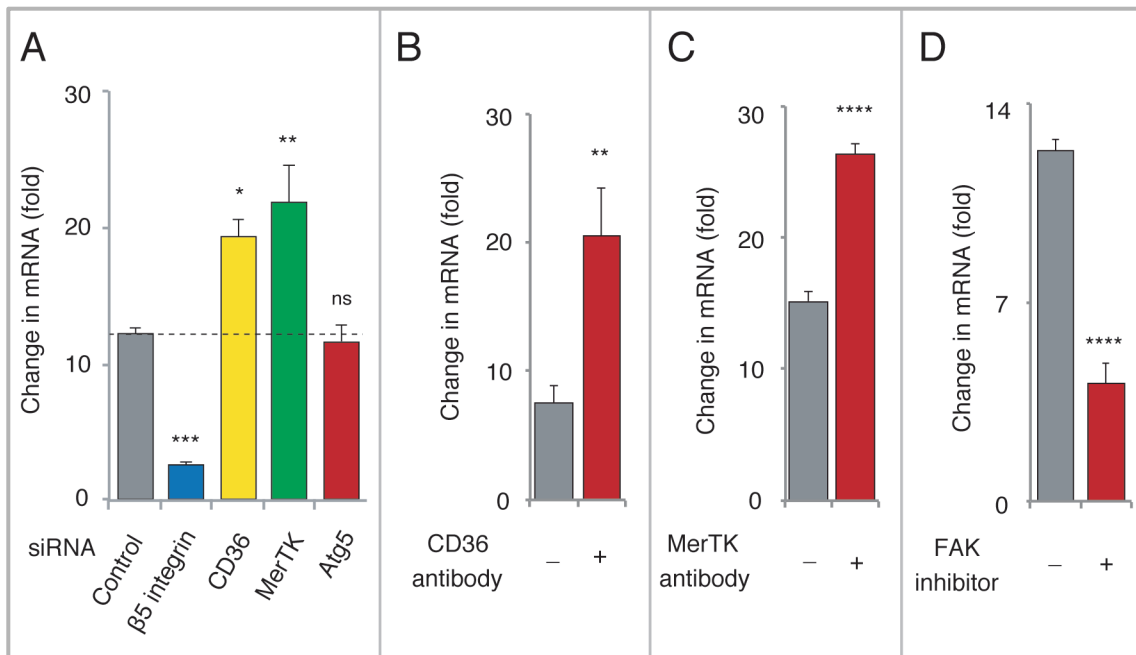


Figure 4.5. POS binding activates the α v β 5 integrin/FAK/PGC-1 α pathway in undifferentiated ARPE-19 cells. (A) Upregulation of PGC-1 α mRNA levels in response to POS was significantly suppressed in the ARPE-19 cells pretreated with siRNA against β 5 integrin, enhanced in those pretreated with siRNA against CD36 or MerTK, and not influenced in those pretreated with siRNA against Atg5. Mean \pm SEM, n = 6 per group, **** P < 0.0001 by ANOVA, followed by a post hoc Tukey's test * P < 0.05, ** P < 0.01, *** P < 0.001, ns [not significant], compared with the control group. (B) Upregulation of PGC-1 α mRNA levels in response to POS was enhanced in the ARPE-19 cells pretreated with CD36 antibody (2 μ g/mL) versus control. Mean \pm SEM, n = 6 per group, two-tailed Student's t -test, ** P < 0.01. (C) Upregulation in PGC-1 α mRNA in response to POS was enhanced in the ARPE-19 cells pretreated with MerTK antibody (3.44 μ g/mL) versus control. Mean \pm SEM, n = 6 per group, two-tailed Student's t -test, **** P < 0.0001. (D) Upregulation in PGC-1 α mRNA in response to POS was suppressed in the ARPE-19 cells pretreated with FAK inhibitor 14 (500 μ M) versus control. Mean \pm SEM, n = 6 per group, two-tailed Student's t -test, **** P < 0.0001.

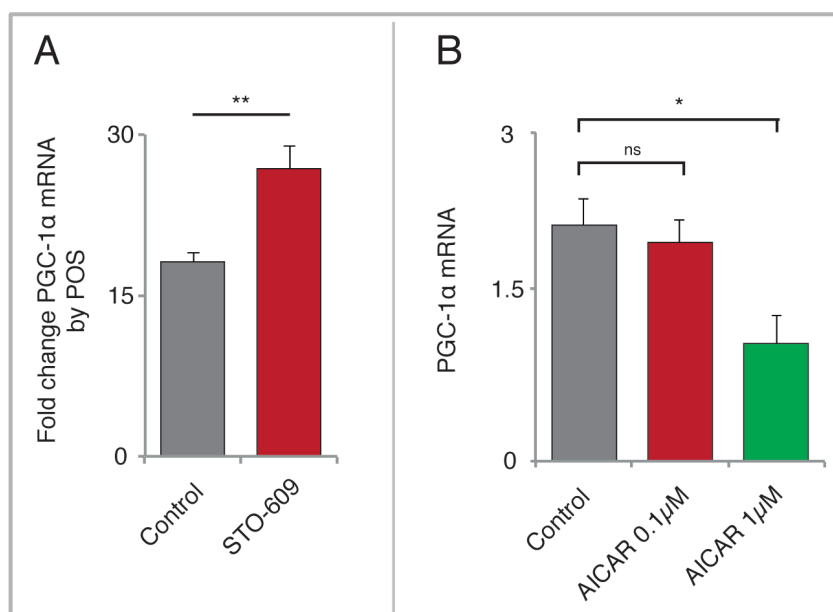


Figure 4.6. The upregulation of PGC1- α was independent of AMPK activity. (A) Pretreatment of undifferentiated ARPE-19 cells with STO-609 (10 μ g/ml) for 10 min enhanced the upregulation of PGC1- α mRNA level by POS. Mean \pm SEM, n = 6 per group, two-tailed Student's *t*-test, $**P < 0.01$. (B) Pretreatment with AICAR for 12 h decreased the PGC1- α mRNA level in the ARPE-19 cells. Mean \pm SEM, n = 6 per group, $*P < 0.05$ by ANOVA, followed by a post hoc Tukey's test $*P < 0.05$, compared with control.

4.3.2 POS exerts antisenescent effects through PGC-1 α in RPE cells

PGC-1 α is a master regulator of mitochondrial biogenesis (Lehman et al., 2002; Lin et al., 2002) and a potent suppresser of oxidative stress (St-Pierre et al., 2006). Increased PGC-1 α expression in muscle rescued age-related muscle wasting and metabolic decline in mice (Wenz et al., 2009). Therefore, it was hypothesized that POS treatment-induced PGC-1 α upregulation increases mitochondrial biogenesis and decreases ROS production, and confers overall anti-senescent effects in RPE cells. This might be important to counteract the metabolic stress by POS. Increased levels of peroxidase 1

(GPx1), GPx4, superoxide dismutase 1 (SOD1), and catalase were confirmed, but not of SOD2 (Figure 4.7A). The overall ROS levels decreased in the RPE cells treated with POS (Figure 4.7B). When PGC-1 α was silenced using small interfering RNA (siRNA), POS treatment increased rather than decreased ROS production in the RPE cells (Figure 4.7C), which indicated an important role of PGC-1 α in the decrease in ROS levels by POS. The efficacy of PGC-1 α silencing in the ARPE-19 cells was also analyzed (Figure 4.7).

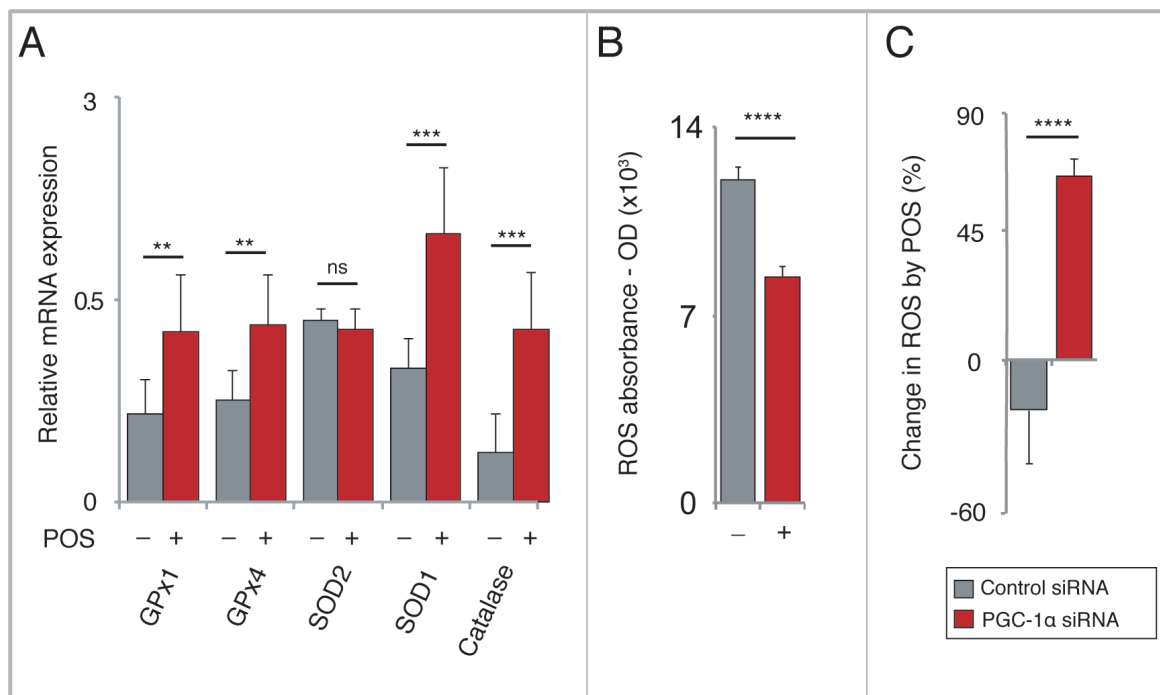


Figure 4.7. POS increased antioxidant enzymes and decreased ROS level in undifferentiated ARPE-19 cells through PGC-1 α . (A) mRNA levels of anti-oxidant enzymes including GPx1, GPx4, SOD1 and catalase, but not of SOD2, were upregulated in the ARPE-19 cells treated with POS. Mean \pm SEM, n = 6 per group, two-tailed Student's *t*-test, ** P < 0.01, *** P < 0.001; ns, not significant. (B) ROS levels in the ARPE-19 cells evaluated by H₂DCFDA were downregulated in the ARPE-19 cells treated with POS. Mean \pm SEM, n = 16 per group, two-tailed Student's *t*-test, **** P < 0.0001. (C) ROS levels were downregulated in response to POS in the ARPE-19 cells transfected with control siRNA, but upregulated in cells transfected with PGC-1 α siRNA. Mean \pm SEM, n = 9–12 per group, two-tailed Student's *t*-test, **** P < 0.0001.

The efficacy of PGC-1 α KD was analyzed in the ARPE-19 cells (Figure 4.8).

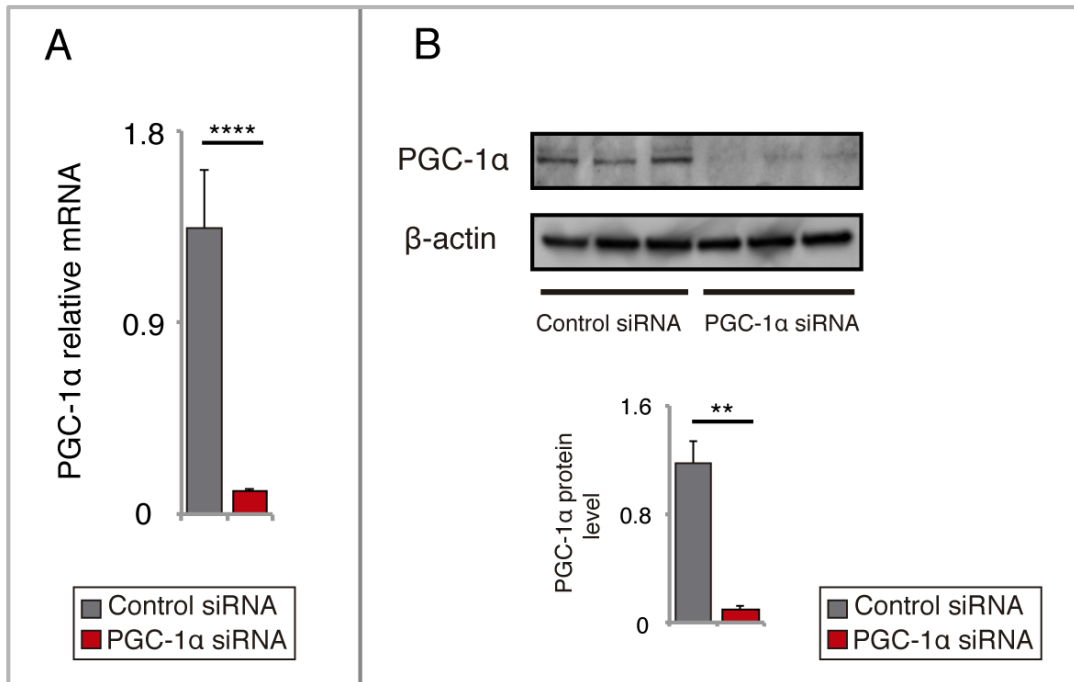


Figure 4.8. Efficacy of PGC-1 α knockdown was analyzed in undifferentiated ARPE-19 cells. (A) PGC-1 α mRNA levels measured by RT-PCR. Mean \pm SEM, n = 8 per group, two-tailed Student's *t*-test, **** P < 0.0001. (B) PGC-1 α protein levels measured by western blot analysis. Mean \pm SEM, n = 3 per group, two-tailed Student's *t*-test, ** P < 0.01).

POS treatment increased relative levels of mitochondrial DNA compared with nuclear DNA (Figure 4.9A), as well as the levels of prohibitin, a mitochondrial marker protein (Figure 4.9B), suggesting increased mitochondrial biogenesis by POS. Functionally, POS treatment upregulated mitochondrial complex I activity, which was abrogated by silencing of PGC-1 α (Figure 4.9C).

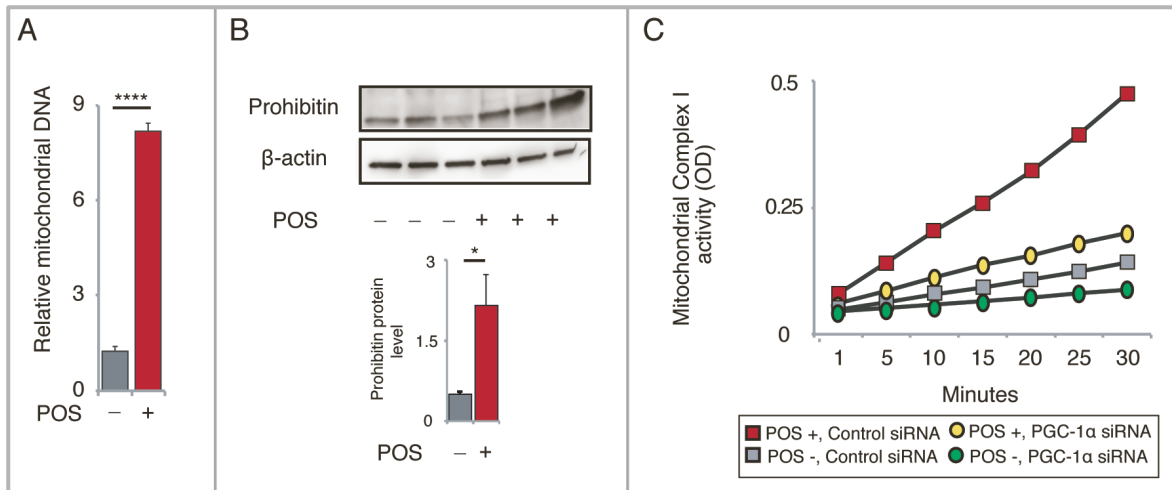


Figure 4.9. POS treatment upregulated mitochondrial biogenesis in undifferentiated ARPE-19 cells through PGC-1 α . (A) Relative mitochondrial DNA level, as determined by cytochrome b/GAPDH, were upregulated in the ARPE-19 cells treated with POS. Mean \pm SEM, $n = 6$ per group, two-tailed Student's t -test, **** $P < 0.0001$. (B) Western blot analysis showed increased protein level of the mitochondrial marker prohibitin in the ARPE-19 cells treated with POS. Mean \pm SEM, $n = 6$ per group, two-tailed Student's t -test, * $P < 0.05$. (C) In the ARPE-19 cells transfected with control siRNA, mitochondrial complex I activity was significantly upregulated in response to the POS treatment ($n = 8$ per group, **** $P = 0.0001$ by ANOVA, followed by a post hoc Tukey's test *** $P < 0.001$). However, in the ARPE-19 cells transfected with PGC-1 α siRNA, the change in mitochondrial complex I activity with POS treatment was not statistically significant.

The effect of POS on the senescence of RPE cells through senescence-associated β -galactosidase (SA- β -gal) activity was also analyzed (Figure 4.10). In the ARPE-19 cells, senescence was induced by 100 μ M H₂O₂ for 2 hours, and SA- β -gal staining was evaluated after 24 hours of incubation (Yu et al., 2009). When the cells were pretreated with POS for 3 hours, it almost completely rescued H₂O₂-induced senescence in the RPE cells transfected with control siRNA. In contrast, silencing of PGC-1 α aggravated H₂O₂-induced senescence and significantly suppressed the counteracting effect by POS (Figure 4.10).

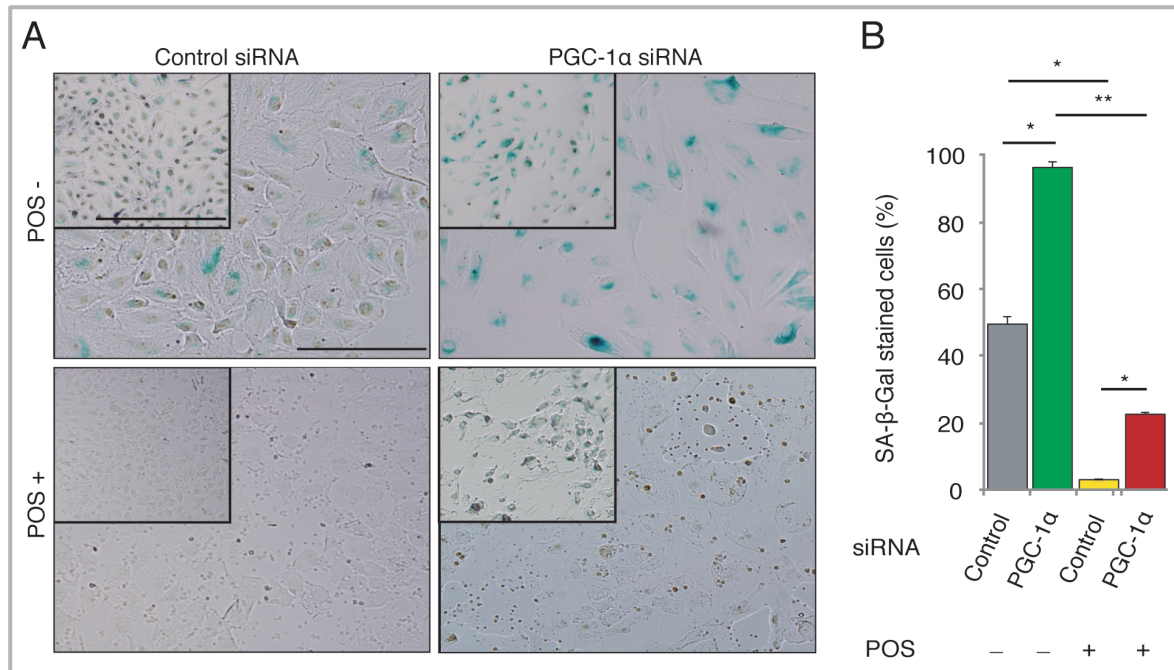


Figure 4.10. POS treatment rescues H_2O_2 -induced senescence through PGC-1 α . (A) Undifferentiated ARPE-19 cells were incubated with or without POS for 3 h and then treated with 100 μM H_2O_2 for 2 h to induce senescence. In the RPE cells pretreated with control siRNA, POS treatment almost completely suppressed SA- β -gal staining by H_2O_2 -induced senescence. In contrast, in the RPE cells transfected with PGC-1 α siRNA, H_2O_2 induced significantly stronger and more frequent SA- β -gal staining in the RPE cells, and the rescue effect by POS treatment was significantly smaller compared with the RPE cells pretreated with control siRNA. (B) Quantification of SA- β -gal staining in the ARPE-19 cells. Mean \pm SEM, $n = 3$ per group, **** $P < 0.0001$ by ANOVA, followed by a post hoc Tukey's test * $P < 0.05$, ** $P < 0.01$. The scale bars in large pictures and in insets are 100 μm and 500 μm , respectively.

4.3.3 PGC-1 α regulates lysosomal activity of POS in RPE cells

Senescence of RPE cells is associated with a decline in the lysosomal activity, and the accumulation of peroxidized lipids and lipofuscin is an important phenotype of aging RPE cells (Kaarniranta et al., 2013; Kim et al., 2013; Valapala et al., 2014). Transcription factor EB (TFEB) is a master regulator of the autophagy/lysosomal pathway (Sardiello et al., 2009; Settembre et al., 2011). TFEB and PGC-1 α can cooperatively regulate the

autophagy/lysosomal pathway and lipid catabolism in a mouse model of Huntington's disease model (Tsunemi et al., 2012) and in starvation (Settembre et al., 2013). It was hypothesized that the $\alpha\beta5$ integrin/FAK/PGC-1 α pathway might be involved in lysosomal degradation in RPE cells to adapt to the metabolic burden with POS. It was observed that when PGC-1 α was silenced, nuclear staining of RPE cells with TFEB antibody was significantly weaker when compared with that of cells transfected with control siRNA (Figure 4.11A). Accordingly, mRNA levels of TFEB target genes including galactosidase α (GLA), hexosaminidase A (HEXA), tripeptidyl peptidase I (TPPI), and cathepsin F (CTSF) were also downregulated by PGC-1 α siRNA versus control siRNA (Figure 4.11B). Similarly, mRNA levels of these TFEB target genes were also downregulated by FAK inhibitor 14 (Figure 4.11C). In addition, in the ARPE-19 cells PGC-1 α silencing significantly decreased the activity of cathepsin D, which is considered a major cathepsin for the degradation of rhodopsin and POS (Kim et al., 2013; Rakoczy et al., 1997; Valapala et al., 2014). (Fig. 4.11D).

These data suggest that the activation of the $\alpha\beta5$ integrin/FAK/PGC-1 α pathway is important for the lysosomal activity in the RPE cells. And if the pathway is not sufficiently activated, RPE cells might not be able to catabolize POS efficiently, leading to abnormal accumulation of lipids. Following this, the role of PGC-1 α in POS degradation was evaluated. Intracellular lipid accumulation was compared in cells transfected with PGC-1 α siRNA with those transfected with control siRNA before and after POS treatment by oil red O staining. Oil red O staining was always more intense in the ARPE-19 cells whose PGC-1 α was silenced when compared with the controls before and after 6 and 12 hours of POS treatment. (Figure 4.12A). Furthermore, the accumulation of peroxidized lipid after POS treatment was analyzed using boron dipyrromethene (BODIPY) C11 dye

(Figure 4.12B), which disclosed that PGC-1 α silencing approximately doubled the accumulation of peroxidized lipids in the RPE cells after POS treatment.

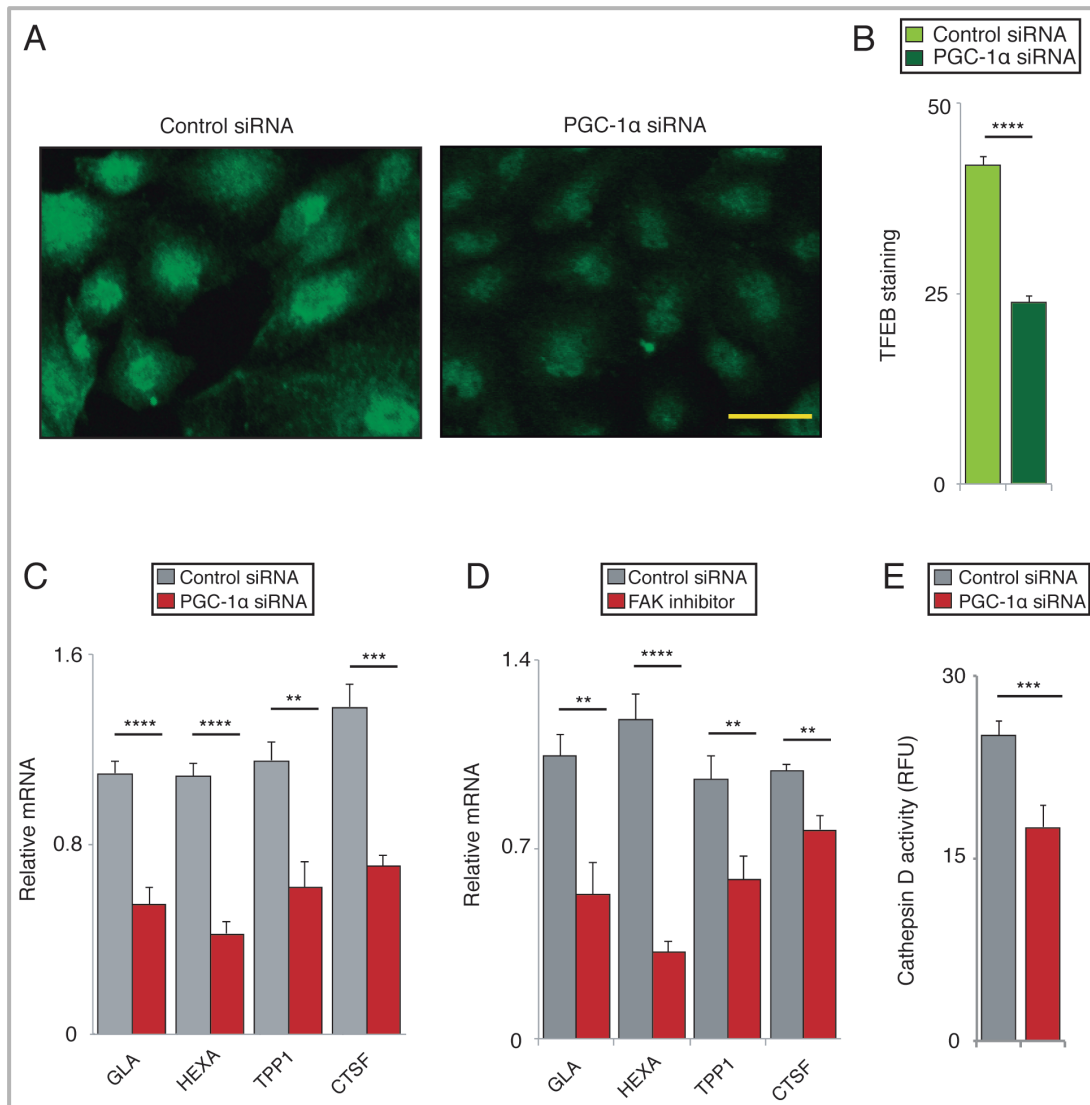


Figure 4.11. PGC-1 α regulates lysosomal activity in undifferentiated ARPE-19 cells. (A) Nuclear immunofluorescence with TFEb antibody was weaker in the ARPE-19 cells transfected with PGC-1 α siRNA compared with those with control siRNA. (B) Quantification of nuclear immunofluorescence with TFEb antibody. Mean \pm SEM, $n = 6$ per group, two-tailed Student's t -test, **** $P < 0.0001$; scale bar, 50 μ m. (C) In the ARPE-19 cells transfected with PGC-1 α siRNA, mRNA levels of TFEB target genes including GLA, HEXA, TPP1, and CTSF were downregulated when compared with those with control siRNA. Mean \pm SEM, $n = 6$ per group, two-tailed Student's t -test, ** $P < 0.01$, *** $P < 0.001$, **** $P < 0.0001$. (D) In the ARPE-19 cells pretreated with FAK inhibitor 14, mRNA levels of TFEB target genes including GLA, HEXA, TPP1, and CTSF were downregulated when compared with those with control pretreatment. Mean \pm SEM, $n = 6$ per group, two-tailed Student's t -test, ** $P < 0.01$, **** $P < 0.0001$. (E) In the ARPE-19 cells transfected with PGC-1 α siRNA, cathepsin D activity was significantly downregulated compared with those with control siRNA. Mean \pm SEM, $n = 11$ – 12 per group, two-tailed Student's t -test, *** $P < 0.001$.

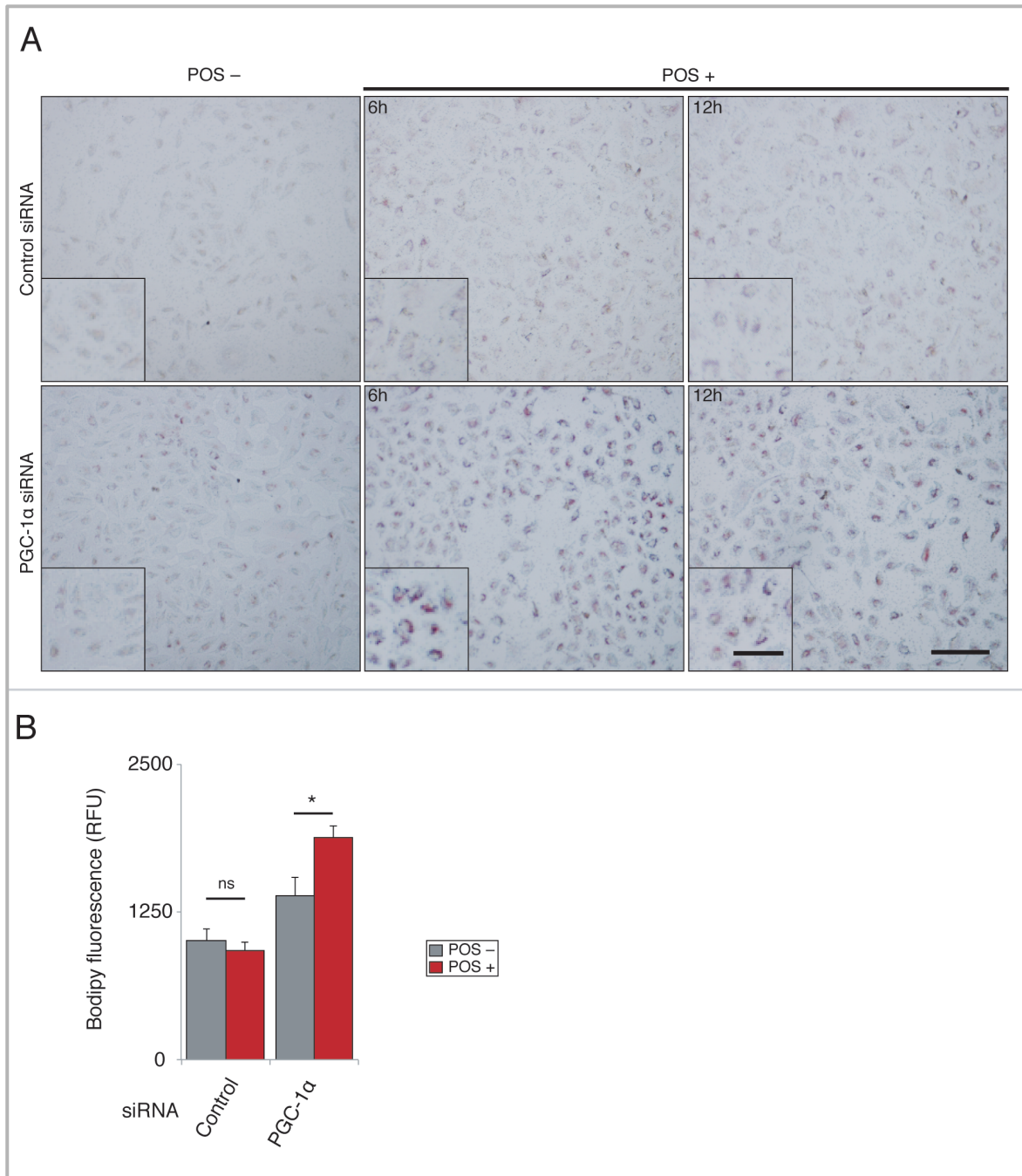


Figure 4.12. PGC-1 α facilitates lysosomal degradation of POS in undifferentiated ARPE-19 cells. (A) In the ARPE-19 cells transfected with PGC-1 α siRNA, oil red O staining was more intense after POS treatment than in those with control siRNA. Scale bar, 200 μ m. (B) In the ARPE-19 cells transfected with PGC-1 α siRNA, the accumulation of peroxidized lipid evaluated by BODIPY C11 fluorescence increased after POS treatment when compared with those with control siRNA. Mean \pm SEM, $n = 6-10$ per group, *** $P < 0.001$ by ANOVA, followed by a post hoc Tukey's test * $P < 0.05$, ns [not significant].

4.3.4 Senescence-related phenotypes in RPE of PGC-1 α knockout (KO) mice

To further elucidate the role of PGC-1 α in lipid metabolism and senescence in the RPE cells, the phenotypes of PGC-1 α KO mice were evaluated in comparison with that of age-matched control littermates. The phenotypes of RPE itself as well as adjacent structures that are affected by aged RPE including the Bruch's membrane and the choriocapillaris were evaluated. The Bruch's membrane is the basement membrane of RPE cells. This structure becomes thicker with age, which makes the transport between the choriocapillaris and the RPE cells more difficult (Ramrattan et al., 1994). Nutrient supply from the choriocapillaris is critical for the integrity of the RPE cells and the outer retina, but it is progressively lost in aged eyes even before the development of AMD (Biesemeier et al., 2014). On the other hand, an intact choriocapillaris is maintained by basal VEGF secretion from RPE cells. Previous study showed that POS phagocytosis upregulate VEGF expression in the RPE cells through PGC-1 α , but not through hypoxia-inducible factor-1 α (Ueta et al., 2012b).

Transmission electron microscopy revealed an accumulation of melanolipofuscin in the RPE (Figure 4.13B and 4.13K vs. 4.13A), thickening of the Bruch's membrane with higher electron density (Figure 4.13D vs. 4.13C; Fig. 4.13F vs. 4.13E), and scarcity of the choriocapillaris (Figure 4.13B vs. 4.13A) in 6-month-old PGC-1 α KO mice in comparison with control littermates. Each of these phenotypes is well known to be associated with aging RPE cells (Biesemeier et al., 2014; de Jong, 2006; Feeney, 1978; Ramrattan et al., 1994).

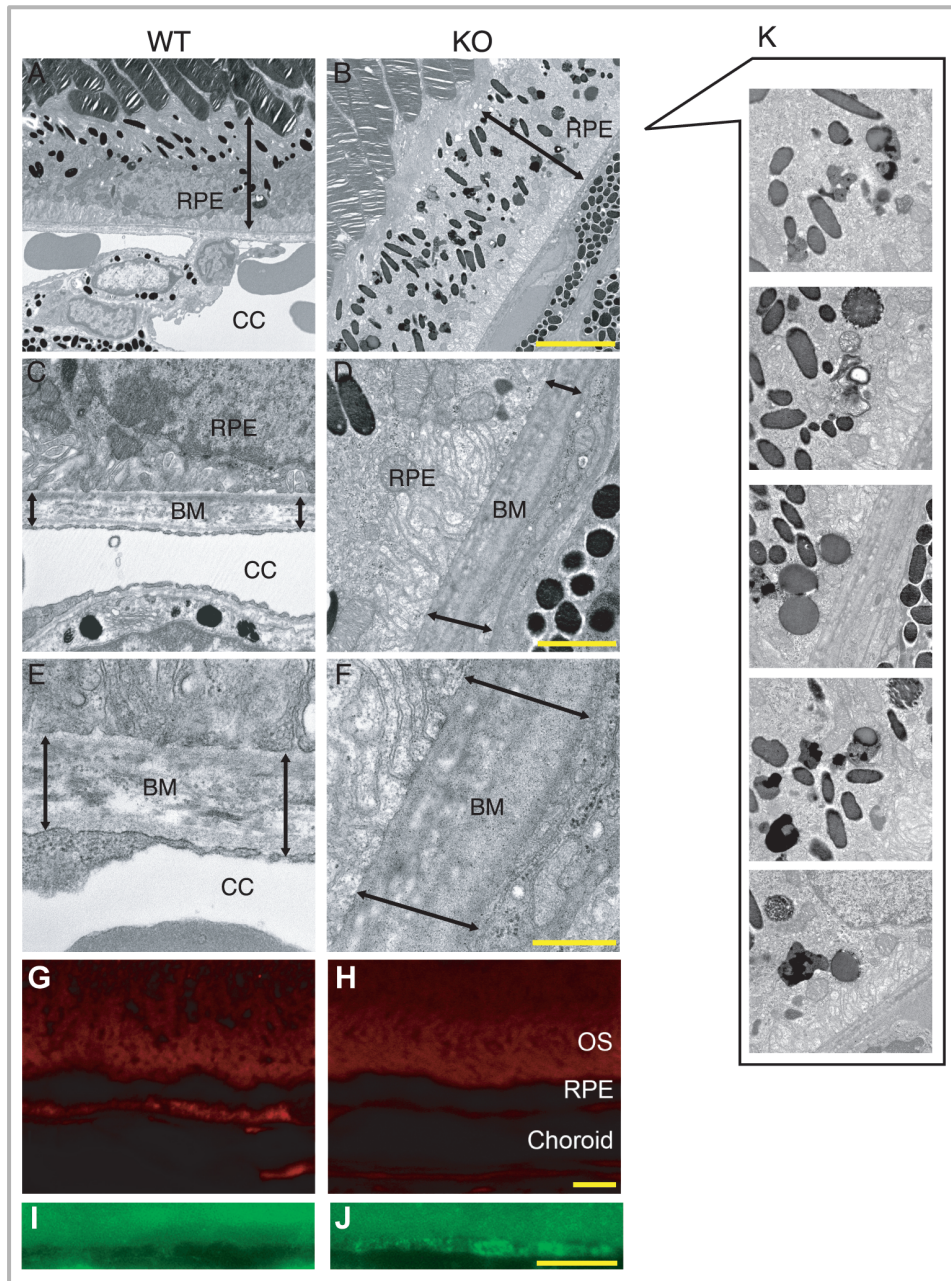


Figure 4.13. Accelerated senescence is observed in the RPE of PGC-1 α KO mice. The phenotypes of the RPE, Bruch's membrane, and choriocapillaris of 6-month-old PGC-1 α KO mice were compared with those of age-matched control littermates. (A and B) Accumulation of melanolipofuscin on TEM was observed in the PGC-1 α KO mice when compared with the control mice. Note that many melanin granules in the KO mice are more whitish, which indicates lipofuscin accumulation in the melanin granules. CC; choriocapillaris; scale bar, 5 μ m. (C and D) Bruch's membrane (BM) and choriocapillaris (CC) on TEM. Note that BM of the KO mice is thicker and has greater electron density than that of the control mice. CC beneath the BM was not often observed in KO mice, while it was abundant in the control mice. Scale bar, 1 μ m. (E and F) Magnified view of BM and CC. Scale bar, 500 nm. (G and H) CC evaluated by UEA-I staining was poor in the KO mice when compared with the control mice. Scale bar, 5 μ m. (I and J) Autofluorescence reflecting lipofuscin accumulation in the RPE was more intense in the KO mice than in the control mice. (K) Magnified views of melanolipofuscin in the RPE cells of the KO mice. Scale bar 1, μ m.

Staining with UEA-I lectin confirmed a poor choriocapillaris vasculature in 6-month-old PGC-1 α KO mice in comparison with age-matched control littermates (Figure 4.13H vs. 4.13G). In addition, this study also evaluated the autofluorescence in the RPE, which reflects the amount of accumulated lipofuscin. Stronger autofluorescence in the RPE of the PGC-1 α KO mice versus the control mice was confirmed (Figure 4.13J vs. 4.13I).

4.4 Discussion

Elucidating the mechanisms underlying POS degradation in the RPE cells is critical for understanding the pathogenesis of AMD. The present study has disclosed for the first time the role of PGC-1 α in POS degradation and that the RPE cells have an inherent α v β 5 integrin/FAK/PGC-1 α signaling pathway to facilitate lysosomal degradation of POS, whose impairment may cause metabolic stress. Moreover, recognition of POS at α v β 5 integrin confers antisenescence effects on RPE cells by decreasing ROS levels and increasing mitochondrial biogenesis. These results explain why in previous studies RPE cells were reportedly more susceptible to oxidative stress (Mukherjee et al., 2007) and aging (Nandrot et al., 2004) when they were not actively phagocytizing POS.

PGC-1 α is a main regulator of metabolism and oxidative stress. Recently, Ueta et al. (2012b) found that expression of PGC-1 α could be upregulated by POS treatment in undifferentiated ARPE-19 cells, whereas, in the present study, the same was confirmed in differentiated ARPE-19 cells and in *ex vivo* RPE. PGC-1 α expression by skeletal muscles

reportedly declines with age (Koltai et al., 2012). Moreover, exercise upregulates PGC-1 α expression and rescues age-related accumulation of oxidative stress in the hippocampus (Marosi et al., 2012). In the RPE cells, high oxygen consumption, light absorption, and lipid peroxidation through POS phagocytosis can result in considerable oxidative stress (Kaarniranta et al., 2013). In fact, light exposure reportedly increases ROS levels *in vivo*, especially in the outer segment layer of photoreceptors in the retina (Roehlecke et al., 2013). Numerous studies have reported that oxidative stress and aging can influence POS phagocytosis. Sublethal exposure to H₂O₂ can inhibit FAK activation in the ARPE-19 cells (Qin and Rodrigues, 2012) and photo-oxidative stress can suppress the expression of β 5 integrin (Olchawa et al., 2013). ARPE-19 cells cultured on the Bruch's membrane from the elderly individuals exhibited decreased POS phagocytic activity when compared with those cultured on the Bruch's membrane from the young (Sun et al., 2007). These reports suggest that the activation of the α v β 5 integrin/FAK/ PGC-1 α pathway decreases in aged RPE cells.

From a therapeutic point of view, modulation of the α v β 5 integrin/FAK/ PGC-1 α pathway can be a useful strategy to combat the aging of RPE cells. Thus, AMPK activation may be suitable for PGC-1 α activation. Although, in the present study, AMPK was not involved in the upregulation of PGC-1 α expression by POS binding, AMPK activation may still be beneficial to RPE cells through posttranslational regulation of PGC-1 α (Jager et al., 2007). Silence information regulator 2-like 1 (Sirt1) is a deacetylase of PGC-1 α and because Sirt1 activity is increased during energy demand, including during fasting and exercise, behavioral modulation may impact RPE senescence. Downstream of the α v β 5 integrin/FAK/PGC-1 α pathway, activation of the autophagy/lysosomal pathway is a potential therapeutic target. The mechanistic target of rapamycin (mTOR) is

reportedly a cause of retinal degeneration due to RPE dedifferentiation (Zhao et al., 2011). The mTOR inhibitor rapamycin can extend the life span of murines, although it remains controversial whether rapamycin can rescue age-related phenotypes (Neff et al., 2013).

The current study identified accelerated aging phenotypes not only in the RPE cells but also in the Bruch's membrane and choriocapillaris of PGC-1 α KO mice. Loss of the choriocapillaris with age and in the early stage of AMD has been confirmed in humans (Biesemeier et al., 2014). Moreover, loss of the choriocapillaris together with a thickened Bruch's membrane hampers smooth nutrient supply to and metabolite release from RPE cells, leading to RPE loss (i.e. dry AMD). On the other hand, loss of the choriocapillaris may be counteracted by neoangiogenesis, leading to choroidal neovascularization (i.e. wet AMD) (Biesemeier et al., 2014). Geographic atrophy and neovascular AMD are the late stage of AMD, in which the degeneration cannot be fully recovered. The choriocapillaris is maintained by VEGF secretion from the RPE cells, and the results of a previous study showed that PGC-1 α is an important regulator of VEGF expression in the RPE cells, especially in response to POS phagocytosis (Ueta et al., 2012b). Therefore, a therapeutic approach targeting PGC-1 α may suppress the progression from the early stage of AMD to the late stage to maintain visual function.

An important limitation of the present study was that undifferentiated ARPE-19 cells were used in most *in vitro* experiments. One reason for using ARPE-19 cells was because the expression of PGC-1 α was silenced using siRNA to elucidate PGC-1 α -dependent mechanisms *in vitro*. Another reason was because the phagocytosis machinery is conserved in different types of RPE cells (Mazzoni et al., 2014) including undifferentiated ARPE-19 cells (Olchawa et al., 2013; Qin and Rodrigues, 2012). Those immortalized cells have some different features in comparison to the original cells in the

native tissue. Especially for RPE cells, gaining polarity through differentiation is considered important (Sonoda et al., 2009). Although phagocytosis machinery is conserved in undifferentiated ARPE-19 cells (Olchawa et al., 2013; Qin and Rodrigues, 2012), they lack many physiological characteristics of the polarized RPE cells, including apical microvilli, well-defined tight junctions, membrane transport capability, polarized secretion of cytokines, and melanocytic pigmentation (Sonoda et al., 2009). Therefore, the results of this study need to be carefully interpreted. The use of differentiated cells of primary culture would be more desirable as an *in vitro* model for more accurate insights.

In conclusion, the present study identified a novel regulatory mechanism for senescence and the lysosomal pathway in the RPE cells on binding of POS, which underscores a role of PGC-1 α (Figure 4.14).

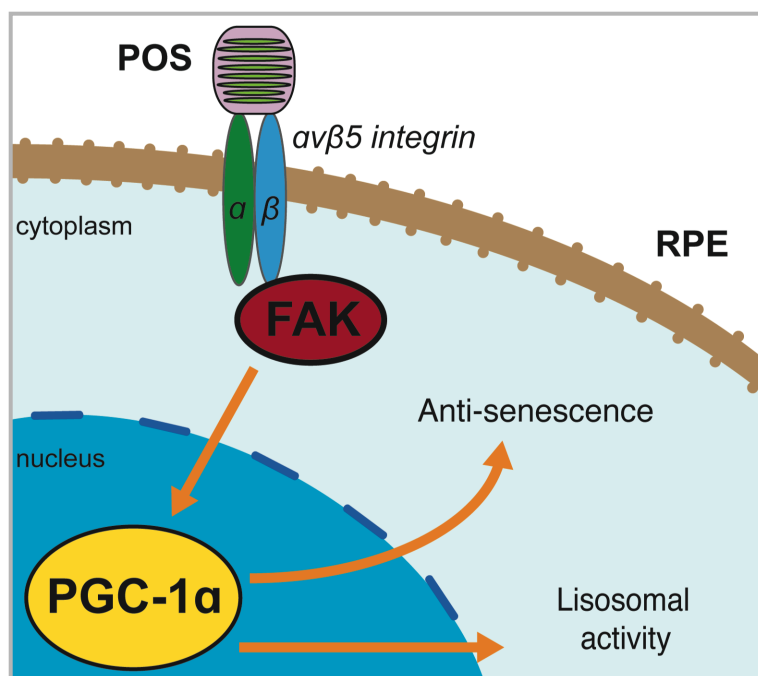


Figure 4.14. Schematic drawing of the signaling pathway revealed in the present study. In the RPE cells, POS binding activates the $\alpha\beta 5$ integrin/FAK/PGC-1 α pathway, which facilitates lysosomal activity and prevents senescence to counteract POS-induced metabolic stress.

5. Protective Role of GPx4 in Laser-Induced Choroidal Neovascularization in Mice

5.1 Introduction

AMD is considered one of the leading causes of irreversible visual loss in the world (de Jong, 2006; Kahn et al., 1977; Klaver et al., 1998). In the late-stage AMD, the growth of abnormal new blood vessels from the choroidal vasculature toward the retinal pigment epithelium (RPE) and neurosensory retina characterizes neovascular AMD. Edema, bleeding, and disruption of photoreceptor cells are some of the features associated with the progression of the disease. The participation of VEGF is widely recognized in the pathogenesis of human neovascular AMD (Rosenfeld et al., 2006), as well as in the animal model of laser-induced choroidal neovascularization (CNV) (Lambert et al., 2013). Laser-induced CNV is a recognized technique widely used to reproduce the structural alterations present in neovascular AMD. This model can efficiently reproduce the inflammatory and angiogenic processes that contribute to the establishment of the disease (Lambert et al., 2013).

Oxidative stress has been associated with the development of neovascular AMD in studies using animal models (Dong et al., 2009; Ebrahim et al., 2006; Hara et al., 2010; Imamura et al., 2006). Accordingly, supplementation with antioxidant vitamins has been reported to suppress the establishment of neovascular AMD (Chew et al., 2013), suggesting that oxidative stress is also involved in human neovascular AMD. The activity of endogenous antioxidant enzymes is considered crucial for the defense against oxidative

stress, and its implication in neovascular AMD has been reported following studies on SOD1-deficient mice (Dong et al., 2009; Imamura et al., 2006). Notwithstanding, it is important to consider that other important antioxidant enzymes, including glutathione peroxidase 4 (GPx4), might be enrolled in the protection against oxidative stress, although this is not yet completely understood.

GPx4, also known as phospholipid hydroperoxide glutathione peroxidase, is an intracellular antioxidant enzyme that belongs to the group of selenoproteins that have a selenocysteine amino acid residue at their enzymatic active site. Ubiquitously expressed, GPx4 directly reduces peroxidized phospholipids produced in cell membranes. In contrast to other GPx isoforms, GPx4 reduces complex lipid hydroperoxides even when they are incorporated in biomembranes or lipoproteins (Thomas et al., 1990).

GPx4 reacts with hydrogen peroxide and many different lipid hydroperoxides, including those originating from lipoproteins and cholesterol. GPx4 has been shown to be critically important because its ablation in mice leads to embryonic lethality at approximately 1 week (Imai et al., 2003). In addition, GPx4 ablation specifically in photoreceptors (Ueta et al., 2012a), cerebral neurons (Wirth et al., 2010), vascular endothelium (Wortmann et al., 2013), or spermatocytes (Imai et al., 2009) causes severe pathological phenotypes.

The current study aimed to evaluate the role of GPx4 in the RPE/choroid tissue using a laser-induced CNV mouse model. The possible influence of GPx4 on VEGF levels following laser-induced CNV was also analyzed.

5.2 Methods

All procedures were performed in accordance with the Association for Research in Vision and Ophthalmology (ARVO) Statement for the Use of Animals in Ophthalmic and Vision Research (Association for Research in Vision and Ophthalmology, 1994) and were approved by the Institutional Animal Research Committee of the University of Tokyo.

5.2.1 Animals

Mice were maintained in a temperature-controlled room, wherein fresh water and rodent-specific diet were available ad libitum. GPx4^{+/-}, GPx4^{+/+}, and GPx4 transgenic mice on a C57BL/6 background were kindly provided by Professor Hiroataka Imai (a co-investigator). To obtain these mice expressing different levels of GPx4, first GPx4^{+/+} wild-type mice were bred with transgene-rescued GPx4 knockout mice GPx4^{-/-}:Tg (GPx4) (Imai et al., 2009) to generate GPx4^{+/-}:Tg (GPx4) and GPx4^{+/-} mice. Then, the GPx4^{+/-}:Tg (GPx4) mice were bred with the GPx4^{+/-} mice to obtain GPx4^{+/-}, GPx4^{+/+}, and GPx4^{+/+}:Tg (GPx4) mice for comparison.

5.2.2 Laser-induced CNV model

Laser photocoagulation was used for the induction of CNV lesions as previously described (Ueta et al., 2012a). A glass cover slip served as a contact lens. Diode laser (DC-3000; Nidek, Osaka, Japan) irradiation was delivered through a slit lamp (SL150;

Topcon, Tokyo, Japan) to the mouse fundus between the major retinal vessels using a spot size of 200 μm , power of 200 mW, and exposure duration of 20 ms. Disruption of the Bruch's membrane was confirmed by central bubble formation immediately after photocoagulation. For each eye, 6 successful laser spots were created. After laser treatment, the mice were maintained on a physiologic 12-h light cycle. On day 7, the mice were deeply anesthetized and perfused with fluorescein isothiocyanate (FITC) dextran in PBS. Then, the mice were sacrificed, and the eyes were enucleated and fixed in 4% paraformaldehyde (PFA) for 20 min. RPE/choroid tissue was separated under a microscope and flat-mounted with the RPE facing up. The CNV area was measured on the basis of pictures analyzed by a blinded examiner using Photoshop CS3. The CNV size was evaluated on day 7 because the size is considered to reach the maximum on days 5 to 7 (Giani et al., 2011; Lambert et al., 2013). In contrast, to evaluate the pathogenic role of VEGF-A, VEGF-A expression in RPE/choroid tissue was evaluated on day 3 (i.e. 72 h after laser treatment) when CNV is considered to be in the active stage of its development.

5.2.3 Assessment of RPE/choroid tissue

After enucleation of the eyes, the extraocular tissues were surgically resected. An incision was performed behind the corneal limbus to make an eye-cup. The anterior components of the eyes were then removed. For the separation of the tissues incubation of the retina and RPE/choroid tissue in dispase solution was used. The RPE/choroid tissue was then separated from the retina and collected for the experiments.

5.2.4 Quantification of mRNA using real-time RT-PCR

All the samples used for real-time RT-PCR were from the RPE/choroid. Thus, the RPE/choroid complexes were microsurgically isolated from the eyes. RNA from homogenized samples of the RPE/choroid tissue was extracted using TRIzol reagent (Invitrogen, Carlsbad, CA), and cDNA was prepared using SuperScript III for RT-PCR (Invitrogen). Real-time PCR was performed using a Thermal Cycler Dice Real Time System (Takara Bio Inc., Shiga, Japan). Expression levels of each gene were normalized to those of GAPDH. Three different primer pairs for VEGF-A were used. An additional primer pair for VEGF 164 was also used to determine the consistency of the results, because changes in the VEGF-A mRNA level in RPE/choroid tissue after CNV induction have not been completely established in the literature (Hu et al., 2009; Mizutani et al., 2009). In the current study, three primer pairs already used in previously published studies (Hu et al., 2009; Mizutani et al., 2009; Xie et al., 2011) were tested and compared with the primer pair specifically designed for this study. First, the validity of the primer sequences shown in the literature was determined using Primer-BLAST, and errors were found in some of the published primer sequences. Therefore, primers with corrected sequences were used (Table 5.1).

Table 5.1. Primers sequences used for real time RT-PCR in the study

Genes	Sequences
Mouse VEGF-A primer 1	Forward: GTACCTCCACCATGCCAAGT Reverse: GCATTCACATCTGCTGTGCT
Mouse VEGF-A primer 2	Forward: AGGCTGCACCCACGACAGAA Reverse: CTTTGGTCTGCATTCACATC
Mouse VEGF-A primer 3	Forward: AGCCGAGCTCATGGACGGGT Reverse: AGTAGCTTCGCTGGTAGACATC
Mouse VEGF 164	Forward: GCCAGCACATAGGAGAGATGAGC Reverse: CAAGGCTCACAGTGATTTTCTGG
Mouse GAPDH	Forward: CACATTGGGGGTAGGAACAC Reverse: AACTTTGGCATTGTGGAAGG

5.2.5 Protein expression analysis using Western Blot analysis and ELISA

The isolated RPE/choroid complexes were placed in 100- μ L radioimmunoprecipitation assay (RIPA) buffer and homogenized at 4°C. Protein concentrations were determined using a Coomassie (Bradford) Protein Assay Kit (Thermo Scientific, Waltham, MA). For Western blot analysis, total protein extracts from the RPE/choroid samples were separated on sodium dodecyl sulfate polyacrylamide gel electrophoresis (SDS-PAGE) gels and transferred onto nitrocellulose membranes followed by blocking with 5% nonfat dry milk in TBS-T (Tris-buffered saline with 0.1% Tween-20). Incubation with primary antibodies was performed for 6 h in TBS-T containing 5% nonfat dry milk. The primary antibodies used were mouse or rabbit antibodies against β -actin (Sigma, St Louis, MO) and against GPx4 obtained from a

primary hybridoma (Imai et al., 2001). The membranes were incubated with anti-mouse/rabbit horseradish peroxidase-labeled secondary antibody (Amersham Biosciences, Chalfont St Giles, UK) for 1 h. The washed membranes were further developed with ECL Plus Western Blotting Detection Reagents (GE Healthcare, Piscataway, NJ). The protein level was calculated by normalization to the β -actin level.

The enzyme-linked immunosorbent assay (ELISA) was used for the evaluation of VEGF-A protein, according to the manufacturer's instructions (R&D Systems, Minneapolis, MN).

5.2.6 Immunohistochemistry using 4-hydroxy-2-nonenal (4-HNE)

Enucleated eyeballs were fixed in 4% PFA for 6 hours and embedded in paraffin, and the posterior retina was cut into 5- μ m-thick sections. Slides were first incubated with blocking solution (2% normal goat serum) overnight, and then with primary antibodies at room temperature for 3 h and secondary antibodies for 1 h. The sections were then coverslipped with mounting medium. For immunostaining, the primary antibodies used were mouse monoclonal antibodies specific to 4-HNE (JaICA, Shizuoka, Japan). Hematoxylin-eosin (HE) staining was used to reveal the morphology of the retina and RPE/choroid tissue. The intensity of immunofluorescence in the RPE/choroid was evaluated using Image-J software.

5.2.7 Statistical analysis

All statistical analyses were performed using JMP10 software (SAS Institute Inc., Cary, NC, USA). For comparison between two unpaired groups, Student's *t*-test was used. For comparison among three or more groups, one-way analysis of variance (ANOVA) was performed, followed by the post hoc Tukey's test. The level of significance was set at $P < 0.05$.

5.3 Results

5.3.1 Laser-induced CNV and VEGF-A expression in the RPE/choroid tissue in mice

To better understand the behavior of VEGF-A in laser-induced CNV in mice, mRNA levels and protein expression of VEGF-A following CNV induction was firstly evaluated in wild mice. According to the literature, different reports have demonstrated conflicting data with regards to VEGF-A mRNA levels in RPE/choroid after laser-induced CNV. Notwithstanding, the literature reveals a well-established consensus regarding the elevation of VEGF-A protein expression in the development of CNV (Hu et al., 2009; Mizutani et al., 2009).

Surprisingly, the mRNA levels of VEGF-A in the RPE/choroid were diminished by CNV induction throughout the first 72 hours during CNV development (Figure 5.1A). On the other hand, the VEGF-A protein levels were increased at 72 hours after laser

treatment, demonstrating consistency with the development of CNV (Figure 5.1B). In accordance with the mRNA results obtained with the VEGF-A primer, the RT-PCR using the additional VEGF primers (VEGF-A primer 2, VEGF 164 primer, and VEGF-A primer 3) (Mizutani et al., 2009; Xie et al., 2011) also revealed decreased VEGF levels, confirming the downregulation of VEGF mRNA following CNV induction (Figure 5.2). Therefore, the opposite behavior of VEGF-A mRNA levels and protein expression following the induction of laser-induced CNV may suggest a possible complex mechanism responsible for the regulation of VEGF expression in RPE/choroid tissue.

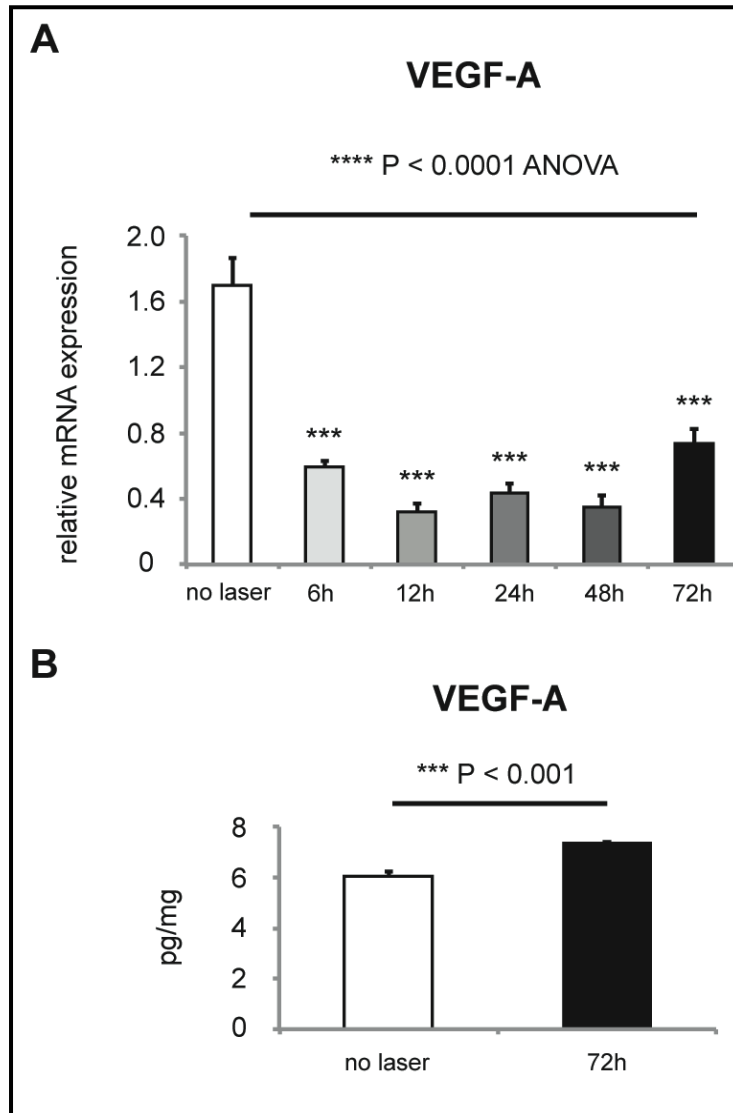


Figure 5.1. VEGF-A expression in the RPE/choroid with laser-induced CNV. (A) Relative VEGF-A mRNA levels in the RPE/choroid of wild-type mice before and after induction of the CNV model at 6, 12, 24, 48 and 72 h. Mean \pm SEM, $n = 10-21$, $***P < 0.0001$ by ANOVA, followed by a post hoc Tukey's test $***P < 0.001$ compared with the no laser group. (B) VEGF-A protein expression in the RPE/choroid of wild-type mice before and after 72 h of CNV induction by laser, measured by ELISA. Mean \pm SEM, $n = 4$, $*** P < 0.001$, Student's *t*-test.

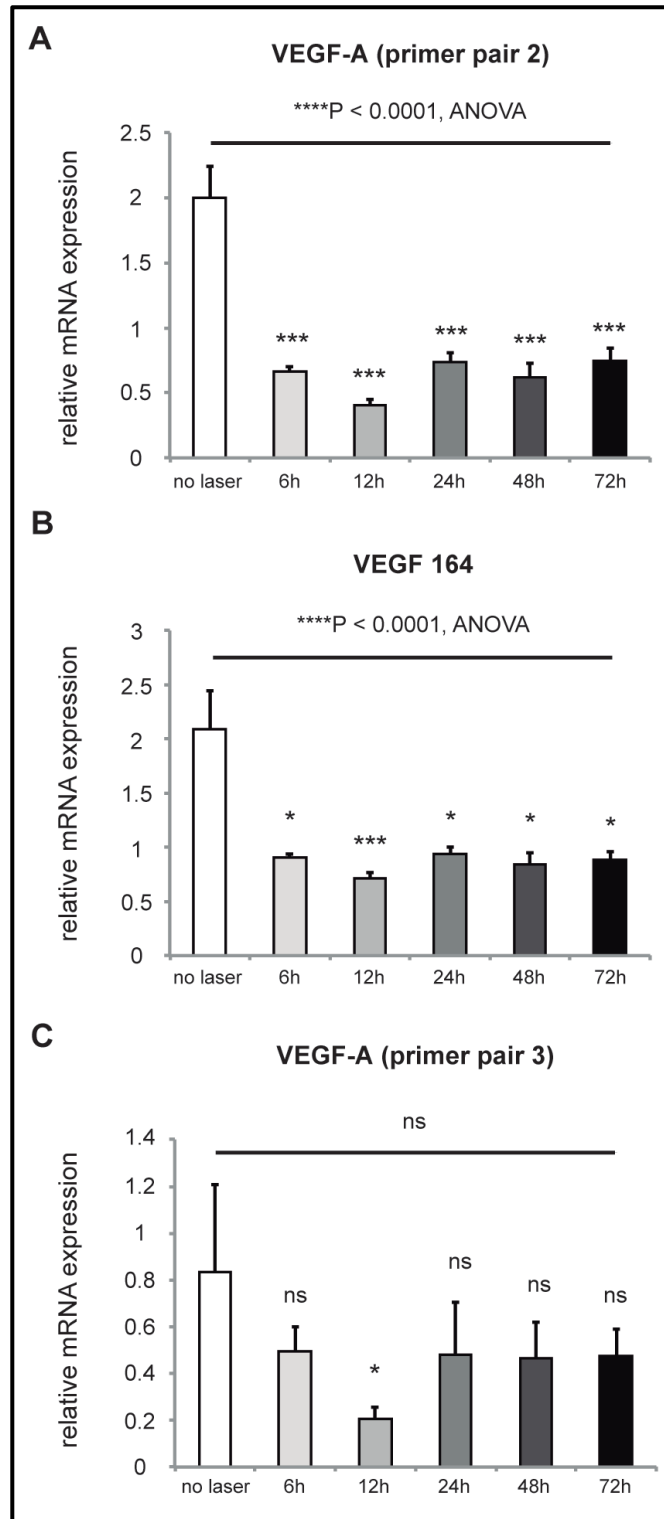


Figure 5.2. Change in VEGF-A mRNA levels in the RPE/choroid after CNV induction in wild-type mice. For the same samples shown in Figure 1, different primer pairs for VEGF-A were used for RT-PCR. The primers sequences are shown in Table 1. (A) A primer pair 2 (Hu et al., 2009) was used. (B) A primer pair for VEGF 164 (Mizutani et al., 2009) was used. (C) A primer pair 3 (Xie et al., 2011) was used. Mean \pm SEM, $n = 10\text{--}21$ per group, **** $P < 0.0001$, ns [not significant] by ANOVA, followed by a post hoc Tukey's test * $P < 0.05$, *** $P < 0.001$, ns [not significant], compared with the no laser group.

5.3.2 Generation of GPx4^{+/-}, GPx4^{+/+}, and GPx4-overexpressing mice used in the study

Figure 5.3 shows the generation of three types of mice expressing different levels of GPx4. All of the mice showed normal growth and development (Figure 5.3A), displaying normal morphology of the retina and RPE/choroid tissue in all three genotypes (Figure 5.3B).

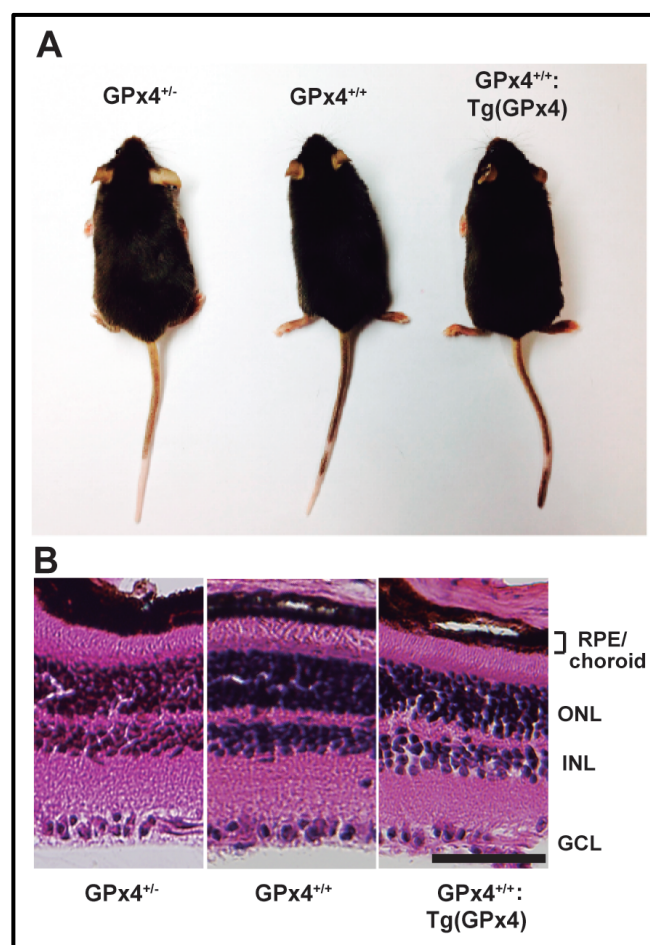


Figure 5.3. GPx4 expression in the RPE/choroid. (A) Similar appearance of GPx4^{+/-}, GPx4^{+/+} and GPx4^{+/+};Tg (GPx4) mice at 3 months of age expressing different levels of GPx4. (B) Hematoxylin-eosin staining of the retina and RPE/choroid of the mice expressing different levels of GPx4. (ONL, outer nuclear layer; INL, inner nuclear layer; GCL, ganglion cells layer; Scale bar, 30 μ m).

The expression levels of GPx4 were determined using Western blot analysis of the RPE/choroid tissue. Western blot analysis revealed different expression levels of GPx4 protein in the RPE/choroid tissue among the three types of mice (Figure 5.4A), which confirmed the validity of using these mice to test the role of GPx4 in the RPE/choroid tissue.

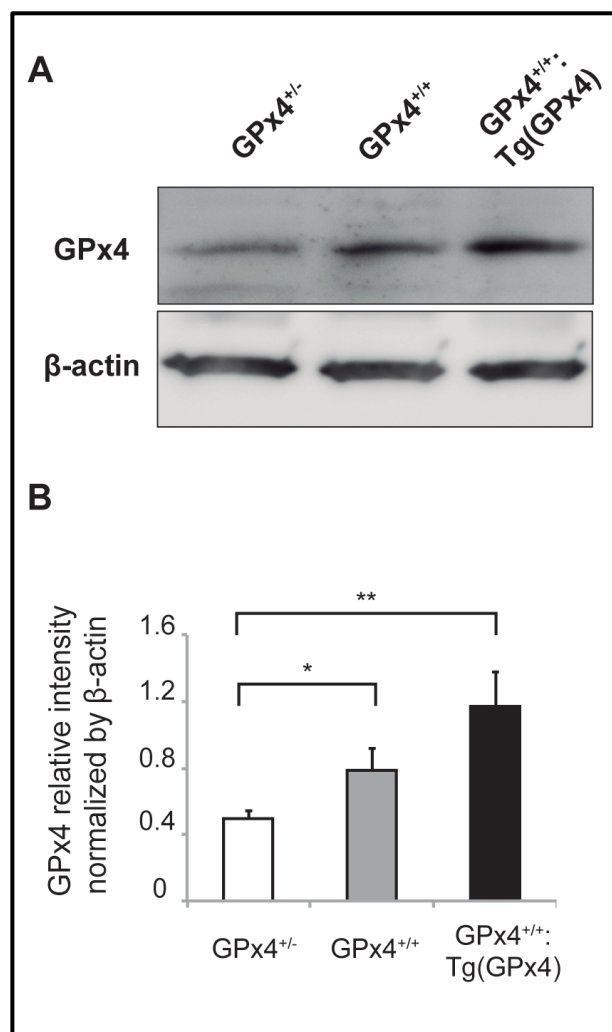


Figure 5.4. GPx4 expression in the mice. (A) Western blot analysis of β -actin and GPx4 protein expression in the RPE/choroid. (B) Statistical evaluation for the comparative differences in GPx4 protein in the RPE/choroid. Mean \pm SEM, $n = 8$, $**P < 0.01$ by ANOVA, followed by a post hoc Tukey's test $*P < 0.05$, $**P < 0.01$, compared with $GPx4^{+/-}$ mice.

To establish that additional GPx isoforms were not associated with the outcomes of this study, Western blot analysis was used to confirm that GPx1 and GPx2 protein expression in the RPE/choroid was similar in these mice (Figure 5.5). No statistically significant difference was observed in the mice used in the study, confirming that the outcomes were related to the GPx4 isoform, and not to GPx1 and GPx2 isoforms.

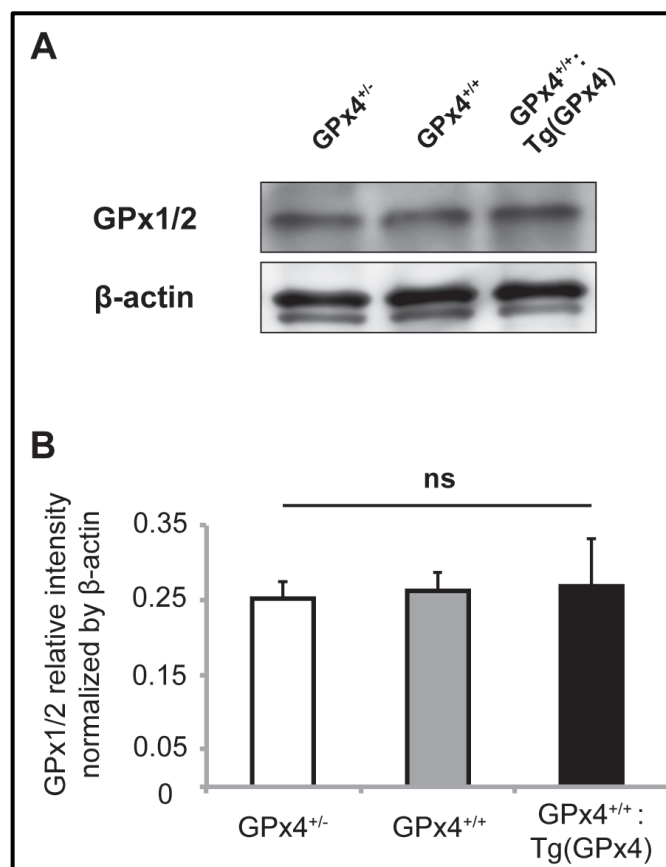


Figure 5.5. Protein expression of GPx1 and GPx2 in the RPE/choroid. (A) Western blot analysis of β-actin and GPx1/2 protein expression in the RPE/choroid. (B) Statistical evaluation for the comparative differences in GPx1/2 protein in the RPE/choroid. Mean ± SEM, n = 5; ns, not significant by ANOVA.

5.3.3 GPx4 and oxidative stress in the mice

GPx4 demonstrated to influence the lipid peroxidation in the RPE/choroid tissue. Immunostaining using specific antibody against 4-HNE revealed increased accumulation of peroxidized lipids in the GPx4^{+/-} mice. In contrast, GPx4-overexpressing mice (i.e. GPx4^{+/+}:Tg [GPx4]) showed significantly less accumulation of oxidized lipids (Figure 5.6). Coherently, the GPx4^{+/+} mice showed an intermediate accumulation of oxidized lipids, suggesting that lipid peroxidation varies according to the amount of GPx4 expressed in the mice. This finding suggests the protective role of endogenous GPx4 against oxidative stress in the RPE/choroid of mice overexpressing GPx4.

5.3.4 Animal model of CNV development using laser-induced CNV

Next, the influence of different levels of GPx4 on CNV development using a laser-induced CNV mouse model was analyzed (Figure 5.7). With increasing GPx4 levels, the CNV size was reduced significantly on day 7 after laser photocoagulation was performed. The literature shows that one week after laser exposure, the size of the CNV is considered to reach its maximum (Giani et al., 2011; Lambert et al., 2013). To evaluate the pathogenic role of VEGF in CNV, expression of VEGF-A in the RPE/choroid tissue was evaluated on day 3 (i.e. 72 hours after laser treatment) when CNV is considered to be in the active stage of its development. As confirmed in the wild-type mice, VEGF-A mRNA was downregulated in all three groups.

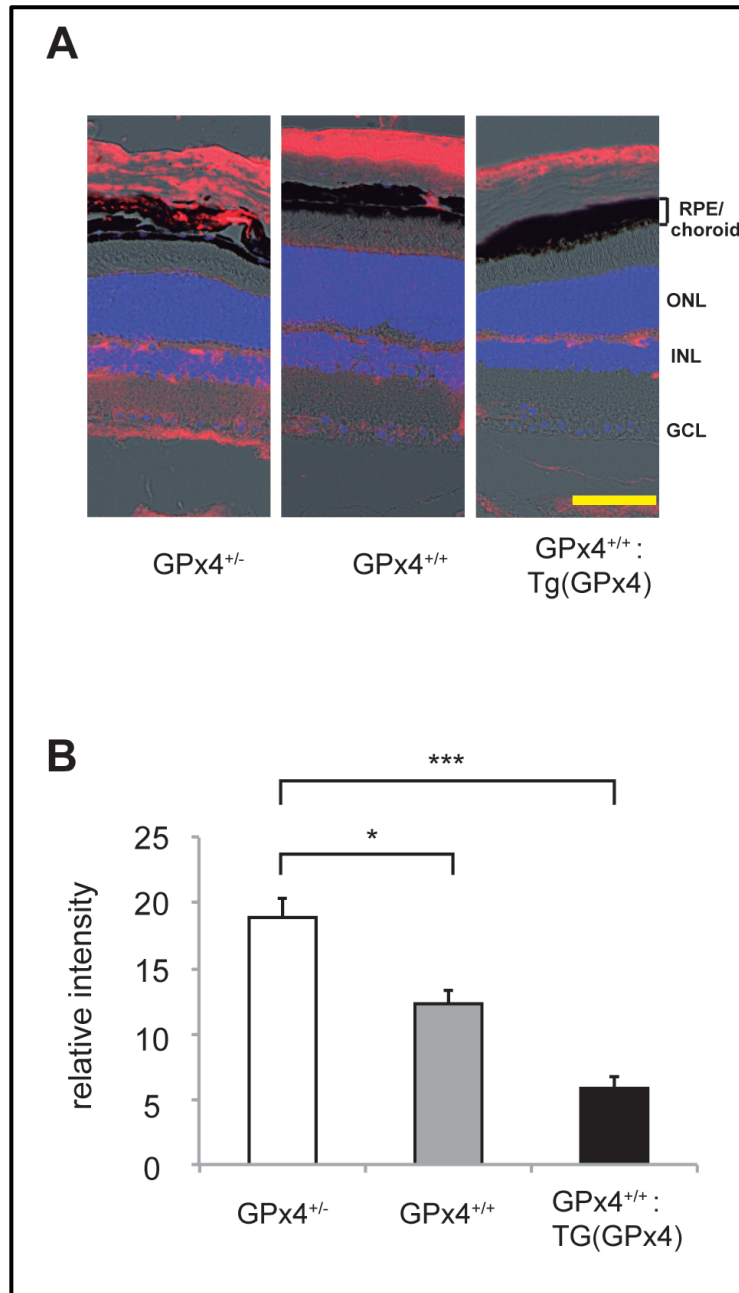


Figure 5.6. Accumulation of peroxidized lipids. (A) Immunoreactivity to 4-hydroxi-2-neonenal (4-HNE, red) in the retina and RPE/choroid of mice expressing different levels of GPx4. Nuclei was counterstained with 4,6-diamidino-2-phenylindole (DAPI, blue). Scale bar, 30 μ m. (B) Statistical evaluation of the immunofluorescence for 4-HNE in the RPE/choroid. Mean \pm SEM, n = 4, *** P < 0.001 by ANOVA, followed by a post hoc Tukey's test * P < 0.05, *** P < 0.001, compared with GPx4^{+/-} mice.

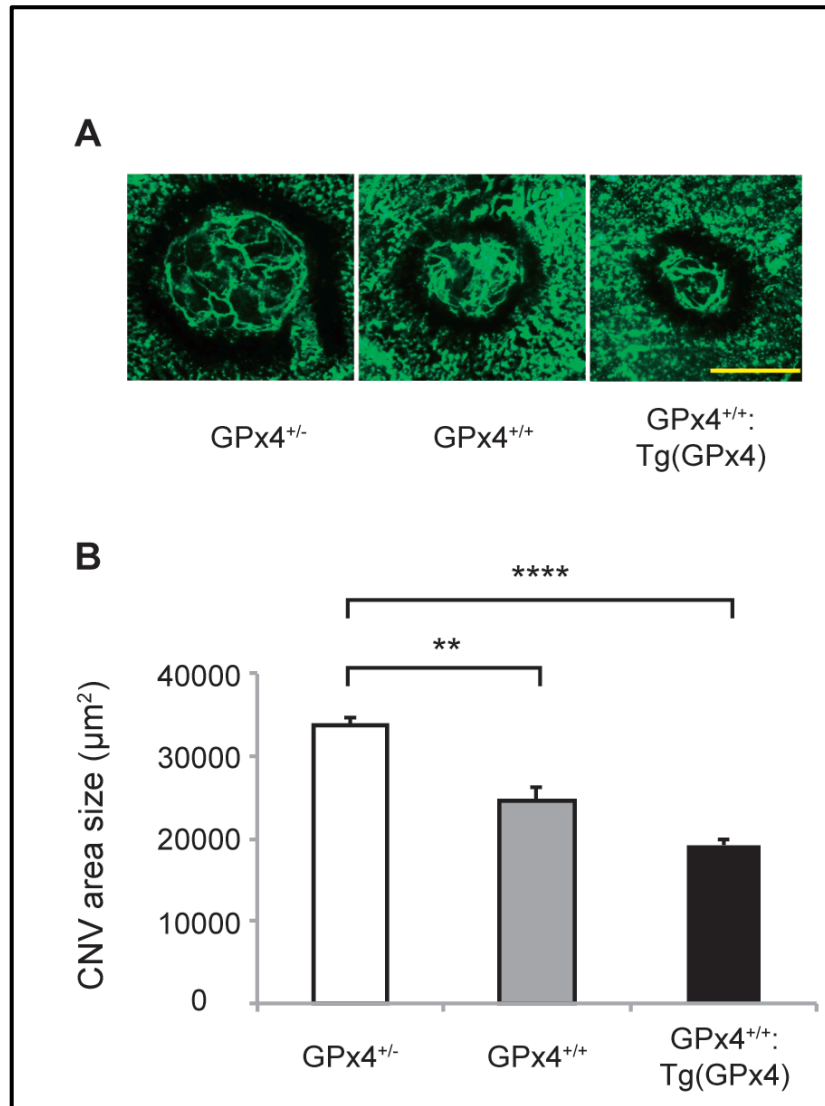


Figure 5.7. Laser-induced CNV model. The CNV area size was evaluated on flatmount culture on day 7. (A) CNV induced by laser exposure in the mice expressing different levels of GPx4. Scale bar, 500 µm. (B) The area size of the CNV in these 3 types of mice (µm²). Mean ± SEM, n = 4–5, *****P* < 0.0001 by ANOVA, followed by a post hoc Tukey's test ***P* < 0.01, *****P* < 0.0001 compared with GPx4^{+/-} mice.

In contrast, with or without laser treatment, the VEGF-A mRNA levels in the RPE/choroid tissue were significantly higher in mice expressing higher levels of GPx4 (Figure 5.8A). However, VEGF-A protein expression exhibited a more peculiar pattern (Figure 5.8B). In the RPE/choroid tissue without CNV induction, the VEGF-A protein levels were higher in mice expressing more GPx4 (*P* = 0.0061 by ANOVA). Three days

after CNV induction, the VEGF-A protein levels were upregulated more in mice expressing lower levels of GPx4. As a result, the VEGF-A protein levels were significantly higher in mice expressing less GPx4 than in mice overexpressing GPx4 ($P = 0.0274$ by ANOVA). In the GPx4^{+/-} and GPx4^{+/+} mice, the difference in the VEGF-A protein levels between mice with laser-induced CNV and those without it was significant ($P = 0.0001$ and $P = 0.0022$ by Student's *t*-test, respectively). In mice overexpressing GPx4, the VEGF-A protein levels did not differ significantly between mice with laser-induced CNV and those without it ($P = 0.45$).

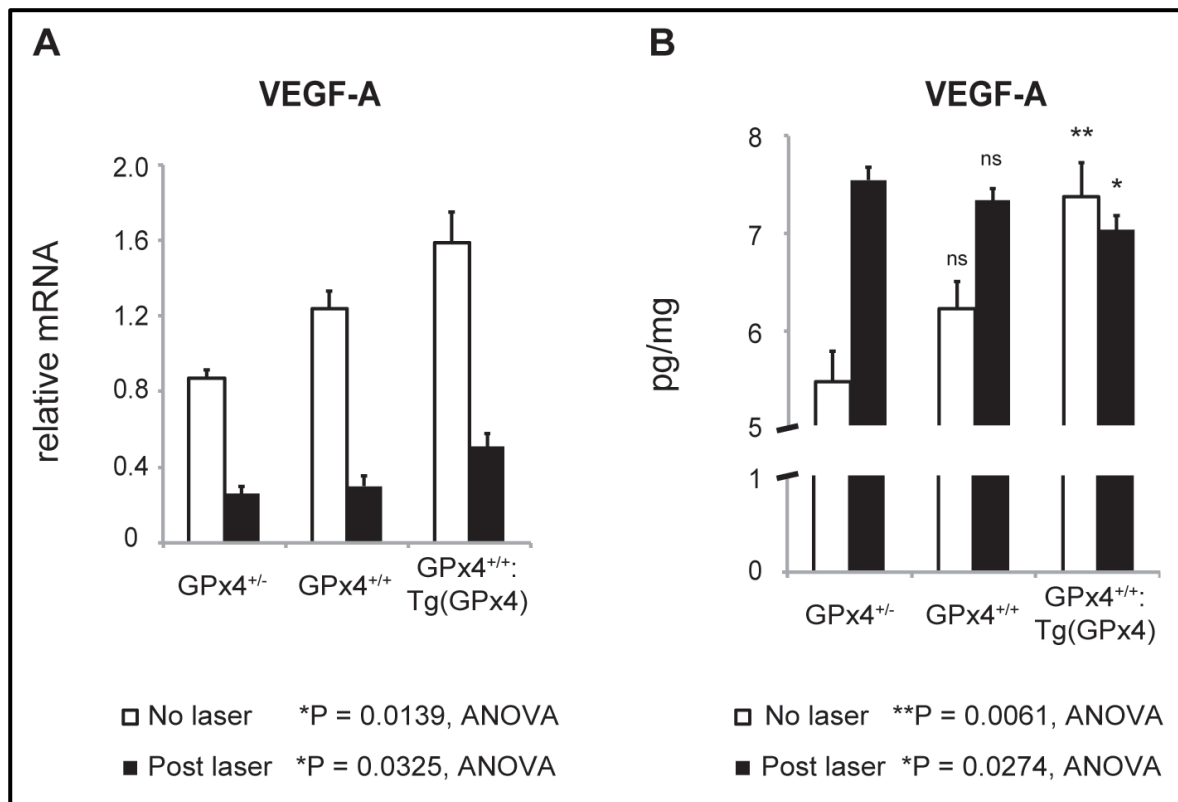


Figure 5.8. VEGF-A expression in the RPE/choroid before and after CNV induction. (A) Relative VEGF-A mRNA levels were measured by RT-PCR before and 3 days after the CNV induction by laser exposure. Mean \pm SEM, $n = 4-6$. P values for ANOVA are described inside the figure. A post hoc Tukey's test * $P < 0.05$, ns [not significant], compared with GPx4^{+/-} mice that underwent the same treatment. (B) VEGF-A protein expression in the RPE/choroid was measured by ELISA before and 3 days after the CNV induction. Mean \pm SEM, $n = 4-6$. P values for ANOVA are described inside the figure. A post hoc Tukey's test * $P < 0.05$, ** $P < 0.01$, ns [not significant], compared with GPx4^{+/-} mice that underwent the same treatment.

5.4 Discussion

The results of the current study demonstrated that GPx4 influences the regulation of VEGF-A expression in the RPE/choroid tissue not only after CNV induction, but also before laser was performed to induce CNV. This suggests that GPx4 might be enrolled in the regulation of VEGF in both physiologic and pathologic conditions. Furthermore, GPx4 confers protection against development of CNV in mice. Because the importance of VEGF in CNV has been well established both in animal studies and in studies using human subjects with CNV (Lambert et al., 2013; Rosenfeld et al., 2006), the role of GPx4 on the basis of VEGF was evaluated in this study. However, to date the relationship between antioxidant enzymes, VEGF-A, and CNV has not been completely understood.

Considering that cells are fully capable of upregulating the intrinsic activity of antioxidant enzymes to protect themselves against deleterious effects generated by oxidative stress reactions, different studies reported the importance of GPx4 opposing lipid peroxidation. In line with the literature, the present study demonstrated less accumulation of peroxidized lipids in the RPE/choroid of GPx4-overexpressing mice. Furthermore, lipid peroxidation varied according to the amount of GPx4 expressed in the mice. As the pathogenesis of CNV is associated with increased recruitment of inflammatory mediators and enhanced generation of ROS and AGEs, it is reasonable that GPx4 might play a role in the cellular defense against neovascularization.

GPx4^{+/-} mice and GPx4-overexpressing mice were used in the present study to evaluate the importance of GPx4. This strategy was used because it was not possible to produce live conditional knockout mice in which GPx4 expression was abrogated specifically in the RPE. A possible explanation for this might be that in the RPE65-Cre

mice used, Cre was expressed from the early stage of development. However, by using mice expressing different levels of GPx4, it was possible to clearly demonstrate the protective role of GPx4 against CNV.

With the objective of better perceiving the behavior of VEGF in CNV development, the time course of VEGF-A mRNA expression in the RPE/choroid tissue was explored. Although increased VEGF-A protein expression in mouse RPE/choroid tissue after CNV induction has been well established, the change in the VEGF-A mRNA level has not been thoroughly investigated. Only few reports describing the VEGF-A mRNA level in mice with laser-induced CNV were found in the literature. In two of them, the VEGF-A mRNA level increased three days after CNV induction (Liu et al., 2011; Mizutani et al., 2009) while in another one, no change was apparent during one week after CNV induction (Hu et al., 2009). In a recent comprehensive review on the methodology of the CNV model, the variation in VEGF-A mRNA levels was not discussed (Lambert et al., 2013). In the present study, using several different primer pairs, it was confirmed that VEGF-A mRNA is downregulated after CNV induction by laser treatment.

According to the literature, discrepancies between mRNA and protein levels can occur (Futcher et al., 1999; Gygi, et al., 1999). Based on the analysis of the different biochemical and physical contributors to the correlation of mRNA and protein abundance, mRNA levels explain around 40% of the variability in protein levels (Schwanhäusser et al., 2011). One of the reasons for this variance could be related to the complexity of post-transcriptional mechanisms (Greenbaum et al., 2003). During the course of the cell cycle, mRNA expression levels can vary or remain stable. Cho et al. (1998) showed that genes which presented a small variation in mRNA expression during the cell cycle tended to have little or no correlation with the final protein levels, while those that presented a large

variation of mRNA expression during the cell cycle had higher correlation between mRNA expression and protein levels (Cho et al., 1998). Another reason for discrepancies could be related to the levels of ribosomal occupancy (Greenbaum et al., 2003). Greenbaum et al. (2003) found no correlation between mRNA and proteins when the ribosomal occupancy rates were low (Arava et al., 2003). Moreover, the authors also showed that genes which were highly expressed tended to present higher correlation levels between mRNA expression and proteins. Another point to consider is the ability of genes to respond quickly to a stimulus. Several transcription factors and genes with specific function in the cell-cycle control have unstable mRNAs and proteins, which predispose them to rapid transcriptional or translational regulation (Schwanhäusser et al., 2011). Many genes with stable mRNAs but unstable proteins can be quickly regulated at translation. These observations are consistent with the idea that several fast responding genes have short protein or mRNA half-lives, which might contribute to the weak correlation between mRNA and protein levels.

By all those reasons, the discrepancy in the levels of mRNA and protein in the current study supports the post-translational regulation of VEGF. For example, the activation of proteolytic enzymes such as matrix metalloproteinase (MMP)-9 (Xu et al., 2012), and a disintegrin and a metalloproteinase domain (ADAM)-15 (Xie et al., 2008) regulate the extracellular VEGF protein levels and affect choroidal neovascularization. In addition, the RPE/choroid tissue consists of heterogeneous cellular components – the cells from the RPE, and the endothelial cells of the choroidal vessels – which naturally increase the complexity of such evaluation as variations of specific cellular populations are combined. Although the mechanism of VEGF regulation was beyond the scope of the current study, it is an interesting topic for a future investigation.

In agreement with the difference in GPx4 expression, a dose-dependent increase in VEGF-A protein expression in the RPE/choroid tissue under physiological conditions was observed. In contrast, as GPx4 expression increased, the elevation in VEGF-A protein level mediated by laser-induced CNV was suppressed. Consequently, after CNV induction, the VEGF-A protein levels were reduced in the GPx4-overexpressing mice. Under physiologic conditions, the decreased and increased VEGF-A protein expression in the GPx4^{+/-} and GPx4-overexpressing mice, respectively, were unexpected results. However, these changes could be associated with the established importance of VEGF that is known to maintain the physiologic choroidal vasculature (Kurihara et al., 2012). Furthermore, VEGF overexpression itself did not induce pathologic CNV (Oshima et al., 2004). On the other hand, the situation was completely different in the RPE/choroid tissue after CNV induction. The VEGF-A protein levels were significantly upregulated by CNV induction in the GPx4^{+/-} mice, while the levels did not significantly change in the GPx4 transgenic mice. This result confirms the notion that GPx4 could confer protection against CNV growth.

In the present study, the importance of GPx4 in the RPE/choroid tissue using a laser-induced CNV model was evaluated. Previously reports demonstrated that SOD1 knockout mice reportedly developed numerous age-related changes in the RPE/choroid tissue including naturally occurring CNV (Imamura et al., 2006; Xie et al., 2011) or ischemic retinopathy (Dong et al., 2009). The protective role of GPx4 against the oxidative stress in the retina was confirmed (Lu et al., 2009). However, the effect of an antioxidant enzyme on laser-induced CNV or VEGF-A expression in the RPE/choroid tissue is not completely clear. In a study evaluating the role of thioredoxin 1, laser was applied at the threshold intensity and the ratio of the number of CNV to the number of

laser spots was analyzed (Inomata et al., 2008). Because evaluating CNV size is the most widely accepted methodology for the laser-induced CNV model (Giani et al., 2011; Lambert et al., 2013), the present study demonstrated for the first time the importance of an endogenous antioxidant enzyme in a laser-induced CNV model with VEGF-A expression in the RPE/choroid tissue.

Finally, the current study revealed that GPx4 influences the expression of VEGF-A in the RPE/choroid tissue under both physiologic and pathologic conditions. Furthermore, GPx4 confers protection against CNV development *in vivo*. Therefore, GPx4 could be a potential target for CNV treatment.

6. Discussion

Different factors are closely associated with the development of AMD. Both genetic and environmental risk factors have been already established as contributors to the disease. The basis of the pathogenesis of AMD relies on the complex formed by the RPE, choroid and photoreceptor cells. There is a strong interaction among those structures, constantly exchanging metabolites and nutrients. The choroidal blood supply is fundamental for the RPE cells, while the photoreceptors depend on the RPE cells to maintain their physiologic activity and continued work of phototransduction. Therefore, the RPE cells represent the most important structure regulating the retinal environment, playing a crucial role in the abnormalities related to the pathogenesis of AMD.

Owing to the fact that AMD is characterized by progression, early stage disease usually advances to the late-stage AMD, either geographic atrophy or neovascular AMD. Thus, it was my interest to investigate the mechanisms associated with the senescence of RPE cells that might contribute to the pathogenesis of the disease.

On the basis of the results reported in this study, phagocytosis of POS protects the RPE cells against senescence-related modifications. Binding of POS to the RPE cells leads to the activation of PGC-1 α , which is responsible for increasing mitochondrial biogenesis and decreasing the generation of ROS in the treated cells. Additionally, higher expression of antioxidant enzymes in the RPE cells treated with POS was also demonstrated here. Supporting the results showed in this study, Mukherjee et al. (2007) described that POS phagocytosis was associated with increased refractoriness to oxidative stress-induced apoptosis in ARPE cells. Furthermore, Nandrot et al. (2004) reported that impaired

phagocytic activity of the RPE cells led to lipofuscin accumulation, which is associated with the aging phenomenon.

Autophagy is an important process associated with removal of cellular debris and damaged organelles (Kim et al., 2013). Functioning as a mechanism for cell repair, it is particularly important for long-lived postmitotic cells (Kim et al., 2013). It has been postulated that autophagy-related proteins are strongly expressed in the eye, suggesting this process is possibly critical for maintaining the health of the RPE and retina (Krohne et al., 2010). Furthermore, the accumulation of end metabolic products with age, such as oxidized lipids and lipofuscin, are considered to interfere with lysosomal degradative processes in RPE cells *in vitro*, suggesting that any interference with autophagy might be a possible mechanism for cellular dysfunction and progression of disease (Vives-Bauza et al., 2008).

The final step of autophagy process is lysosome-dependent. Intracellular constituents or any material undergoing autophagy are delivered for lysosomal degradation. Lysosomes are responsible for the synthesis and release of potent hydrolytic enzymes that will act on the autophagosome, thus originating the autophagolysosome (Kim et al., 2013).

Kim et al. (2013) described an association between POS phagocytosis by the RPE cells and autophagy. They demonstrated that in mice with Atg5-deficient RPE cells, phagosomes failed to move from the apical surface to the basal surface of the RPE cells, and most importantly, phagosome maturation as well as phagosome-lysosome fusion was defective in preventing degradation. As a consequence, disrupted POS degradation, diminished chromophore levels, and decreased visual function were observed. Therefore, POS phagocytosis and autophagy are linked to maintain a proper functioning of the visual

cycle. Additionally, Valapala et al. (2014) described that in mice with Cryba1-deficient RPE cells, lysosomal pH was elevated and cathepsin D activity was decreased, thereby blocking autophagy in their RPE cells. They also showed that loss of Cryba1, and the consequently interrupted lysosomal process, were associated with age-related abnormalities in the cellular architecture of RPE cells. Although no damage to autophagosome generation was observed, nor on to fusion with lysosomes, the terminal degradative stage of the autophagic process was inhibited.

TFEB is already known as regulator of the lysosomal biogenesis, positively controlling genes associated with the coordinate lysosomal expression and regulation network (Sardiello et al., 2009). The authors observed an increase in the expression of different lysosomal genes after TFEB overexpression. Following the same behavior, activity of lysosomal enzymes, such as cathepsin D, was demonstrated to be significantly enhanced after overexpression of TFEB. Additionally, the abrogation of TFEB activity using a specific siRNA to KD TFEB expression was associated with the downregulation of different lysosomal genes. Accordingly, cytosolic TFEB translocated to the nucleus in response to abnormal lysosomal storage conditions, resulting in activation of its target genes. Thus, the nuclear translocation of TFEB is considered an important mechanism of TFEB activation (Sardiello et al., 2009).

The results of the present study suggest that PGC-1 α , activated by the binding of POS to the α v β 5 integrin receptor, is associated with the activation of TFEB in the RPE cells. Nuclear staining of RPE cells with TFEB antibody was strongly decreased by the abrogation of PGC-1 α expression. Additionally, the KD of PGC-1 α in the RPE cells downregulated the expression of TFEB-target genes. Following the same tendency, cathepsin D activity was also significantly decreased in the RPE cells deprived of PGC-1 α expression.

TFEB has been proved to be associated with autophagy, despite its role in lysosomal biogenesis coordination. Settembre et al. (2011) demonstrated that TFEB overexpression significantly increased the number of autophagosomes *in vitro*. This increase persisted even when cells were treated with specific lysosomal inhibitors of autophagosomes and degradation. The sustained elevation indicated that TFEB activates the formation of autophagosomes. Additionally, the KD of TFEB expression *in vitro* using siRNA resulted in decreased levels of autophagy-related protein in either normal or starved conditions, and in the presence or absence of lysosomal inhibitors of autophagosomes. This suggests that the biogenesis of autophagosomes and lysosomes are coregulated by TFEB (Settembre et al., 2011). They also evaluated the delivery of autophagosomes to lysosomes, demonstrating that the number of autophagolysosomes was higher in cells overexpressing TFEB than in control ones, indicating that the autophagic flux was directly increased by TFEB. In accordance with that, overexpression of TFEB also enhanced the degradation of long-lived proteins, while the KD of TFEB decreased its degradation (Settembre et al., 2011).

Considering the fact that impaired lysosomal activity leads to abnormal accumulation of lipids as a consequence of the inability to proceed to an efficient degradation of internalized POS in the RPE cells, the role of PGC-1 α in POS degradation was also evaluated. It was demonstrated in the current study that PGC-1 α protects the RPE cells against intracellular lipid accumulation. Furthermore, PGC-1 α was also associated with a protective role against the accumulation of peroxidized lipids in the RPE cells after POS treatment.

In agreement with these findings, PGC-1 α KO mice demonstrated important features of senescence in the RPE cells, choriocapillaris and Bruch's membrane. Moreover, choriocapillaris atrophy and lipofuscin accumulation were also observed in the mice

lacking PGC-1 α expression. It is important to remember that VEGF has a physiologic role in the development of the choroidal blood vessels. According to Ueta et al. (2012b), PGC-1 α is a regulator of VEGF expression in RPE cells following POS phagocytosis. Thus, in the early-stage AMD, PGC-1 α plays a physiologic role in the maintenance of the choriocapillaris. However, in the late-stage neovascular AMD, the overexpression of VEGF is associated with a pathologic effect on the generation of abnormal choroidal blood vessels, and PGC-1 α may possibly contribute to this scenario.

In the late stage neovascular AMD, characterized by choroidal neovascularization, dysregulation of growth factor secretion by the RPE cells is one of the most important factors in the pathogenesis of the disease. Hypoxia, wound healing processes following the loss of RPE cells and inflammation have been implicated in the establishment of CNV (Strauss, 2005). Although different types of growth factors have been associated with CNV, the most important angiogenic factor responsible for the development of abnormal choroidal blood vessels is VEGF. Different studies have demonstrated the RPE cells to be the most important source of VEGF secretion in CNV (Strauss, 2005). RPE cells of patients with vascular AMD show higher secretion rates of VEGF when compared with those of patients without CNV (Strauss et al., 2003).

Two pathways have been associated with the generation of VEGF in the RPE cells: one is mediated by the complement system, and the other one is regulated by oxidative stress. Both of them have been described as intermediating the production of VEGF (Ambati and Fowler, 2012). Although independently regulating the VEGF secretion, oxidative stress and complement system can work synergistically in the generation of choroidal and retinal new blood vessels. Oxidative stress might stimulate the complement-induced secretion of VEGF in the RPE cells (Thurman et al., 2009). Besides VEGF, many vascular molecules secreted by the RPE are capable of potentiating VEGF secretion in

response to the activation of complement system (Fukuoka et al., 2003) and oxidative stress (Higgins et al., 2003). RPE cells are constantly exposed to a wide variety of stressors, which contributes to impairment of their physiologic role in the maintenance of the surrounding structures. Damaged RPE cells then originate a proinflammatory environment, considered a key modulator of CNV development and progression. Besides induction of proangiogenic VEGF, active complement factors start recruiting leukocytes to the choroidal tissue (Nozaki et al., 2006). Thus, oxidative stress imposed on the RPE cells by the photo-oxidation products activates the complement system, contributing to the establishment of neovascularization.

According to the results demonstrated in the present study, GPx4 expression is strongly associated with protection against CNV. Not only was the size of the CNV lesions influenced by the antioxidant molecule, but the expression of VEGF was also regulated by GPx4.

It is important to remember that isolated VEGF overexpression in the RPE cells is not sufficient for the development of CNV. For CNV to be successfully established, it is necessary that both the Bruch's membrane and the RPE cells to be compromised, allowing the growth of abnormal new blood vessels towards the retina (Oshima et al., 2004). In agreement with the literature, the current study reported that in physiologic conditions, the expression of VEGF, although increased, was not associated with the development of CNV. Probably the presence of intact and fully functional RPE cells and Bruch's membrane contributed to the maintenance of the health status. Additionally, VEGF expression is needed for the normal development of the choroidal vasculature. On the other hand, the situation changes completely when it comes to the pathologic scenario. After laser-induced CNV, the overexpression of GPx4 significantly downregulated the expression of VEGF; thus, protecting against CNV formation.

Aging-related changes in the RPE cells, which are responsible for lipofuscin accumulation, impaired POS degradation by the autophagy/lysosomal pathway, leading to generation of ROS, decreased mitochondrial function and lipid accumulation. Consequently, the RPE structure becomes compromised, which contributes to the establishment of the new blood vessel growth from the choroid. Oxidative stress is also associated with the accumulation of AGEs in the Bruch's membrane. The developing neovascular tissue shows high expression of AGEs, while the RPE cells contain active receptors for AGEs in the basal membrane. Thus, RPE cells are fully capable of secreting VEGF in response to AGEs exposure (Handa et al., 1999; Lu et al., 1998), contributing to the development of neovascularization.

7. Conclusions

The results of the present study demonstrate for the first time the existence of a specific pathway responsible for the degradation of POS by the RPE cells. Accordingly, binding of POS activates the $\alpha v\beta 5$ integrin/FAK/PGC-1 α signaling route in the RPE, stimulating the intracellular digestion of the internalized POS by lysosomal activity, protecting the cells against metabolic stress. Recognition of POS is associated with an antisenescence effect in the RPE cells. This is particularly important in the scenario of the early stage AMD, wherein aging of RPE cells represents the basis of the pathogenesis of the disease. Thus, this pathway may represent a possible target for future therapeutic interventions in early stage AMD, avoiding the progression of the disease.

The current study also disclosed for the first time the protective effect of the antioxidant enzyme GPx4 in the regulation of VEGF expression in the RPE/choroid. GPx4 was shown to regulate VEGF levels in both physiologic and pathologic conditions. Moreover, GPx4 showed a protective effect in the development of CNV. Therefore, GPx4 may be a potential target for the treatment of late stage neovascular AMD.

8. Clinical Viewpoints and Future Perspective

The current research confirmed important roles of PGC-1 α combating the aging process in the RPE cells. This study suggests that insufficient induction of PGC-1 α in response to POS binding may be an important factor for the aging of RPE cells. In addition, aged phenotypes in RPE of PGC-1 α -deficient mice were firstly revealed. Therefore, enforcing PGC-1 α activity may be a preventive measure for the development of AMD, a major cause of blindness worldwide. Well-known activators of PGC-1 α among nutrients and lifestyle modifications include resveratrol, polyphenol (Wang et al., 2014), calorie restriction (Martin-Montalvo and de Cabo, 2013), and endurance exercise (Pilegaard et al., 2003; Suwa et al., 2008). These PGC-1 α -activating factors need to be further evaluated for the potential anti-aging effects in RPE cells.

Another point investigated in the current study was the role of GPx4 in a mouse model of neovascular AMD. For the next step, the effect of the augmented GPx4 expression using a virus vector for the inhibition of CNV should be elucidated in the future.

9. Bibliography

- Adamis, A.P., Shima, D.T., Yeo, K.T., Yeo, T.K., Brown, L.F., Berse, B., . . . Folkman, J. (1993). Synthesis and secretion of vascular permeability factor/vascular endothelial growth factor by human retinal pigment epithelial cells. *Biochemical and Biophysical Research Communication*, *193*, 631–638.
- Age-Related Eye Disease Study Research Group. (2000). Risk factors associated with age-related macular degeneration: a case-control study in the age-related eye disease study: Age-Related Eye Disease Study Report Number 3. *Ophthalmology*, *107*, 2224–2232.
- Age-Related Eye Disease Study Research Group. (2001). A randomized, placebo-controlled, clinical trial of high-dose supplementation with vitamins C and E, β -carotene, and zinc for age-related macular degeneration and vision loss: AREDS report no. 8. *Archives of Ophthalmology*, *119*, 1417–1436.
- Age-Related Eye Disease Study 2 Research Group. (2013). Lutein + zeaxanthin and omega-3 fatty acids for age-related macular degeneration: The age-related eye disease study 2 (AREDS2) randomized clinical trial. *The Journal of the American Medical Association*, *309*, 2005–2015.
- Ambati, J., Ambati, B.K., Yoo, S.H., Ianchulev, S., & Adamis, A.P. (2003). Age-related macular degeneration: etiology, pathogenesis, and therapeutic strategies. *Survey of Ophthalmology*, *48*, 257–293.
- Ambati, J., & Fowler, B.J. (2012). Mechanisms of age-related macular degeneration. *Neuron*, *75*, 26–39.
- Arany, Z., Foo, S.Y., Ma Y., Ruas, J.L., Bommi-Reddy, A., Girnun, G., . . . Spiegelman, B.M.

- (2008). HIF-independent regulation of VEGF and angiogenesis by the transcriptional coactivator PGC-1 alpha. *Nature*, *451*, 1008–1012.
- Arany, Z., He, H., Lin, J., Hoyer, K., Handschin, C., Toka, O., . . . Spiegelman, B.M. (2005). Transcriptional coactivator PGC-1 alpha controls the energy state and contractile function of cardiac muscle. *Cell Metabolism*, *1*, 259–271.
- Arava, Y., Wang, Y., Storey, J.D., Liu, C.L., Brown, P.O., & Herschlag, D. (2003). Genome-wide analysis of mRNA translation profiles in *saccharomyces cerevisiae*. *Proceedings of the National Academy of Sciences of the United States of America*, *100*, 3889–94.
- Association for Research in Vision and Ophthalmology (ARVO). (1994). ARVO statement for the use of animals in ophthalmic and visual research. *Investigative Ophthalmology & Visual Sciences*, *35*, v–vi.
- Beatty, S., Boulton, M., Henson, D., Koh, H.H., & Murray, I.J. (1999). Macular pigment and age related macular degeneration. *British Journal of Ophthalmology*, *83*, 867–877.
- Beatty, S., Murray, I.J., Henson, D.B., Carden, D., Koh, H., & Boulton, M.E. (2001). Macular pigment and risk for age-related macular degeneration in subjects from a Northern European population. *Investigative Ophthalmology & Visual Sciences*, *42*, 439–446.
- Bibb, C., & Young, R.W. (1974). Renewal of fatty acids in the membranes of visual cell outer segments. *Journal of Cell Biology*, *61*, 327–343.
- Biesemeier, A., Taubitz, T., Julien, S., Yoeruek, E., & Schraermeyer, U. (2014). Choriocapillaris breakdown precedes retinal degeneration in age-related macular degeneration. *Neurobiology of Aging*, *35*, 2562–2573.
- Blaauwgeers, H.G., Holtkamp, G.M., Rutten, H., Witmer, A.N., Koolwijk, P., Partanen, T.A., . . . Schlingemann, R.O. (1993). Polarized vascular endothelial growth factor secretion by human retinal pigment epithelium and localization of vascular endothelial growth factor

- receptors on the inner choriocapillaris. Evidence for a trophic paracrine relation. *American Journal of Pathology*, 155, 421–428
- Bok, D. (1993). The retinal pigment epithelium: a versatile partner in vision. *Journal of Cell Science Supplement*, 17, 189–195.
- Bora, N.S., Matta, B., Lyzogubov, V.V., & Bora, P.S. (2014). Relationship between the complement system, risk factors and prediction models in age-related macular degeneration. *Molecular Immunology*, 63, 176–183.
- Boulton, M. (1998). The role of melanin in the RPE. In M.F. Marmor & T.J. Wolfensberger (Eds.), *The Retinal Pigment Epithelium*, (pp. 68–65). Oxford: University Press.
- Bowes Rickman, C., Farsiu, S., Toth, C.A., & Klingeborn, M. (2013). Dry age-related macular degeneration: mechanisms, therapeutic targets, and imaging. *Investigative Ophthalmology & Visual Sciences*, 13, 54, 68–80.
- Bressler N. M., Bressler S. B. (2013a). Neovascular (Exsudative or “Wet”) Age-Related Macular Degeneration. In A.P. Schachat & S.R. Sadda (Eds.). *Retina*. (pp 1183–1212). Oxford: Elsevier.
- Bressler S. B., & Bressler N. M. (2013b). Age-related Macular Degeneration: Non-neovascular Early MD, Intermediate ARMD, and Geographic Atrophy. In A.P. Schachat & S.R. Sadda (Eds.). *Retina*. (pp 1150–1182). Oxford: Elsevier.
- Burke, J.M., & Zareba, M. (2009). Sublethal photic stress and the motility of RPE phagosomes and melanosomes. *Investigative Ophthalmology & Visual Sciences*, 50, 1940–1947.
- Burns, M.S., & Hartz, M.J. (1992). The retinal pigment epithelium induces fenestration of endothelial cells *in vivo*. *Current Eye Research*, 11, 863–873.

- Cao, W., Tombran-Tink, J., Elias, R., Sezate, S., Mrazek, D., & McGinnis, J.F. (2001). *In vivo* protection of photoreceptors from light damage by pigment epithelium-derived factor. *Investigative Ophthalmology & Visual Sciences*, *42*, 1646–1652.
- Chew, E.Y., Clemons, T.E., Agro'n, E., Sperduto, R.D., Sangiovanni, J.P., Kurinij, N., & Davis, M.D. (2013). Long-term effects of vitamins C and E, b-carotene, and zinc on age-related macular degeneration: AREDS report no. 35. *Ophthalmology*, *120*, 1604–1611.
- Cho, R.J., Campbell, M.J., Winzler, E.A., Steinmetz, L., Conway, A., Wodicka, L., . . . Davis, R.W. (1998). A genome-wide transcriptional analysis of the mitotic cell cycle. *Molecular Cell*, *2*, 65–73.
- Chowers, I., Kim, Y., Farkas, R.H., Gunatilaka, T.L., Hackam, A.S., Campochiaro, P.A., . . . Zack, D.J. (2004). Changes in retinal pigment epithelial gene expression induced by rod outer segment uptake. *Investigative Ophthalmology & Visual Sciences*, *45*, 2098–2106.
- Cuervo, A.M., Bergamini, E., Brunk, U.T., Dröge, W., Ffrench, M., & Terman, A. (2005). Autophagy and aging: the importance of maintaining “clean” cells. *Autophagy*, *1*, 131–140.
- Curcio, C.A., Sloan, K.R., Kalina, R., & Hendrickson, A.E. (1990). Human photoreceptor topography. *Journal of Comparative Neurology*, *292*, 497–523.
- de Jong, P.T. (2006). Age-related macular degeneration. *The New England Journal of Medicine*, *355*, 1474–1485.
- Delori, F.C., Goger, D.G., & Dorey, C.K. (2001). Age-related accumulation and spatial distribution of lipofuscin in RPE of normal subjects. *Investigative Ophthalmology & Visual Sciences*, *42*, 1855–1866.

- Dong, A., Xie, B., Shen, J., Yoshida, T., Yokoi, K., Hackett, S.F., & Campochiaro, P.A. (2009). Oxidative stress promotes ocular neovascularization. *Journal of Cell Physiology*, *219*, 544–552.
- Dunn, K.C., Aotaki-Ken, A.E., Putkey, F.R., & Hjelmeland, L.M. (1996). A human retinal pigment epithelial cell line with differentiated properties. *Experimental Eye Research*, *62*, 155–169.
- Dunn, K.C., Marmorstein, A.D., Bonilha, V.L., Rodriguez-Boulan, E., Giordano, F., & Hjelmeland, L.M. (1998). Use of ARPE-19 cell line as a model of RPE polarity: basolateral secretion of FGF5. *Investigative Ophthalmology & Visual Sciences*, *39*, 2744–2749.
- Ebrahem, Q., Renganathan, K., Sears, J., VasANJI, A., Gu, X., Lu, L., . . . Anand-Apte, B. (2006). Carboxyethylpyrrole oxidative protein modifications stimulate neovascularization: Implications for age-related macular degeneration. *Proceedings of the National Academy of Sciences of the United States of America*, *103*, 13480–13484.
- Feeney, L. (1978). Lipofuscin and melanin of human retinal pigment epithelium. Fluorescence, enzyme cytochemical, and ultrastructural studies. *Investigative Ophthalmology & Visual Sciences*, *17*, 583–600.
- Feng, W., Yasumura, D., Matthes, M.T., LaVail, M.M., & Vollrath, D. (2002). Mertk triggers uptake of photoreceptor outer segments during phagocytosis by cultured retinal pigment epithelial cells. *The Journal of Biological Chemistry*, *277*, 17016–17022.
- Finnemann, S.C. (2003). Focal adhesion kinase signaling promotes phagocytosis of integrin-bound photoreceptors. *The European Molecular Biology Organization Journal*, *22*, 4143–4154.
- Finnemann, S.C., Bonilha, V.L., Marmorstein, A.D., & Rodriguez-Boulan, E. (1997). Phagocytosis of rod outer segments by retinal pigment epithelial cells requires

- alpha(v)beta5 integrin for binding but not for internalization. *Proceedings of the National Academy of Sciences of the United States of America*, 94, 12932–12937.
- Finnemann S.C., & Nandrot E.F. (2006). MerTK activation during RPE phagocytosis *in vivo* requires $\alpha\beta 5$ integrin. *Advances in Experimental and Medical Biology*, 572, 499–503.
- Finnemann, S.C., & Rodriguez-Boulan, E. (1999). Macrophage and retinal pigment epithelium phagocytosis: apoptotic cells and photoreceptors compete for $\alpha\beta 3$ and $\alpha\beta 5$ integrins, and protein kinase C regulates $\alpha\beta 5$ binding and cytoskeletal linkage. *The Journal of Experimental Medicine*, 190, 861–874.
- Finnemann, S.C., & Silverstein, R.L. (2001). Differential roles of CD36 and alphavbeta5 integrin in photoreceptor phagocytosis by the retinal pigment epithelium. *The Journal of Experimental Medicine*, 194, 1289–1298.
- Friedman, D.S., O’Colmain, B.J., Muñoz, B., Tomany, S.C., McCarty, C., de Jong, P.T., . . . Kempen, J. (2004). Eye Diseases Prevalence Research Group. Prevalence of age-related macular degeneration in the United States. *Archives of Ophthalmology*, 122, 564–572.
- Fukuoka, Y., Strainic, M., & Medof, M.E. (2003). Differential cytokine expression of human retinal pigment epithelial cells in response to stimulation by C5a. *Clin Exp Immunol*, 131, 248–253.
- Futcher, B., Latter, G.I., Monardo, P., McLaughlin, C.S. & Garrels, J.I. (1999). A sampling of the yeast proteome. *Molecular Cell Biology*, 19, 7357–7368.
- Gao, H., & Hollyfield, J.G. (1992). Aging of the human retina. Differential loss of neurons and retinal pigment epithelial cells. *Investigative Ophthalmology & Visual Sciences*, 33, 1–17.
- Giani, A., Thanos, A., Roh, M.I., Connolly, E., Trichonas, G., Kim, I., . . . Miller, J.W. (2011). *In vivo* evaluation of laser-induced choroidal neovascularization using spectral domain

- optical coherence tomography. *Investigative Ophthalmology & Visual Sciences*, 52, 3880–3887.
- Greenbaum, D., Colangelo, C., Williams, K., & Gerstein, M. (2003). Comparing protein abundance and mRNA expression levels on a genomic scale. *Genome Biology*, 4, 117, 1–8.
- Gygi, S.P., Rochon, Y., Franza, B.R. & Aebersold, R. (1999). Correlation between protein and mRNA abundance in yeast. *Molecular Cell Biology*, 19, 1720–1730.
- Hageman, G.S., Luthert, P.J., Victor Chong, N.H., Johnson, L.V., Anderson, D.H., & Mullins, R.F. (2001). An integrated hypothesis that considers drusen as biomarkers of immune-mediated processes at the RPE — Bruch’s membrane interface in aging and age-related macular degeneration. *Progress in Retinal and Eye Research*, 20, 705–732.
- Hall, M.O., & Abrams, T. (1987). Kinetic studies of rod outer segment binding and ingestion by cultured rat RPE cells. *Experimental Eye Research*, 45, 907–922.
- Handa, J.T. (2012). How does the macula protect itself from oxidative stress? *Molecular Aspects of Medicine*, 33, 418–435.
- Handa, J.T., Verzijl, N., Matsunaga, H., Aotaki-Keen, A., Luttj, G.A., te Koppele, J.M., . . . Hjelmeland, L.M. (1999). Increase in the advanced glycation end product pentosidine in Bruch’s membrane with age. *Investigative Ophthalmology & Visual Sciences*, 40, 775–779.
- Handschin, C., & Spiegelman, B.M. (2006). Peroxisome proliferator-activated receptor gamma coactivator 1 coactivators, energy homeostasis, and metabolism. *Endocrine Reviews*, 27, 728–735.
- Hara, R., Inomata, Y., Kawaji, T., Sagara, N., Inatani, M., Fukushima, M., & Tanihara, H. (2010). Suppression of choroidal neovascularization by N-acetyl-cysteine in mice. *Current Eye Research*, 35, 1012–1020.

- Higgins, G.T., Wang, J.H., Dockery, P., Cleary, P.E., & Redmond, H.P. (2003). Induction of angiogenic cytokine expression in cultured RPE by ingestion of oxidized photoreceptor outer segments. *Investigative Ophthalmology & Visual Sciences*, *44*, 1775–1782.
- Hildebrand, G.D., & Fielder, A.R. (2011). Anatomy and physiology of the retina. In J. Reynolds & S. Olitsky (Eds.), *Pediatric Retina* (pp. 39-65). Berlin: Springer-Verlag.
- Hu, W., Criswell, M.H., Fong, S.L., Temm, C.J., Rajashekhar, G., Cornell, T.L., & Clauss, M.A. (2009). Differences in the temporal expression of regulatory growth factors during choroidal neovascular development. *Experimental Eye Research*, *88*, 79–91.
- Imai, H., Hakkaku, N., Iwamoto, R., Suzuki, J., Suzuki, T., Tajima, Y., . . . Nakagawa, Y. (2009). Depletion of selenoprotein GPx4 in spermatocytes causes male infertility in mice. *The Journal of Biological Chemistry*, *284*, 32522–32532.
- Imai, H., Hirao, F., Sakamoto, T., Sekine, K., Mizukura, Y., Saito, M., . . . Nakagawa, Y. (2003). Early embryonic lethality caused by targeted disruption of the mouse PHGPx gene. *Biochemistry and Biophysical Research Communications*, *305*, 278–286.
- Imai, H., Suzuki, K., Ishizaka, K., Ichinose, S., Oshima, H., Okayasu, I., . . . Nakagawa, Y. (2001). Failure of the expression of phospholipid hydroperoxide glutathione peroxidase in the spermatozoa of human infertile males. *Biology of Reproduction*, *64*, 674–683.
- Imamura, Y., Noda, S., Hashizume, K., Shinoda, K., Yamaguchi, M., Uchiyama, S., . . . Tsubota, K. (2006). Drusen, choroidal neovascularization, and retinal pigment epithelium dysfunction in SOD1-deficient mice: a model of age-related macular degeneration. *Proceedings of the National Academy of Sciences of the United States of America*, *103*, 11282–11287.

- Inomata, Y., Tanihara, H., Tanito, M., Okuyama, H., Hoshino, Y., Kinumi, T., . . . Nakamura, H. (2008). Suppression of choroidal neovascularization by thioredoxin-1 via interaction with complement factor H. *Investigative Ophthalmology & Visual Sciences*, *49*, 5118–5125.
- Jager, R.D., Mieler, W.F., & Miller, J.W. (2008). Age-related macular degeneration. *The New England Journal of Medicine*, *358*, 2606–2617.
- Jager, S., Handschin, C., St-Pierre, J., & Spiegelman, B.M. (2007). AMP-activated protein kinase (AMPK) action in skeletal muscle via direct phosphorylation of PGC-1alpha. *Proceedings of the National Academy of Sciences of the United States of America*, *104*, 12017–12022.
- Kaarniranta, K., Sinha, D., Blasiak, J., Kauppinen, A., Veréb, Z., Salminen, A., . . . Petrovski, G. (2013). Autophagy and heterophagy dysregulation leads to retinal pigment epithelium dysfunction and development of age-related macular degeneration. *Autophagy*, *9*, 973–984.
- Kahn, H.A., Leibowitz, H.M., Ganley, J.P., Kini, M.M., Colton, T., Nickerson, R.S., & Dawber, T.R. (1977). The Framingham Eye Study. I. Outline and major prevalence findings. *American Journal of Epidemiology*, *106*, 17–32.
- Kannan, R., Zhang, N., Sreekumar, P.G., Spee, C.K., Rodriguez, A., Barron, E., & Hinton, D.R. (2006). Stimulation of apical and basolateral VEGF-A and VEGF-C secretion by oxidative stress in polarized retinal pigment epithelial cells. *Molecular Vision*, *12*, 1649–1659.
- Kawasaki, R., Yasuda, M., Song, S.J., Chen, S.J., Jonas, J.B., Wang, J.J., . . . Wong, T.Y. (2010). The prevalence of age-related macular degeneration in Asians: a systematic review and meta-analysis. *Ophthalmology*, *117*, 921–927.
- Kim, J.Y., Zhao, H., Martinez, J., Doggett, T.A., Kolesnikov, A.V., Tang, P.H., . . . Ferguson, T.A. (2013). Noncanonical autophagy promotes the visual cycle. *Cell*, *154*, 365–376.

- King, G.L., & Suzuma, K. (2000). Pigment-epithelium-derived factor—a key coordinator of retinal neuronal and vascular functions. *The New England Journal of Medicine*, *342*, 349–351.
- Klaver, C.C., Wolfs, R.C., Vingerling, J.R., Hofman, A., & de Jong, P.T. (1998). Age-specific prevalence and causes of blindness and visual impairment in an older population: the Rotterdam Study. *Archives of Ophthalmology*, *116*, 653–658.
- Klein, R., Klein, B.E., & Linton, K.L. (1992). Prevalence of age-related maculopathy: the Beaver Dam Eye Study. *Ophthalmology*, *99*, 933–943.
- Koike, M., Shibata, M., Ohsawa, Y., Nakanishi, H., Koga, T., Kametaka, S., . . . Uchiyama, Y. (2003). Involvement of two different cell death pathways in retinal atrophy of cathepsin D-deficient mice. *Molecular and Cellular Neurosciences*, *22*, 146–161.
- Koltai, E., Hart, N., Taylor, A.W., Goto, S., Ngo, J.K., Davies, K.J., & Radak, Z. (2012). Age-associated declines in mitochondrial biogenesis and protein quality control factors are minimized by exercise training. *American Journal of Physiology - Regulatory, Integrative and Comparative Physiology*, *303*, 127–134.
- Krohne, T.U., Stratmann, N.K., Kopitz, J., & Holz, F.G. (2010). Effects of lipid peroxidation products on lipofuscinogenesis and autophagy in human retinal pigment epithelial cells. *Experimental Eye Research*, *90*, 465–471.
- Kurihara, T., Westenskow, P.D., Bravo, S., Aguilar, E., & Friedlander, M. (2012). Targeted deletion of Vegfa in adult mice induces vision loss. *The Journal of Clinical Investigation*, *122*, 4213–4217.
- Kurz, T., Terman, A., Gustafsson, B., & Brunk, U.T. (2008). Lysosomes and oxidative stress in aging and apoptosis. *Biochimica et Biophysica Acta*, *1780*, 1291–1303.

- Lambert, V., Lecomte, J., Hansen, S., Blacher, S., Gonzalez, M.L., Struman, I., . . . Noel, A. (2013). Laser induced choroidal neovascularization model to study age-related macular degeneration in mice. *Nature Protocols*, *11*, 2197–2211.
- LaVail, M.M. (1976). Rod outer segment disk shedding in rat retina: relationship to cyclic lighting. *Science*, *194*, 1071–1074.
- Lehman, J.J., Barger, P.M., Kovacs, A., Saffitz, J.E., Medeiros, D.M., & Kelly, D.P. (2002). Peroxisome proliferator-activated receptor gamma coactivator-1 promotes cardiac mitochondrial biogenesis. *The Journal of Clinical Investigation*, *106*, 847–56.
- Leone, T.C., Lehman, J.J., Finck, B.N., Schaeffer, P.J., Wende, A.R., Boudina, S., . . . Kelly, D.P. (2005). PGC-1alpha deficiency causes multi-system energy metabolic derangements: muscle dysfunction, abnormal weight control and hepatic steatosis. *PLOS Biology*, *3*, e101.
- Lin, J., Wu, H., Tarr, P.T., Zhang, C.Y., Wu, Z., Boss, O., . . . Spiegelman, B.M. (2002). Transcriptional co-activator PGC-1 alpha drives the formation of slow-twitch muscle fibres. *Nature*, *418*, 797–801.
- Lin, J., Wu, P.H., Tarr, P.T., Lindenberg, K.S., St-Pierre, J., Zhang, C.Y., . . . Spiegelman, B.M. (2004). Defects in adaptive energy metabolism with CNS-linked hyperactivity in PGC-1alpha null mice. *Cell* *119*, 121–135.
- Liu, C., Li, S., Liu, T., Borjigin, J., & Lin, J.D. (2007). Transcriptional coactivator PGC-1alpha integrates the mammalian clock and energy metabolism. *Nature*, *447*, 477–481.
- Liu, J., Jha, P., Lyzogubov, V.V., Tytarenko, R.G., Bora, N.S., & Bora, P.S. (2011). Relationship between complement membrane attack complex, chemokine (C-C motif) ligand 2 (CCL2) and vascular endothelial growth factor in mouse model of laser-induced choroidal neovascularization. *The Journal of Biological Chemistry*, *286*, 20991– 21001.

- Lopez, P.F., Sippy, B.D., Lambert, H.M., Thach, A.B., & Hinton, D.R. (1996). Transdifferentiated retinal pigment epithelial cells are immunoreactive for vascular endothelial growth factor in surgically excised age-related macular degeneration-related choroidal neovascular membranes. *Investigative Ophthalmology & Visual Sciences*, *37*, 855–868.
- Lu, L., Oveson, B.C., Jo, Y.J., Lauer, T.W., Usui, S., Komeima, K., . . . Campochiaro, P.A. (2009). Increased expression of glutathione peroxidase 4 strongly protects retina from oxidative damage. *Antioxidants & Redox Signaling*, *11*, 715–724.
- Lu, M., Kuroki, M., Amano, S., Tolentino, M., Keough, K., Kim, I., . . . Adamis, A.P. (1998). Advanced glycation end products increase retinal vascular endothelial growth factor expression. *The Journal of Clinical Investigation*, *101*, 1219–1224.
- Marosi, K., Bori, Z., Hart, N., Sárga, L., Koltai, E., Radák, Z., & Nyakas, C. (2012). Long-term exercise treatment reduces oxidative stress in the hippocampus of aging rats. *Neuroscience*, *226*, 21–8.
- Martin-Montalvo, A., & de Cabo, R. (2013). Mitochondrial metabolic reprogramming induced by calorie restriction. *Antioxidants & Redox Signaling*, *19*, 310–320.
- Mazzoni, F., Safa, H., & Finnemann, S.C. (2014). Understanding photoreceptor outer segment phagocytosis: use and utility of RPE cells in culture. *Experimental Eye Research*, *126*, 51–60.
- McBee, J.K., Palczewski, K., Baehr, W., & Pepperberg, D.R. (2001). Confronting complexity: the interlink of phototransduction and retinoid metabolism in the vertebrate retina. *Progress in Retinal and Eye Research*, *20*, 469–529.
- Mizutani, T., Ashikari, M., Tokoro, M., Nozaki, M., & Ogura, Y. (2009). Suppression of laser-induced choroidal neovascularization by a CCR3 antagonist. *Investigative Ophthalmology & Visual Sciences*, *54*, 1564–1572.

- Mukherjee, P.K., Marcheselli, V.L., de Rivero Vaccari, J.C., Gordon, W.C., Jackson, F.E., & Bazan, N.G. (2007). Photoreceptor outer segment phagocytosis attenuates oxidative stress-induced apoptosis with concomitant neuroprotectin D1 synthesis. *Proceedings of the National Academy of Sciences of the United States of America*, *104*, 13158–13163.
- Nakahira, K., Haspel, J.A., Rathinam, V.A., Lee, S.J., Dolinay, T., Lam, H.C., . . . Choi, A.M. (2011). Autophagy proteins regulate innate immune responses by inhibiting the release of mitochondrial DNA mediated by the NALP3 inflammasome. *Nature Immunology*, *12*, 222–230.
- Nandrot, E.F., Kim, Y., Brodie, S.E., Huang, X., Sheppard, D., & Finnemann, S.C. (2004). Loss of synchronized retinal phagocytosis and age-related blindness in mice lacking $\alpha v \beta 5$ integrin. *The Journal of Experimental Medicine*, *200*, 1539–1545.
- Nandrot, E.F., Silva, K.E., Scelfo, C., & Finnemann, S.C. (2012). Retinal pigment epithelial cells use a MerTK-dependent mechanism to limit the phagocytic particle binding activity of $\alpha v \beta 5$ integrin. *Biology of the Cell*, *104*, 326–341.
- Neff, F., Flores-Dominguez, D., Ryan, D.P., Horsch, M., Schröder, S., Adler, T., . . . Ehninger, D. (2013). Rapamycin extends murine lifespan but has limited effects on aging. *The Journal of Clinical Investigation*, *123*, 3272–3291.
- Nguyen-Legros, J., & Hicks, D. (2000). Renewal of photoreceptor outer segments and their phagocytosis by the retinal pigment epithelium. *International Review of Cytology*, *196*, 245e313.
- Nozaki, M., Raisler, B.J., Sakurai, E., Sarma, J.V., Barnum, S.R., Lambris, J.D., . . . Ambati, J. (2006). Drusen complement components C3a and C5a promote choroidal neovascularization. *Proceedings of the National Academy of Sciences of the United States of America*, *103*, 2328–2333.

- Olchawa, M.M., Herrnreiter, A.M., Skumatz, C.M., Zareba, M., Sarna, T.J., & Burke, J.M. (2013). Photosensitized oxidative stress to ARPE-19 cells decreases protein receptors that mediate photoreceptor outer segment phagocytosis. *Investigative Ophthalmology & Visual Sciences*, *54*, 2276–2287.
- Oshima, Y., Oshima, S., Nambu, H., Kachi, S., Hackett, S.F., Melia, M., . . . Campochiaro, P.A. (2004). Increased expression of VEGF in retinal pigmented epithelial cells is not sufficient to cause choroidal neovascularization. *Journal of Cell Physiology*, *201*, 393–400.
- Oyster, C. (1999). Retinal III: regional variation and spatial organization. In C. Oyster (Ed.), *The Human Eye-Structure and Function* (pp. 649–700), Sunderland: Sinauer Associates.
- Panda-Jonas S., Jonas, J.B., & Jakobczk-Zmija M. (1996). Retinal pigment epithelial cell count, distribution and correlations in normal human eyes. *American Journal of Ophthalmology*, *121*, 181–189.
- Pilegaard, H., Saltin, B., & Neufer, P.D. (2003). Exercise induces transient transcriptional activation of the PGC-1alpha gene in human skeletal muscle. *The Journal of Physiology*, *546*, 851–858.
- Qin, S., & Rodrigues, G.A. (2012). Roles of $\alpha v\beta 5$, FAK and MerTK in oxidative stress inhibition of RPE cell phagocytosis. *Experimental Eye Research*, *94*, 63–70.
- Rakoczy, P.E., Lai, C.M., Baines, M., Di Grandi, S., Fitton, J.H., & Constable, I.J. (1997). Modulation of cathepsin D activity in retinal pigment epithelial cells. *Biochemical Journal*, *324*, 935–940.
- Ramrattan, R.S., van der Schaft, T.L., Mooy, C.M., de Bruijn, W.C., Mulder, P.G., & de Jong, P.T. (1994). Morphometric analysis of Bruch's membrane, the choriocapillaris, and the choroid in aging. *Investigative Ophthalmology & Visual Sciences*, *35*, 2857–2864.
- Roehlecke, C., Schumann, U., Ader, M., Brunssen, C., Bramke, S., Morawietz, H., & Funk, R.H.

- (2013). Stress reaction in outer segments of photoreceptors after blue light irradiation. *PLOS ONE*, 8: e71570.
- Roof, D.J., & Makino, C.L. (2000). The structure and function of retinal photoreceptors. In D.A. Albert & F.A. Jakobiec (Eds.), *Principles and Practice of Ophthalmology* (pp. 1624–1673). Philadelphia: Saunders.
- Rosenfeld, P.J., Brown, D.M., Heier, J.S., Boyer, D.S., Kaiser, P.K., Chung, C.Y., & Kim, R.Y. (2006). Ranibizumab for neovascular age-related macular degeneration. *The New England Journal of Medicine*, 355, 1419–1431.
- Salminen, A., Kaarniranta, K., & Kauppinen, A. (2012). Inflammaging: disturbed interplay between autophagy and inflammasomes. *Aging*, 4, 166–175.
- Sardiello, M., Palmieri, M., di Ronza, A., Medina, D.L., Valenza, M., Gennarino, V.A., . . . Ballabio, A. (2009). A gene network regulating lysosomal biogenesis and function. *Science*, 325, 473–477.
- Schmidt-Erfurth, U., Chong, V., Loewenstein, A., Larsen, M., Souied, E., Schlingemann, R., . . . Bandello, F. (2014). *British Journal of Ophthalmology*, 98, 1144–1167.
- Schwanhäusser, B., Busse, D., Li, N., Dittmar, G., Schuchhardt, J., Wolf, J., . . . Selbach, M. (2011). Global quantification of mammalian gene expression control. *Nature*, 473, 337–42.
- Settembre, C., De Cegli, R., Mansueto, G., Saha, P.K., Vetrini, F., Visvikis, O., . . . Ballabio, A. (2013). TFEB controls cellular lipid metabolism through a starvation-induced autoregulatory loop. *Nature Cell Biology*, 15, 647–658.
- Settembre, C., Di Malta, C., Polito, V.A., Garcia Arencibia, M., Vetrini, F., Erdin, S., . . . Ballabio, A. (2011). TFEB links autophagy to lysosomal biogenesis. *Science*, 332, 1429–1433.

- Smith, W., Assink, J., Klein, R., Mitchell, P., Klaver, C.C., Klein, B.E., . . . de Jong, P.T. (2001). Risk factors for age-related macular degeneration: pooled findings from three continents. *Ophthalmology*, *108*, 697–704.
- Sonoda, S., Spee, C., Barron, E., Ryan, S.J., Kannan, R., & Hinton, D.R. (2009). A protocol for the culture and differentiation of highly polarized human retinal pigment epithelial cells. *Nature Protocols*, *4*, 662–673.
- Steinberg, R.H. (1985). Interactions between the retinal pigment epithelium and the neural retina. *Documenta Ophthalmologica*, *60*, 327–346.
- St-Pierre, J., Drori, S., Uldry, M., Silvaggi, J.M., Rhee, J., Jäger, S., . . . Spiegelman, B.M. (2006). Suppression of reactive oxygen species and neurodegeneration by the PGC-1 transcriptional coactivators. *Cell*, *127*, 397–408.
- Strauss, O. (2005). The retinal pigment epithelium in visual function. *Physiological Reviews*, *85*, 845–881.
- Strauss, O., Heimann, H., Foerster, M.H., Agostini, H., Hansen, L.L., & Rosenthal, R. (2003). Activation of L-type Ca²⁺ channels is necessary for growth factor-dependent stimulation of VEGF secretion by RPE cells. *Investigative Ophthalmology & Visual Sciences*, e-abstract 3926.
- Sun, K., Cai, H., Tezel, T.H., Paik, D., Gaillard, E.R., & Del Priore, L.V. (2007). Bruch's membrane aging decreases phagocytosis of outer segments by retinal pigment epithelium. *Molecular Vision*, *13*, 2310–2319.
- Suwa, M., Nakano, H., Radak, Z., & Kumagai, S. (2008). Endurance exercise increases the SIRT1 and peroxisome proliferator-activated receptor gamma coactivator-1alpha protein expressions in rat skeletal muscle. *Metabolism*, *57*, 986–998.
- Thomas, J.P., Maiorino, M., Ursini, F., & Girotti, A.W. (1990). Protective action of phospholipid

- hydroperoxide glutathione peroxidase against membrane-damaging lipid peroxidation. *In situ* reduction of phospholipid and cholesterol hydroperoxides. *The Journal of Biological Chemistry*, 265, 454–461.
- Thurman, J.M., Renner, B., Kunchithapautham, K., Ferreira, V.P., Pangburn, M.K., Ablonczy, Z., . . . Rohrer, B. (2009). Oxidative stress renders retinal pigment epithelial cells susceptible to complement-mediated injury. *The Journal of Biological Chemistry*, 284, 16939–16947.
- Tsunemi, T., Ashe, T.D., Morrison, B.E., Soriano, K.R., Au, J., Roque, R.A., . . . La Spada, A.R. (2012). PGC-1 α rescues Huntington's disease proteotoxicity by preventing oxidative stress and promoting TFEB function. *Science Translational Medicine*, 4, 142ra97.
- Ueta, T., Inoue, T., Furukawa, T., Tamaki, Y., Nakagawa, Y., Imai, H., & Yanagi, Y. (2012a). Glutathione peroxidase 4 is required for maturation of photoreceptor cells. *The Journal of Biological Chemistry*, 287, 7675–7682.
- Ueta, T., Inoue, T., Yuda, K., Furukawa, T., Yanagi, Y., & Tamaki, Y. (2012b). Intense physiological light upregulates vascular endothelial growth factor and enhances choroidal neovascularization via peroxisome proliferator-activated receptor γ coactivator-1 α in mice. *Arteriosclerosis, Thrombosis and Vascular Biology*, 32, 1366–1371.
- Valapala, M., Wilson, C., Hose, S., Bhutto, I.A., Grebe, R., Dong, A., . . . Cano, M. (2014). Lysosomal-mediated waste clearance in retinal pigment epithelial cells is regulated by CRYBA1/ β A3/A1-crystallin via V-ATPase-MTORC1 signaling. *Autophagy*, 10, 480–496.
- Viscomi, C. Bottani, E. Civiletto, G., Cerutti, R., Moggio, M., Fagiolari, G., . . . Zeviani, M. (2011). *In vivo* correction of COX deficiency by activation of the AMPK/PGC-1 α axis. *Cell Metabolism*, 14, 80–90.

- Vives-Bauza, C., Anand, M., Shirazi, A.K., Magrane, J., Gao, J., Vollmer-Snarr, H.R., . . . Finnemann, S.C. (2008). The age lipid A2E and mitochondrial dysfunction synergistically impair phagocytosis by retinal pigment epithelial cells. *The Journal of Biological Chemistry*, *283*, 24770–24780.
- Walsh, N., Valter, K., & Stone, J. Cellular and subcellular patterns of expression of bFGF and CNTF in the normal and light stressed adult rat retina. (2001). *Experimental Eye Research*, *72*, 495–501.
- Wang, S., Moustaid-Moussa, N., Chen, L., Mo, H., Shastri, A., Su, R., . . . Shen, C.L. Novel insights of dietary polyphenols and obesity. (2014). *The Journal of Nutritional Biochemistry*, *25*, 1–18.
- Weiter, J.J., Delori, F.C., Wing, G.L., & Fitch, K.A. (1986). Retinal pigment epithelial lipofuscin and melanin and choroidal melanin in human eyes. *Investigative Ophthalmology & Visual Sciences*, *27*, 145–152.
- Wenz, T., Rossi, S.G., Rotundo, R.L., Spiegelman, B.M., & Moraes, C.T. (2009). Increased muscle PGC-1alpha expression protects from sarcopenia and metabolic disease during aging. *Proceedings of the National Academy of Sciences of the United States of America*, *106*, 20405–20410.
- Westenskow, P.D., Moreno, S.K., Krohne, T.U., Kurihara, T., Zhu, S., Zhang, Z.N., . . . Friedlander, M. (2012). Using flow cytometry to compare the dynamics of photoreceptor outer segment phagocytosis in iPS-derived RPE cells. *Investigative Ophthalmology & Visual Sciences*, *53*, 6282–6290.
- Winkler, B.S., Boulton, M.E., Gottsch, J.D., & Sternberg, P. (1999). Oxidative damage and age-related macular degeneration. *Molecular Vision*, *5*, 32.

- Wirth, E.K., Conrad, M., Winterer, J., Wozny, C., Carlson, B.A., Roth, S., . . . Schweizer, U. (2010). Neuronal selenoprotein expression is required for interneuron development and prevents seizures and neurodegeneration. *The Journal of the Federation of American Societies for Experimental Biology*, *24*, 844–852.
- Witmer, A.N., Vrensen, G.F., Van Noorden, C.J., & Schlingemann, R.O. (2003). Vascular endothelial growth factors and angiogenesis in eye disease. *Progress in Retinal and Eye Research*, *22*, 1–29.
- Wortmann, M., Schneider, M., Pircher, J., Hellfritsch, J., Aichler, M., Vegi, N., . . . Beck, H. (2013). Combined deficiency in glutathione peroxidase 4 and vitamin E causes multiorgan thrombus formation and early death in mice. *Circulation Research*, *113*, 408–417.
- Xie, B., Shen, J., Dong, A., Swaim, M., Hackett, S.F., Wyder, L., . . . Campochiaro, P.A. (2008). An Adam15 amplification loop promotes vascular endothelial growth factor-induced ocular neovascularization. *The Journal of the Federation of American Societies for Experimental Biology*, *22*, 2775–2783.
- Xie, P., Kamei, M., Suzuki, M., Matsumura, N., Nishida, K., Sakimoto, S., . . . Nishida, K. (2011). Suppression and regression of choroidal neovascularization in mice by a novel CCR2 antagonist, INCB3344. *PLOS ONE*, *6*, e28933.
- Xu, J., Zhu, D., Sonoda, S., He, S., Spee, C., Ryan, S.J., Hinton, & D.R. (2012). Over-expression of BMP4 inhibits experimental choroidal neovascularization by modulating VEGF and MMP-9. *Angiogenesis*, *15*, 213–227.
- Yang, C.S., Kim, J.J., Lee, H.M., Jin, H.S., Lee, S.H., Park, J.H., . . . Jo, E.K. (2014). The AMPK-PPARGC1A pathway is required for antimicrobial host defense through activation of autophagy. *Autophagy*, *10*, 785–802.

- Young, R.W. (1971). Shedding of discs from rod outer segments in the rhesus monkey. *Journal of Ultrastructure Research*, 34, 190–203.
- Yu, A.L., Fuchshofer, R., Kook, D., Kampik, A., Bloemendal, H., & Welge-Lüssen, U. (2009). Subtoxic oxidative stress induces senescence in retinal pigment epithelial cells via TGF- β release. *Investigative Ophthalmology & Visual Sciences*, 50, 926–935.
- Zhao, C., Yasumura, D., Li, X., Matthes, M., Lloyd, M., Nielsen, G., . . . Vollrath, D. (2011). mTOR-mediated dedifferentiation of the retinal pigment epithelium initiates photoreceptor degeneration in mice. *The Journal of Clinical Investigation*, 121, 369–383.